PONTIFICIA UNIVERSIDAD CATOLICA DE CHILE

ESCUELA DE INGENIERIA

STUDY OF TRANSPORT PHENOMENA DURING FRYING USING GLASS MICROMODELS

PABLO CORTES

Thesis submitted to the Office of Research and Graduate Studies in partial fulfillment of the requirements for the Degree of Doctor in Engineering Sciences

Advisor:

PEDRO BOUCHON

Santiago de Chile, August, 2011

PONTIFICIA UNIVERSIDAD CATOLICA DE CHILE
ESCUELA DE INGENIERIA

STUDY OF TRANSPORT PHENOMENA DURING FRYING USING GLASS MICROMODELS

PABLO CORTES

Members of the Committee:

PEDRO BOUCHON

JOSE MANUEL DEL VALLE

FRANCO W. PEDRESCHI

LUIS A. SEGURA

KESHAVAN NIRANJAN

CRISTIAN VIAL

Thesis submitted to the Office of Research and Graduate Studies in partial fulfillment of the requirements for the Degree of Doctor in Engineering Sciences

Santiago de Chile, August, 2014

A mi familia

ACKNOWLEDGMENTS

At the end of this long road, I would like to look back and thank to all the people who in one way or another helped me to complete this great challenge.

I would like to thank:

First of all, to my advisor Pedro Bouchon for his trust, unconditional support, motivation and patience during the development of this thesis. Thanks a lot for all these times that I needed that somebody pushed me and you were there.

To my labmates and friends Maria Salomé Mariotti, Sergio Benavides, Veronica Dueik, Maria Carolina Moreno, Mariel Farfán, Teresa Molina and Nicolás Ovalle who were mainstays not only in the development of the thesis but also in the daily life at the University. To secretaries Maria Inés Valdebenito, Debbie Meza, and Danitza Herrera for all the support received.

Specials thanks to Professor Mashairo Kawaji of City College of New York for accepting me as an internship student in his laboratory. I would also thank to Professor Luis Segura and Guillermo Badillo for their support and help in micromodels fabrication.

I also would like to thank the members of the doctoral thesis committee Professors José Manuel del Valle, Franco Pedreschi, Luis Segura, Keshavan Niranjan and Cristián Vial for their suggestions and comments made to this thesis.

I would like to thank the Chilean National Commission for Science and Technology Research (CONICYT), the VRI and School of Engineering from Pontificia Universidad Católica de Chile, that allowed me to carry out my doctoral studies in optimal conditions; to Becas Chile and Fulbright for funding my internship in City College of New York; to FONDECYT Project number 1131083 and project Anillo ACT1105/2012: Healthy food matrix design, for sponsoring my research.

PONTIFICIA UNIVERSIDAD CATÓLICA DE CHILE
ESCUELA DE INGENIERÍA

STUDY OF TRANSPORT PHENOMENA DURING FRYING USING GLASS MICROMODELS

Thesis submitted to the Office of Research and Graduate Studies in partial fulfillment of the requirements for the Degree of Doctor in Engineering Sciences by

PABLO ANDRES CORTES SEGOVIA

New trends in nutrition and the growing demand for healthier foods have been the driving force for the development of fried products with lower oil content. Despite the efforts done to fully understand the phenomenon of oil absorption during frying, due to the multiple changes taking place during this complex and rapid process, a thorough description of the process still remains unclear. So far, oil absorption phenomena during frying have been studied in several ways, using different microscopy techniques, chemical methods, and significant efforts have been carried out to model the process. Due to its complexity, most of this work has been made using a macroscopic approach, since key fluxes are affected by many factors that interact in numerous ways, at different stages.

This thesis aimed to address the transport phenomena that occur during frying from a microscopic perspective in order to arrive to a better understanding of the mechanisms involved during the process. Accordingly, the fundamental hypothesis of this thesis established that it is possible to study and gain a better understanding of the water evaporation and oil absorption phenomena, which occur during frying, from a microscopic point of view, using glass micromodels. Therefore, the main objective of this research was to obtain visual evidence of the mechanisms involved in the evaporation of water and oil absorption during frying using glass micromodels, to

mimic a porous food matrix, in order to establish the flow mechanisms and sequence during the process, identifying when and how the movements of the fluids occur.

Micromodels are transparent pores and constrictions networks that simulate the complexity of a natural porous media. They have been used to study flow in porous media in many areas of science and technology, such as in the oil industry, where its application has contributed to the understanding of flow phenomena and to the optimization of the extraction process. In food processing, they have been used to understand key phenomena in drying, vacuum impregnation, and freeze-drying.

The first step considered the implementation of a photolithographic technique to fabricate the glass micromodels in a reproducible manner. Two set-ups were designed to simulate the frying process, and different cameras were used to capture static images and videos, which were later processed to obtain quantitative information of the phenomenon. The first study was aimed to visualize the different stages during the immersion and cooling periods, to understand most important mechanisms involved throughout the process. Among the main results of this study, it was possible to get visual evidence of the immersion and cooling periods, previously described in the literature. Specifically, it was possible to observe the movement (or evolution) of the evaporation front, and bubbling dynamics. Regarding oil absorption phenomena, it was possible to conclude that only a small fraction of oil penetrated into the glass micromodel during the immersion period. During cooling, suction began just a few seconds after the micromodel was removed from the oil bath and was abruptly stopped when the continuity of the surface oil layer on the open side of the micromodel was lost. This allowed the entry of air, which quickly penetrated into the empty capillaries, until the internal pressure equaled the external one.

Subsequently, the effect of gravity in moisture loss and oil absorption kinetics was studied, aiming to decouple the gravity effect from other factors. Micromodels were placed into the oil bath with different arrangements with respect to gravity ($g>0$, $g=0$,

g<0), in order to understand its effect in capillary penetration. It was observed that when g<0, the drying rate of the matrix was slowed-down and affected the evaporation front, which was less stable as indicated by its higher fractal dimension (1.818 ± 0.032). Largely, evaporation fronts tended to take the form of temperature profiles as reflected by infrared thermal imaging. Overall, g severely affected oil content. Specifically, when g=0, a minimum amount of oil absorption was found.

Finally, the effect of different food matrices in transport phenomena was analyzed. To do so, three different micromodels were designed, based on the porous pattern of apples, potatoes and carrots. Micromodels that mimicked the structure of an apple showed the higher drying rate, and absorbed the highest amount of oil. Carrot micromodels showed lower drying rates, with a less stable evaporation front as indicated by their higher fractal dimension (1.826 ± 0.015). The lower porosity of carrot micromodels significantly reduced oil suction during the cooling period, with 34.8% of the total available volume occupied by oil. Meanwhile, the volume occupied by oil in potato and apple micromodels was 37.0% and 41.5%, respectively.

Overall, the work presented herein allowed getting direct visual evidence of the mechanisms involved in the evaporation of water and oil absorption during oil immersion, in order to establish the most important flow mechanisms and sequence during the process, identifying when and how the movements of the fluids within the matrix occur. Oil immersion of a glass micromodel has certainly some differences from oil immersion of a food material. For instance, glass micromodels are non-hygroscopic, have a fixed structure and are 100% saturated with water. Food materials, on the other hand, are composted of several components and the porous structure develops during the process. In starchy foods for instance, a major food category, starch gelatinization affects the formation and structure of the porous media that is developed during frying, where pores may also expand or collapse during the process. But, the use of glass micromodels allows the direct observation of transport phenomena, which has not been possible to be achieved in a food system. This evidence may lay the foundations for

further knowledge about these phenomena and contribute to the improvement of predictive models, technology design and processing strategies to develop fried products with lower oil content. In addition, the work developed throughout this thesis and developed technique illustrates how glass micromodels may be used to visualize and provide valuable information to understand key transport phenomena during processing in other fields.

Members of the Doctoral Thesis Committee

Pedro Bouchon
Franco Pedreschi
José Manuel del Valle
Luis Segura
Keshavan Niranjan
Cristian Vial

Santiago, August 2014

PONTIFICIA UNIVERSIDAD CATÓLICA DE CHILE
ESCUELA DE INGENIERÍA

ESTUDIO DE LOS FENOMENOS DE TRANSPORTE DURANTE EL PROCESO DE FRITURA USANDO MICROMODELOS DE VIDRIO

Tesis enviada a la Dirección de Investigación y Postgrado en cumplimiento parcial de los requisitos para el grado de Doctor en Ciencias de la Ingeniería.

PABLO ANDRES CORTES SEGOVIA

RESUMEN

Las nuevas tendencias en nutrición y la creciente demanda por alimentos más sanos han sido las fuerzas motrices para el desarrollo de productos fritos con un menor contenido final de aceite. A pesar de los esfuerzos realizados por comprender a cabalidad el fenómeno de absorción de aceite durante la fritura, debido a que múltiples cambios ocurren durante este rápido y complejo proceso, la descripción completa de éste sigue siendo poco clara. Hasta el momento, el fenómeno de absorción de aceite en alimentos fritos, ha sido estudiado de diferentes maneras, utilizando diferentes técnicas de microscopia, métodos químicos, y se han realizado importantes esfuerzos por modelarlo. Debido a su complejidad, la mayoría del trabajo ha sido realizado desde un enfoque macroscópico, ya que los flujos claves son afectados por muchos factores que interactúan de numerosas maneras, en niveles diferentes. Esta tesis busca abordar el fenómeno de transporte ocurrido durante la fritura desde una perspectiva microscópica con el fin de lograr un mejor entendimiento de los mecanismos envueltos en el proceso. En consecuencia, la hipótesis fundamental de esta tesis fue que es posible estudiar y ganar un mejor entendimiento de la evaporación de los fenómenos de evaporación de agua y absorción de aceite, los cuales ocurren durante la inmersión en aceite desde un punto de vista microscópico mediante el uso de micromodelos. Por lo tanto, el objetivo principal de esta investigación fue obtener evidencia visual de los mecanismos responsables de la evaporación de agua y absorción de aceite durante la inmersión en

aceite usando micromodelos de vidrio, para imitar una matriz alimentaria porosa, con el fin de establecer los mecanismos de flujo y secuencia durante el proceso, identificando cuando y como ocurren los movimientos de los fluidos. Los micromodelos son redes estrechas y transparentes de poros que simulan la complejidad de un medio natural poroso. Los micromodelos de vidrio han sido utilizados para estudiar flujo en medios porosos en muchas áreas de la ciencia y tecnología, como por ejemplo en la industria del petróleo, donde su aplicación ha contribuido a la comprensión de los fenómenos de flujo y en la optimización de los procesos de extracción. En el procesamiento de alimentos han sido usados para entender fenómenos claves en secado, impregnación a vacío y secado en frío.

El primer paso consideró la implementación de la técnica fotolitográfica para la fabricación de los micromodelos de una manera reproducible. Además, se diseñaron 2 tipos de sistemas para simular el proceso de fritura, y se usaron varios tipos de cámaras para capturar imágenes estáticas y videos, los cuales fueron posteriormente procesados; con el fin de obtener información cuantitativa del fenómeno. El primer estudio estuvo centrado en visualizar las distintas etapas durante el periodo de inmersión y enfriamiento, con el objetivo de entender los principales mecanismos involucrados. Dentro de los principales resultados de este estudio, cabe destacar que fue posible obtener evidencia visual de los periodos de inmersión y enfriamiento, previamente descritos en la literatura. Específicamente, fue posible observar el movimiento (o evolución) del frente de evaporación y la dinámica del burbujeo. Respecto al fenómeno de absorción de aceite, fue posible concluir que solamente una pequeña fracción de aceite penetraba dentro del micromodelo de vidrio durante el periodo de inmersión. Durante el enfriamiento, la succión comenzó solo algunos segundos después de ser retirado el micromodelo del baño de aceite y se detuvo abruptamente cuando la continuidad de la capa de aceite superficial en el lado abierto del micromodelo se perdió. Esto permitió la entrada de aire, el cual penetró rápidamente en los capilares que aún se encontraban vacíos hasta que la presión interna alcanzó la externa. Los frentes de evaporación tienden en gran medida a tomar las formas de los perfiles de temperatura,

como se refleja en la termografía infrarroja. En general, g afectó severamente el contenido de aceite. Específicamente, cuando g=0, una absorción mínima de aceite fue observada.

Posteriormente, se estudió el efecto de la gravedad en la cinética de pérdida de humedad y absorción de aceite, con el objetivo de desacoplar la gravedad de los otros factores. Los microdelos fueron ubicados dentro del baño de aceite, usando diferentes orientaciones con respecto de la gravedad (g>0; g=0; g <0) con el fin de entender su efecto en la penetración capilar. Se observó que cuando g<0 la velocidad de secado de la matriz disminuyó y afectó el frente de evaporación, el cual fue menos estable como se indica por su mayor dimensión fractal (1.818±0.032). Finalmente, el efecto de diferentes matrices alimentarias sobre los fenómenos de transporte fue analizado. Para lo cual, se diseñaron tres micromodelos diferentes, basados en los patrones porosos de manzanas, papas y zanahorias. Los micromodelos que imitaban la estructura de una manzana mostraron las mayores velocidades de secado, y alcanzaron un mayor contenido de aceite final. Los micromodelos de zanahoria mostraron menores velocidades de secado, con un frente de evaporación menos estable, como se indica en su mayor dimensión fractal (1.826 ± 0.015). La menor porosidad de los micromodelos de zanahoria redujo significativamente la succión de aceite durante el periodo de enfriamiento, con un 34, 8 % del volumen total disponible ocupado por aceite. Por otro lado, el volumen ocupado por el aceite en los micromodelos de papa y manzana fue 37,0% y 41,5%, respectivamente.

En general, el trabajo presentado en este documento permite obtener evidencia visual directa de los mecanismos implicados en la evaporación del agua y la absorción de aceite, con el fin de establecer los mecanismos de flujo más importantes y su secuencia durante el proceso, identificando cuándo y cómo los movimientos de los fluidos dentro de la matriz se producen. La inmersión de un micromodelo de vidrio en aceite, tiene ciertamente algunas diferencias respecto de la inmersión de un material alimentario. Por ejemplo, los micromodelos de vidrio no son higroscópicos, poseen una estructura fija y

son 100% saturados con agua. Por otro lado, los materiales alimentarios están compuestos por variados componentes y la estructura porosa se desarrolla durante su procesamiento. En alimentos amiláceos por ejemplo, una de las principales categorías de alimentos; la gelatinización del almidón afecta la formación de la estructura del medio poroso la cual se desarrolla durante la fritura, donde los poros pueden además expandirse o colapsar durante el proceso. Sin embargo, el uso de micromodelos permite la observación directa del fenómeno de transporte, lo cual no ha sido posible alcanzar en los sistemas alimenticios. Esta evidencia podrá establecer las bases para conocimientos futiros en estos fenómenos y contribuir a la mejora de modelos predictivos, diseños de procesos y tecnologías de procesamiento para desarrollar productos fritos con menores contenidos de aceite. Junto a ello, el trabajo y técnicas desarrolladas en esta tesis ilustran como los micromodelos podrían ser usados para visualizar y proveer de valiosa información que permita entender fenómenos de transporte determinantes del procesamiento en otros campos.

Miembros del Comité de Tesis Doctoral

Pedro Bouchon
Franco Pedreschi
José Manuel del Valle
Luis Segura
Keshavan Niranjan
Cristian Vial

Santiago, Agosto 2014.

LIST OF CONTENTS

LIST OF FIGURES

LIST OF TABLES

LIST OF PAPERS

This thesis is based on the following papers, referred in the text by their respective chapters:

CHAPTER 2: Cortes, P., Badillo, G., Segura, L. A., & Bouchon, P. (2014). **Experimental evidence of water loss and oil-uptake during simulated deep-frying process using glass micromodels**. *Journal of Food Engineering*, 140, 19-27.

CHAPTER 3: Cortes , P., Segura, L. A., Kawaji, M, & Bouchon, P. (2014). **The effect of gravity on moisture and oil absorption profiles during a simulated frying process using glass micromodels**. *Food and Bioproducts Processing*, submitted.

CHAPTER 4: Cortes, P., Badillo, G., Segura, L. A., & Bouchon, P. (2014). **The effect of the microstructural characteristics on humidity loss and oil absorption profiles during a mimic deep-frying process using glass micromodels.** *LWT Food Science and Technology*, submitted.

PROCEEDINGS

Parts of the work have also been presented at three international congresses and one national congress under the following references:

Cortés P.; Bouchon P.; Segura L. Visualization of fluids displacements mechanisms during simulated frying process using glass micromodels. In: 11th International congress on Engineering and Food ICEF 2011. May 22-26, Atenas, Greece. (Best poster award).

Cortes P., Segura L., Bouchon P. Moisture and oil profiles, and visualization of displacements mechanisms during simulated frying process using glass micromodels. In: 8° Congreso Iberoamericano de Ingeniería de Alimentos 2011. October 23-26, Lima, Perú.

Cortés P., Segura L., Bouchon P. Study of oil uptake during frying of glass micromodels using fluorescence microscopy. In: IFT 2012 Annual Meeting and Food Expo. June 26-28, Las Vegas, USA.

Cortes P., Segura L., Bouchon P. Efecto de la gravedad sobre los perfiles de humedad y la absorción de aceite durante un proceso de fritura simulada usando micromodelos de vidrio. In: XIX Congreso nacional de ciencia y tecnología de los alimentos. October 2013, Antofagasta, Chile. (Best poster award).

1. INTRODUCTION

New trends in nutrition have driven research on the development of fried food products with lower oil content. A significant effort has been made to elucidate and understand the mechanisms responsible for oil absorption. The oil absorption of fried products has both nutritional and economic implications. The consumption of fat is considered one of the key factors contributing to obesity and the development of chronic non-communicable diseases (NCDs) such as cardiovascular diseases, hypertension and possibly some types of cancer. Intake of fat, and especially saturated fat, contributes to higher incidence of NCDs (I. Sam Saguy & Dana, 2003). High oil content in fried products also leads to increased production costs and can cause various problems during processing.

Deep-fat frying is a complex unit operation which has been widely studied in an effort to understand key transport phenomena. In this process, food is immersed in an edible fat that is brought to a temperature well above the boiling point of water, producing food water evaporation and the formation of a crust. The process can be divided into four stages (Farkas, Singh, & Rumsey, 1996): 1) *initial heating*, during which the surface of the product is heated to the boiling point of water, 2) *the surface boiling stage*, which is denoted by the rapid loss of surface moisture and an important increase of the heat transfer coefficient (surface boiling regime), 3) *the falling rate period* during which the bulk of the moisture is lost and the inner temperature approaches the water boiling-point and 4) *the bubble-end point*, when the bubbling stops.

1.1. Oil uptake

Frying is a process that involves simultaneous heat and mass transfer resulting in a countercurrent flow of water vapor (bubbles) and oil on the food surface (R. Moreira, Palau, & Sun, 1995; Olivier Vitrac, Dufour, Trystram, & Raoult-Wack, 2002). It has been suggested that oil is mainly absorbed during the cooling period, since the vigorous

escape of water vapor would preclude oil absorption during most of the immersion period. This has been inferred following different indirect experimental procedures such as the addition of a dyed-oil fraction at the end of the process (Ufheil & Escher, 1996) or the extraction of surface oil through successive washing with solvents upon immersion during the post-frying cooling period (R. G. Moreira, Sun, & Chen, 1997). The first experimental observations of Ufheil and Escher (1996) with potato slices suggested that oil absorption occurs during cooling. The researchers added the potato slices to a bath of oil stained at different times in the process, and then quantified the oil content of the chips with an extraction-refractometric methodology. They concluded that oil seems to penetrate during the immersion period of frying and that large amounts of oil are absorbed in the surface layer during the cooling period.

During the immersion period, intense drying occurs at a temperature above the boiling point of water. Thus, the solid food matrix is an obstacle to the growth of water bubbles and produces a pressure gradient within the food. This overpressure depends on the initial structure of the material. The more resistant the structure, the greater the internal over-pressure. Vitrac et al (2000) confirmed these observations by measuring the internal pressure within a starch food model system during the immersion and cooling periods. These authors measured an overpressure of 45 kPa during the immersion period which prevents oil migration into the material. By contrast, it was also found that rapid cooling of the crust in the hygroscopic domain after the immersion period generates an immediate vapor condensation in equilibrium with the solid matrix which results in a pressure drop to 35 kPa. The process was repeated using materials with different compositions and structures. This showed that the pressure values depend on the material's bulk density and porosity.

Thus, during the immersion period, when the product has a high content of free water susceptible to evaporation, the water vapor escape associated with overpressure is a barrier to oil absorption. However, when the product is removed from the heating medium, the temperature of the product decreases and the vapor condenses, resulting in

a sudden decrease in pressure inside of the product. The difference between internal and external pressure creates a "vacuum effect" and causes the penetration of the surface oil (Gamble, Rice, & Selman, 1987; R. G. Moreira & Barrufet, 1996). The oil absorption involves a balance between adhesion forces (capillary condensation and water) and oil drain during the cooling period (Halder, Dhall, & Datta, 2007a; Ufheil & Escher, 1996).

Using a combined approach using solvent washing coupled to spectrometry, Bouchon et al (2003) found that a small amount of oil may be absorbed during frying. They call this "*structural oil*." The authors identified three types of oil when frying a thick potato cylinder: i) *structural oil*, which represents the oil absorbed during immersion period, ii) *penetrated surface oil*, which represents the oil suctioned into the food during cooling and iii) *surface oil*, the remaining portion. The results showed that only a small amount of oil seemed to penetrate during frying and that most oil penetrated after cooling. The oil was located either on the surface of the product or was suctioned into the porous crust microstructure, with an inverse relationship between them for increasing frying times, as confirmed through infrared spectroscopy of high spatial resolution (Bouchon et al., 2003). This experimental approach is the closest yet to a direct measurement of oil at different frying times. It is not yet possible to engage in direct observation of the phenomena.

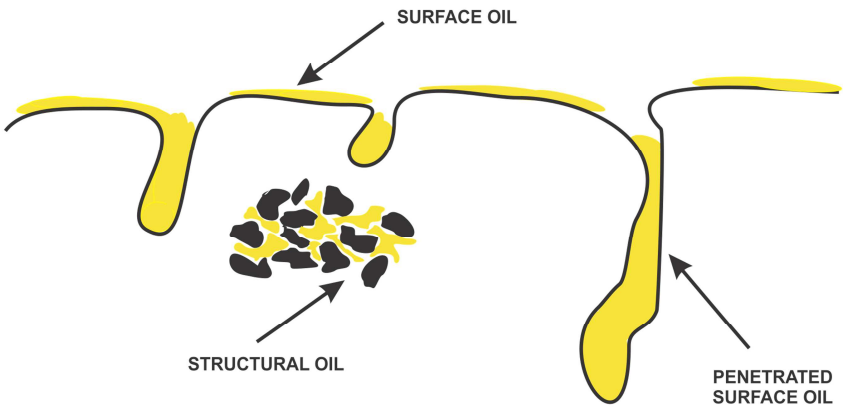

Figure 1-1: Types of oil that can be identified in a fried product (Bouchon et al., 2003)

As a consequence, the main driving forces that control oil absorption and have been used to model the process are linked to capillary pressure (R. G. Moreira & Barrufet, 1998) and/or to the pressure drop generated during cooling (Bouchon & Pyle, 2005a; Mellema, 2003; Ziaiifar, Achir, Courtois, Trezzani, & Trystram, 2008). The oil suction mechanism refers to the oil suctioned into the product due to water-vapor condensation, a mechanism that may be mediated by capillary forces. The only difference is a greater pressure gradient.

Moreno et al. (2010) studied the oil absorption capacity of laminated dough after deep-fat frying, using formulations based either on potato flakes or wheat gluten. These thin products were dehydrated up to a final moisture content of 2%. Interestingly, they found that gluten-based products absorbed most of the oil during frying, whereas potato-flake-based products absorbed most of it during cooling. . Differences were attributed to the characteristics of the porous network developed by gluten-based products during frying, which could influence the capillary flow of oil within the product.

During post-frying cooling, the oil adhered to the surface of the product when it is removed from the oil bath, fills the accessible pores in competition with air. Normally, the oil is drained from the product surface so that the available surface oil is limited (Yamsaengsung & Moreira, 2002). The main driving forces are the capillary pressure and the possible pressure drop generated by vapor condensation within the product. Resistance to oil migration is related to oil viscosity, pore connectivity and free water for removal or displacement created by cell dislocation. As a result, variations in patterns of oil absorption can be obtained using different structures or oil products (Halder, Dhall, & Datta, 2007b). For instance, products that are sufficiently dried may be impregnated with oil during the process, as in thin laminated dough (Moreno et al., 2010).

In addition, potentially toxic compounds may be generated during frying. These may appear in the oil as a result of this deterioration due to the action of oxygen, heat and

water (Danowska-Oziewicz & Karpinska-Tymoszczyk, 2005). The compounds modify the physicochemical properties of the oil, thus promoting its absorption. The formation of surfactants only partially explains the increase in oil absorption during prolonged frying, as the literature, theory and new data have yielded conflicting results that do not support the theory that prolonged frying produces surfactants that reduce the contact angle and/or the interfacial tension in a manner that would significantly influence oil absorption (Dana & Saguy, 2006; I. Sam Saguy & Dana, 2003).

1.2. Oil uptake mechanisms

Oil absorption during frying is a complex phenomenon which is not clearly understood. There is a need to study the initial product structures and their development, the different exchanges between the food matrix and the heating medium, and the variations that both the product and the oil undergo in their physicochemical and thermal properties. In addition, the rate at which these changes occur complicates the study of this phenomenon (Ziaiifar et al., 2008). Over the past 20 years, several of the heat and mass transfer phenomena occurring during or immediately after deep frying have been described. Research, through indirect measurements, seems to point out that oil does would not penetrate the food product as long as there is an overpressure inside of it (Dana & Saguy, 2006; Farinu & Baik, 2005; Mellema, 2003). However, direct observation of this phenomenon has not yet been possible.

The models of the frying process that have been developed have helped generate predictions of temperature profiles in the different regions of the fried product (thin and thick products with different geometries), the thickness of the crust, and moisture loss. However, none of these models describes the oil absorption process, much less the amount and location of the oil retained by the product (Farinu & Baik, 2005).

As we noted earlier, Moreira and Barrufet (1998) developed a model for oil absorption during cooling in tortilla chips. The main cause of oil penetration of the product was attributed to the capillary force and the “suction” effect of vapor condensation. They

selected the suction effect based on the fact that they observed suction while the temperature of the product was above the temperature of boiling water after frying. Ni and Datta (1999) developed a multiphase porous medium model to predict heat transfer, moisture loss, and oil absorption during frying. They conceptualized the fried product as a multiphase porous medium and argued that the gas phase (vapor and air) moved through convective and diffusive flows, while the liquid phase (water and oil) moved by convective and capillaries flows. However, this model assumed that the oil penetrated the product during the immersion period and did not consider the cooling period, which differs from the physical reality of the process known to date.

More recently, (Bouchon & Pyle, 2005a, 2005b) developed a two-part model focused on the frying and cooling processes. They used the Whasburn equation for the oil absorption model, adding two new terms to the capillary pressure (Equation 1-1):

$$\frac{dh}{dt} = \frac{r^2}{8 \cdot \mu \cdot h} \cdot \left(P_{atm} - P_v + \left[\left(2\gamma \cos\phi\right)/r\right] \pm \rho g h \cos\alpha\right) \qquad \text{(Eq.1-1)}$$

The first term represents the unbalanced air pressure due to the change in the vapor pressure of the water during cooling. The second term is related to the influence of gravity on the oil drain in different positions during cooling and can favor or disfavor oil absorption, such as shown in Figure 1-2.

Note that all of the models described above have been developed from a macroscopic perspective. As Figure 1-2 shows, many authors have used models with an ideal pore for explaining the oil absorption phenomenon (Mellema, 2003). But food matrices are much more complex than this because the pores are interconnected and may be filled or partially filled with water, air, vapor or oil, and their evolution will depend on the condition of neighboring pores (mainly their temperature and pressure).

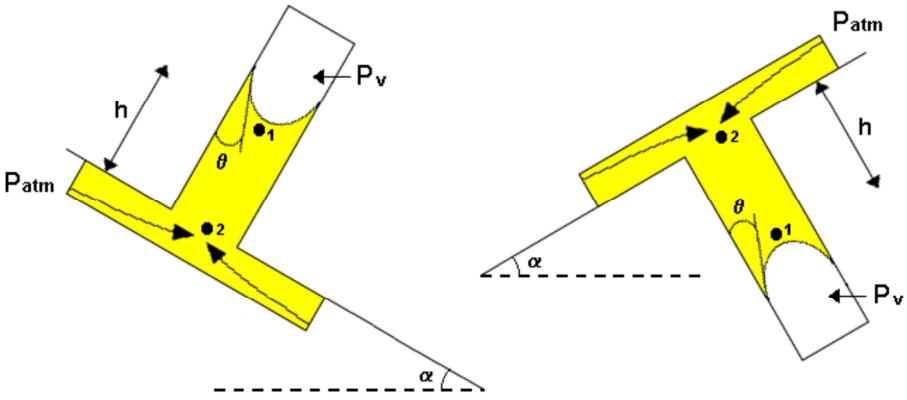

Figure 1-2: Capillary penetration of oil (viscosity μ, surface tension γ and density φ) on a regular pore of radius r in different configurations. Left: gravity restricts penetration. Right: gravity favors penetration (Bouchon and Pyle, 2005a).

The importance of the microstructural changes that occur during deep frying has been recognized in modeling of the mass and heat transport. They also are important for understanding the mechanisms because the crust microstructure plays a key role in determining the amount of oil absorbed. It is thus essential to connect the food microstructure to the transport phenomena involved in the process (Farinu & Baik, 2005; Ziaiifar et al., 2008).

It is noteworthy that our current knowledge of the frying process is mainly macroscopic and takes into account only some aspects of the evolution of the food and the complex interactions between different factors (Ziaiifar et al., 2008). The evolution of the microstructure (for example, the initial cell structure and its evolution) and its mechanical properties, as well as the coupling between mass and heat phenomena are poorly understood. Recent efforts to simulate the microstructure of various food materials and mimic numerous food processes have attracted attention in food science literature. Several approaches have been applied to predict transport phenomena in food materials. The pore network approaches have several advantages over the continuum approach (diffusion model) because in the latter case, the microscopic complexities of

the matrix are often lumped (*e.g.* effective diffusivities), which are empirical constants (Gueven & Hicsasmaz, 2013). In order to achieve this goal, it is reasonable to use tools derived from other areas of science such as transparent micromodels.

1.3. Micromodels

Micromodels are transparent pore and constriction networks that simulate the complexity of a natural porous medium. They have been developed to help researchers display flow processes at the pore level (Buckley, 1991). Micromodels are useful for elucidating and understanding the fundamentals of transport mechanisms, their interactions, and their evolution over time because they allow researchers to visualize complex fluid/fluid/solid interactions and their relationships with geometry and pore-space topology during the displacement processes (Oyarzún & Segura, 2009). The multiple events occurring in the micromodels illustrate mechanisms of the multiphase flow. The applications of the micromodels are varied. They allow researchers to see the movement of the fluid interface and to distinguish between a variety of mechanisms with similar behaviors with respect to other phenomena. A great deal of work has been done in order to understand the importance of pore geometry and topology, fluid properties, and the interaction of capillary forces and gravity for determining the course of displacement of two phases (Buckley, 1991).

Micromodels can be manufactured using different techniques and transparent materials. The basic steps include the capture of the key characteristics of the microstructure of the natural porous media to be mimicked, the generation of the pattern that contains those features, and the transfer of this network to the transparent material in order to build the micromodel. Statistical information about the microscopic characteristics of food networks is available in the literature, including pore size distribution, mean values and standard deviation, which have been calculated using different techniques (Karathanos, Kanellopoulos, & Belessiotis, 1996; Rahman, Al-Zakwani, & Guizani, 2005).

Micromodels were originally used as an important tool in the development of the petroleum industry. Their use later spread to other areas of science and to the study of different types of phenomena. Micromodels also have been used to better understand transport phenomena in food processes such as drying (Laurindo & Prat, 1998; SanMartin, Laurindo, & Segura, 2011; L. A. Segura & Toledo, 2005b), vacuum impregnation (Badillo, Segura, & Laurindo, 2011) and freeze-drying (L. A. Segura & Oyarzún, 2012). To date, no studies have considered their use in frying.

The pioneering work of Lenormand *et al.* (1988) in immiscible displacement of two fluids in a transparent model helped establish the basis for experiments of this kind and their application in engineering problems. The author performed extensive studies using pore network simulations and experiments with transparent micromodels in drain-type displacement where a wetting fluid (mercury in this study) is displaced by another non-wetting fluid (different types of oils). The goal was to show the displacement mechanisms of two immiscible fluids according to capillary number (C) and viscosity ratio (M). Capillary number is a dimensionless number that is a ratio between viscous and capillary forces. It represents the type of forces that dominate during the process. For instance, in porous media for low capillary numbers, the flow is dominated by capillary forces whereas for high capillary numbers, the capillary forces are negligible compared to the viscous forces:

$$\boldsymbol{C = \frac{q \cdot \mu_w}{A \cdot \gamma \cdot \cos \varphi}} \qquad \text{(Eq. 1-2)}$$

where the numerator is the displacing fluid flow q (m^3/s) multiplied by the viscosity of the wetting fluid μ (kg/ms) and the denominator is the flow cross-sectional area A (m^2) multiplied by the interfacial tension of the wetting fluid (γ in N/m) and the cos of contact angle (φ for water/glass ~ °0), and for M:

$$\boldsymbol{M} = \frac{\boldsymbol{\mu_{nw}}}{\boldsymbol{\mu_{w}}} \qquad \text{(Eq. 1-3)}$$

where M is the ratio between the viscosity of non-wetting fluid (in the case of the immersion period it is vapor) and the viscosity of the wetting fluid (water), yielding a relative viscosity of the non-wetting fluid on the wetting.

Lenormand and Zarcone (1984) described three basic mechanisms in order to explain the immiscible displacing fluid within a porous network as a function of capillary contact. Here, capillary forces are much greater than viscous forces, and the fluid of lower viscosity is displaced by a higher-viscosity fluid in a piston-like flow pattern. These researchers showed that the displacement can be described using a statistical theory called invasion-percolation in order to identify the three regimes governing the process.

Figure 1-3 shows the flow patterns obtained using the dynamic model developed by Lenormand et al. (1988). The similarity in the flow patterns using micromodels experimentally determined by the same authors was notable (R. Lenormand et al., 1988). These authors established the existence of a "phase diagram" for the displacement of two immiscible phases (see Figure 1-3) depending on the capillary number C and the viscosity ratio M. In the stable displacement, the driving force due to the viscosity of the invading fluid is represented by a model called Growth Dominated by Gradient (CGC). The viscous fingering to the viscosity of the displaced fluid is represented by the diffusion-limited aggregation (DLA) model. In the extreme case, M reaches zero. In capillary fingering, viscous forces are negligible compared to the capillary. This phenomenon is modeled by invasion percolation. In Figure 1-3, one can qualitatively distinguish between the values of C and M that define the existing flow patterns and the regions on the diagram.

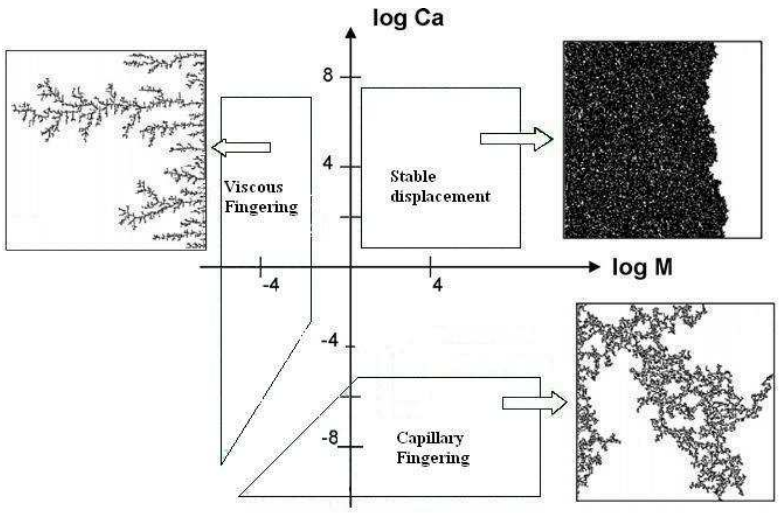

Figure 1-3: Phase diagram of Lenormand *et al*. (1986) for two-phase flow as a function of the capillary number C and the ratio of viscosities M (Badillo et al., 2011).

The complex way in which transport phenomena occurring within a food matrix are coupled makes it more difficult to study these phenomena. The flow in a porous medium is affected by several factors including the direction in which this flow occurs in relation to the force of gravity. Laurindo and Prat (1996) studied the effect of gravity on the drying front of a micromodel. In this study, the researchers considered three basic situations depending on bond B, which is defined as:

$$B = \Delta\rho \cdot g a^2 \cdot \sin\theta / \gamma \quad \text{(Eq.1-4)}$$

where **α** is the distance between two nodes of the network, **g** is the gravity vector intensity, $\Delta\rho = \rho_{liquid} - \rho_{gas}$, **θ** is the angle between the open side of micromodel and the horizontal plane, and **γ** is the interfacial tension between wetting fluid and non-wetting fluid (N/m). The first case is the one where the micromodel is placed horizontally and the gravity forces are negligible, *i.e.* B = 0. The second case is where the micromodel is placed vertically with the open side up and the gravity forces tend to stabilize the invasion process, *i.e.* B > 0. Finally, in the third case, the micromodel is placed with the open side down and gravity forces tend to destabilize the invasion process, *i.e.* B < 0.

Many experimental and theoretical studies have been carried out to better understand the mechanisms of heat and mass transfer during the frying process. This has helped researchers to understand the transport phenomena during frying and the relationship between water content/loss, thermo-physical properties of the food, and the frying medium.

1.4. Hypothesis and objectives

The literature review clearly shows that deep-fat frying and associated oil uptake are complex phenomena. This unit operation is affected by many factors that interact in numerous ways, acting as coupled processes with some dominating others at different stages. Most of the data gathered and studies performed to date have considered a macroscopic approach. There is a need to understand the phenomena which physically occur during the frying process with focus on oil absorption. This thesis seeks to address the transport phenomena that occur during frying from a microscopic perspective in order to arrive at a better understanding of the mechanisms and the phenomenon itself. Accordingly, the fundamental hypothesis of this thesis established that it is possible to study and gain a better understanding of the water evaporation and oil absorption phenomena, which occur during frying, from a microscopic point of view, using glass micromodels.

Therefore, the main objective of this research is to obtain visual evidence of the mechanisms involved in the evaporation of water and oil absorption during frying using glass micromodels and to establish the flow mechanisms, identifying when and how the movements of the fluids within the food matrix occur. This is expected to explain the relationship between the phenomena and the properties of the matrix and the fluids involved (air, water, oil, and water vapor) in order to establish a sequence of events and define which mechanisms dominate in each stage of the frying process.

In order to achieve this goal, the thesis was organized around the following specific objectives:

- To develop an experimental procedure, which allows mimicking the deep-fat frying process using glass micromodels, to get direct evidence and understand the sequence of transport phenomena occurring during oil immersion, through the observation of the actual movement of fluids within the model (Chapter 2).
- To analyze the effect of gravity on the dynamics of water evaporation and oil uptake using glass micromodels (Chapter 3).
- To study the effect of different porous media on moisture loss and oil patterns during frying, using glass micromodels, to get a better understanding of the relationship between microstructure and transport phenomena.

Accordingly, a general overview of the outline of the thesis is summarized in Figure 1.4.

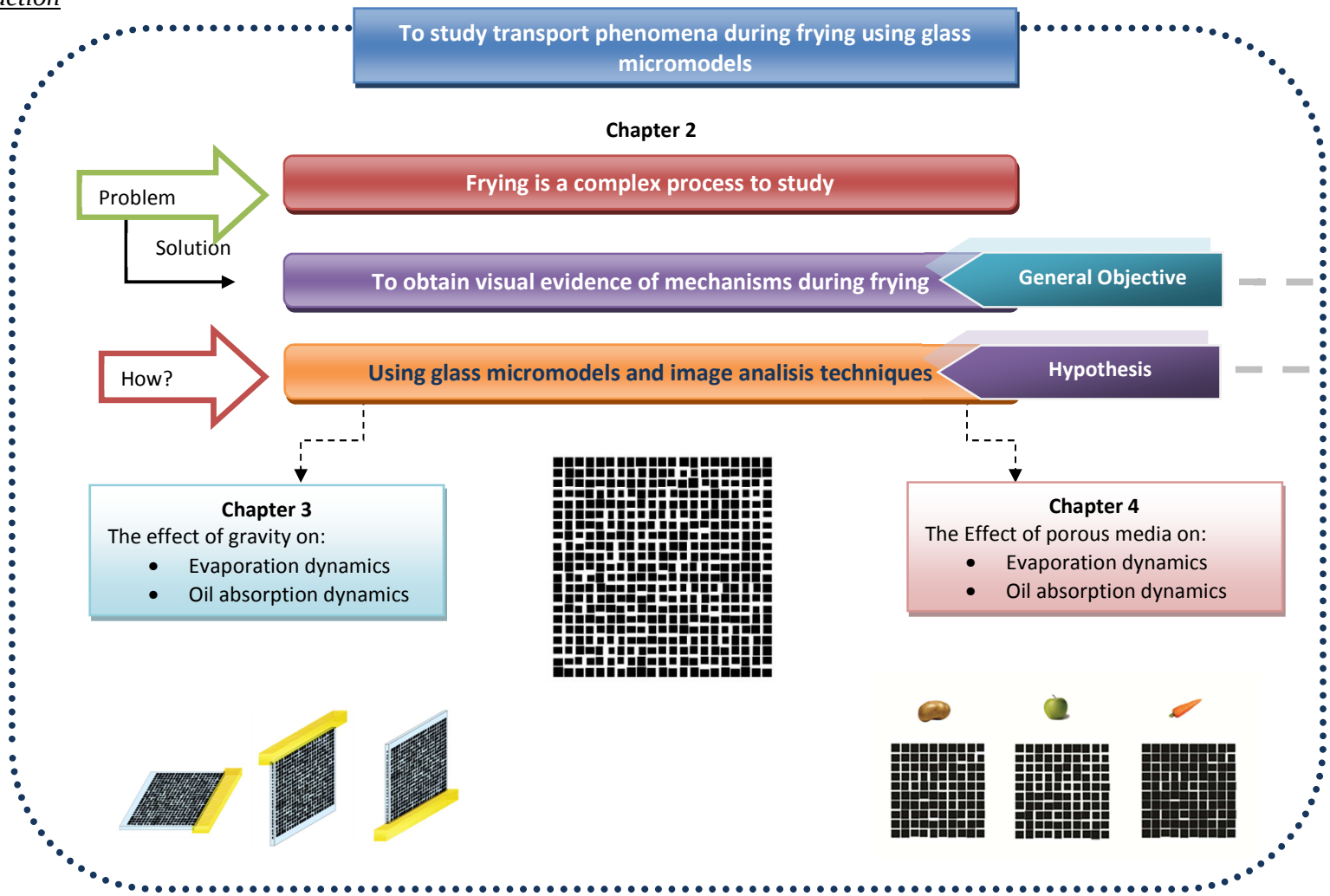

Figure 1-4: Overview of the studies comprising this thesis

1.5. References

Badillo, G.M., Segura, L.A., Laurindo, J.B., (2011). Theoretical and experimental aspects of vacuum impregnation of porous media using transparent etched networks. International Journal of Multiphase Flow 37(9), 1219-1226.

Bouchon, P., Aguilera, J.M., Pyle, D.L., (2003). Structure oil-absorption relationships during deep-fat frying. Journal of Food Science 68(9), 2711-2716.

Bouchon, P., Pyle, D.L., (2005a). Modelling Oil Absorption During Post-Frying Cooling: I: Model Development. Food and Bioproducts Processing 83(4), 253-260.

Bouchon, P., Pyle, D.L., (2005b). Modelling Oil Absorption During Post-Frying Cooling: II: Solution of the Mathematical Model, Model Testing and Simulations. Food and Bioproducts Processing 83(4), 261-272.

Buckley, J.S., (1991). Multiphase displacements in micromodels, in: Morrow, N.R. (Ed.), *Interfacial phenomena in petroleum recovery*. Marcel Dekker Inc., New York, pp. 157-189.

Dana, D., Saguy, I.S., (2006). Review: Mechanism of oil uptake during deep-fat frying and the surfactant effect-theory and myth. Advances in Colloid and Interface Science 128-130, 267-272.

Danowska-Oziewicz, M., Karpinska-Tymoszczyk, M., (2005). Quality changes in selected frying fats during heating in a model system. Journal of Food Lipids 12(2), 159-168.

Farinu, A., Baik, O.D., (2005). Deep fat frying of foods-transport phenomena. Food Reviews International 21(4), 389-410.

Farkas, B.E., Singh, R.P., Rumsey, T.R., (1996). Modeling heat and mass transfer in immersion frying .1. Model development. Journal of Food Engineering 29(2), 211-226.

Gamble, M.H., Rice, P., Selman, J.D., (1987). Distribution and morphology of oil deposits in some deep fried products
Journal of Food Science 52(6), 1742.

Gueven, A., Hicsasmaz, Z., (2013). *Pore structure in food - simulation, measurement and applications* Springer, New York.

Introduction

Halder, A., Dhall, A., Datta, A.K., (2007a). An improved, easily implementable, porous media based model for deep-fat frying - Part I: Model development and input parameters. Food and Bioproducts Processing 85(C3), 209-219.

Halder, A., Dhall, A., Datta, A.K., (2007b). An improved, easily implementable, porous media based model for deep-fat frying - Part II: Results, validation and sensitivity analysis. Food and Bioproducts Processing 85(C3), 220-230.

Karathanos, V.T., Kanellopoulos, N.K., Belessiotis, V.G., (1996). Development of porous structure during air drying of agricultural plant products. Journal of Food Engineering 29(2), 167-183.

Laurindo, J.B., Prat, M., (1996). Numerical and experimental network study of evaporation in capillary porous media. Phase distributions. Chemical Engineering Science 51(23), 5171-5185.

Laurindo, J.B., Prat, M., (1998). Numerical and experimental network study of evaporation in capillary porous media. Drying rates. Chemical Engineering Science 53(12), 2257-2269.

Lenormand, R., Touboul, E., Zarcone, C., (1988). Numerical models and experiments on immiscible displacements in porous media. Journal of Fluid Mechanics 189(9), 165-187.

Lenormand, R., Zarcone, C., (1984). Role of roughness and edges during imbibition in square capillaries.

Mellema, M., (2003). Mechanism and reduction of fat uptake in deep-fat fried foods. Trends in Food Science & Technology 14(9), 364-373.

Moreira, R., Palau, J., Sun, X.Z., (1995). Simultaneous heat and mass-transfer during the deep fat frying of tortilla chips. Journal of Food Process Engineering 18(3), 307-320.

Moreira, R.G., Barrufet, M.A., (1996). Spatial distribution of oil after deep-fat frying of tortilla chips from a stochastic model. Journal of Food Engineering 27(3), 279-290.

Moreira, R.G., Barrufet, M.A., (1998). A new approach to describe oil absorption in fried foods: a simulation study. Journal of Food Engineering 35(1), 1-22.

Moreira, R.G., Sun, X.Z., Chen, Y.H., (1997). Factors affecting oil uptake in tortilla chips in deep-fat frying. Journal of Food Engineering 31(4), 485-498.

Moreno, M.C., Brown, C.A., Bouchon, P., (2010). Effect of food surface roughness on oil uptake by deep-fat fried products. Journal of Food Engineering 101(2), 179-186.

Introduction

Ni, H., Datta, A.K., (1999). Moisture, oil and energy transport during deep-fat frying of food materials. Food and Bioproducts Processing 77(C3), 194-204.

Oyarzun, C.A., Segura, L.A., (2009). Design and Construction of Glass Micromodels for the Study of Moisture Transport in Softwoods. Drying Technology 27(1), 14-29.

Rahman, M.S., Al-Zakwani, I., Guizani, N., (2005). Pore formation in apple during air-drying as a function of temperature: porosity and pore-size distribution. Journal of the Science of Food and Agriculture 85(6), 979-989.

Saguy, I.S., Dana, D., (2003). Integrated approach to deep fat frying: engineering, nutrition, health and consumer aspects. Journal of Food Engineering 56(2-3), 143-152.

SanMartin, F.A., Laurindo, J.B., Segura, L.A., (2011). Pore-Scale Simulation of Drying of a Porous Media Saturated with a Sucrose Solution. Drying Technology 29(8), 873-887.

Segura, L.A., Oyarzún, C.A., (2012). Experimental evidence of mass transfer mechanisms during freeze-drying in a capillary porous medium. International Journal of Refrigeration 35(8), 2102-2109.

Segura, L.A., Toledo, P.G., (2005). Pore-level modeling of isothermal drying of pore networks. Evaporation and viscous flow. Latin American Applied Research 35(1), 43-50.

Ufheil, G., Escher, F., (1996). Dynamics of oil uptake during deep-fat frying of potato slices. Food Science and Technology-Lebensmittel-Wissenschaft & Technologie 29(7), 640-644.

Vitrac, O., Dufour, D., Trystram, G., Raoult-Wack, A.-L., (2002). Characterization of heat and mass transfer during deep-fat frying and its effect on cassava chip quality. Journal of Food Engineering 53(2), 161-176.

Vitrac, O., Trystram, G., Raoult-Wack, A.L., (2000). Deep-fat frying of food: heat and mass transfer, transformations and reactions inside the frying material. European Journal of Lipid Science and Technology 102(8-9), 529-538.

Yamsaengsung, R., Moreira, R.G., (2002). Modeling the transport phenomena and structural changes during deep fat frying - Part 1: model development. Journal of Food Engineering 53(1), 1-10.

Ziaiifar, A.M., Achir, N., Courtois, F., Trezzani, I., Trystram, G., (2008). Review of mechanisms, conditions, and factors involved in the oil uptake phenomenon during the deep-fat frying process. International Journal of Food Science and Technology 43(8), 1410-1423.

2. EXPERIMENTAL EVIDENCE OF WATER LOSS AND OIL UPTAKE DURING SIMULATED DEEP-FAT FRYING USING GLASS MICROMODELS

Abstract:

Different studies have emphasized the importance of cooling in oil absorption after frying, suggesting that the largest proportion of oil is sucked into the crust after the product is removed from the oil. Microscopy has been a powerful tool to support these determinations, but, direct observation of fluxes has not yet been possible. The aim of this research was to develop an experimental procedure based on the use of glass micromodels to get direct evidence of transport phenomena during oil immersion for the first time. To do so, micromodels were saturated with water and immersed in oil at 190 ºC. Fluids displacements were monitored using video-microscopy as well as fluorescence microscopy. Results showed that only a small fraction of oil penetrated during the immersion period, due to the vigorous escape of bubbles. Once the release of steam stopped, after some initial cooling, oil-uptake began abruptly and oil movement into the pores could be clearly identified. Oil absorption ended as soon as the oil film lost continuity, due to air penetration. Overall, the developed technique illustrates how glass micromodels may be used to visualize and provide valuable information to understand key transport phenomena during processing.

Key words: *micromodel; frying; oil uptake; pore network; capillaries; dehydration.*

2.1. Introduction

Deep-fat frying is a complex unit operation, which has been widely studied to understand key transport phenomena. In relation to oil absorption, it has been suggested that it is the mostly absorbed during the cooling period, since the vigorous escape of water vapour would preclude oil absorption during most of the immersion period. This has been inferred following different indirect experimental procedures, which have considered for instance the addition of a dyed-oil fraction at the end of the process (Ufheil & Escher, 1996) or the extraction of surface-oil through successive washing with solvents upon immersion during the post-frying cooling period (R. G. Moreira et al., 1997). Using a combined experimental approach, Bouchon et al. (2003) found that only a small amount of oil was able to penetrate during frying and that after cooling. They determined that oil was located either on the surface of the product or was suctioned into the porous crust microstructure, with an inverse relationship between them for increasing frying times. However, so far it has not been possible the direct observation of these phenomena.

The main driving forces that have been suggested to control oil absorption and have been used to model the process have been related to capillary pressure (R. G. Moreira & Barrufet, 1998) and/or to the pressure drop generated during cooling (Bouchon & Pyle, 2005a; Mellema, 2003; Ziaiifar et al., 2008). This last mechanism refers to the oil post-cooling suction due to water-vapor condensation, a mechanism that may well be mediated by capillary forces. In this respect, Vitrac et al. (2000) measured the internal pressure inside a food model made of starch during the immersion and post-frying cooling periods. An overpressure of 45 kPa was determined during frying, which prevented the migration of oil inside the material. In contrast, the fast cooling upon frying generated the immediate condensation of water-vapor, which was responsible for a pressure drop down to 35 kPa. Repetitions for materials with different compositions and structures demonstrated that pressure values depended of their apparent density and porosity. Recently, Moreno et al. (2010) studied the oil absorption in thin laminated

dough, using formulations based either on potato flakes or wheat gluten. These thin products are dehydrated to a final moisture content of 2%; thus, little water is left to preclude oil absorption during the immersion period. In contrast to some previous results, they found that gluten-based products absorbed most of the oil during frying, whereas potato-flake-based products absorbed most of it during cooling. Differences were conferred to the characteristics of the porous network developed by gluten-based products during frying, which could influence the capillary flow of oil within the product.

It is noteworthy that our current knowledge in relation to oil absorption is mainly macroscopic and takes into account only some aspects of the evolution of the food matrix (Ziaiifar et al., 2008). Certainly, microscopy has been a powerful tool, but, direct observation of fluxes has not yet been possible. A possibility could be achieved through the use of additional tools from other fields of science, such as the use of micromodels.

Micromodels are transparent pores and constrictions networks that simulate the complexity of a natural porous media, which have been developed to meet the needs to display flow processes at a pore level (Buckley, 1991). Micromodels are useful in elucidating the fundamentals of transport mechanisms because they allow visualizing complex fluid/fluid/solid interactions and their relationships with geometry and pore-space topology during the displacement processes (Oyarzún & Segura, 2009). Their fabrication may be achieved through different techniques. Basic steps consider the capture of the key characteristics of the microstructure of the natural porous media to be mimicked, the generation of the pattern that contains such features and the transfer to the model.

Micromodels have been used to get a better understanding of transport phenomena in different food processes, such as drying (Laurindo & Prat, 1998; SanMartin et al., 2011; L. A. Segura & Toledo, 2005b), vacuum impregnation (Badillo et al., 2011) and freeze-drying (L. A. Segura & Oyarzún, 2012), but as yet, frying has not been considered. In

accordance, the aim of this research was to develop an experimental procedure based on the use of micromodels to get direct evidence, for the first time, of the sequence of transport phenomena occurring during oil immersion, through the observation of the actual movement of fluids within the model, to elucidate among others, whether water removal and oil absorption are simultaneous and/or coupled events.

2.2. Materials and methods

Micromodels (2D transparent porous media) were fabricated using a photolithographic technique, according to the protocol reported by Oyarzún and Segura (2009). The photolithographic process considers two main steps: the design of the pattern (photomask) and the photo-etching process in the glass plate, which are described in detail in the following sections.

2.2.1 Computer-Designed Photomask

One of the critical steps in the fabrication of micromodels is the design of the transparent pattern to be transferred to the glass plates. This pattern usually known as photomask, must be carefully designed to capture all the topological and geometric features of the original porous structure. In this work, we used computer-designed patterns to describe the microstructure of potatoes. The first step was to generate random numbers of throats-radii. Then, a macro was written in Visual Basic Application (VBA), values were loaded and the network was drawn using the vector graphics drawing program AutoCAD (version 2010, Autodesk Inc.). The patterns were printed in transparent films using a laser printer (HP Designjet Z5200) with a resolution of 2,400 x 1,200 dpi.

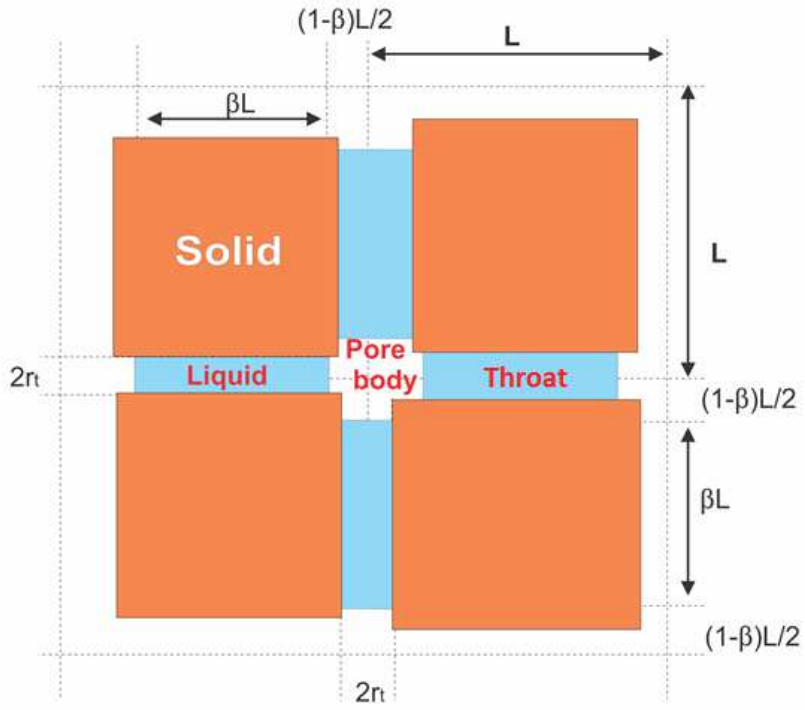

Figure 2-1: Bi-dimensional network of pore-bodies connected by prismatic rectangular pore-throats used in this research, as reported by Segura and Oyarzún (2012).

The network model used in this work was a bi-dimensional network of pore-bodies connected by prismatic rectangular pore-throats, as depicted in Figure 2-1. The radii of the throats in the duct circumscribed rt were chosen randomly according to a probability distribution function given by f(rt) (probability function of the distribution of the radii of pore throats). The depth of each pore throat and body were constant and equal to Rah. The distance between pore centers was constant and equal to L. The length of the throats was constant and equal to a fraction of L, referred as β. The distance between the meniscus of each throat and the adjacent pore center was equal to (1 - β)L/2. This model of network is able to precisely capture the topology and statistical distribution of the pore space of the glass micromodels at the pore scale (Prat, 1993).

Table 2-1: Pore network parameters used in the micromodel design.

Description	Symbol	Value
Pore body to pore body length (m)	L	1×10^{-3}
Throat and body depth (m)	R_{ah}	3.5×10^{-5}
Porosity (dimensionless)	P	0.26
Geometrical parameter (dimensionless)	B	0.71
Throat length (m)	βL	4.28×10^{-3}
Pore radius (m)	r_p	8.7×10^{-4}
Mean aspect ratio (dimensionless)	r_p/r_t	1.18
Total pore space volume (m^3)	V_r	3.01×10^{-7}
Cross-sectional area (m^2)	Σ	1.15×10^{-3}

The size of micromodels was (15 x 14.5 cm^2) and contained 100x100 pores (nodes). The pore network was designed according to the statistical information of the microstructure of potatoes reported by (Karathanos et al., 1996), amplified 100 times. Pore-throat radii had a Log-Normal distribution with a mean size of 150 μm with a standard deviation of ± 60 μm and a center-to-center pore distance of 1,000 μm. The depth of each channel was constant and equal to 35 μm. Additional characteristics of the micromodel are shown in Table 2-1. To provide statistical representativeness of the experiments, micromodels were built using the same pore size distribution, but using 3 different seeds to generate the radii of pore throats. This resulted in 3 different networks with the same distribution.

2.2.2 Photolithographic Process

The photolithographic technique allows etching the pattern printed on the glass plates. A diagram of the manufacturing protocol is shown in Figure 2-2, and a detailed description of the protocol is described below, which is based on that described by Oyarzún and Segura (2009).

Conditioning of glass plates: The plates (2.5 mm thickness) were immersed in a 2% detergent solution and were then submerged in a 4:1:1 solution of H_2SO_4:H_2O_2:H_2O (v/v) for 120 min. Thereafter, the plates were rinsed with distilled water and dried in an oven for 30 min at 150 ºC.

Hydrophobization: The plates were impregnated with hexamethyldisilazane (HMDS) to improve the adhesion of the photoresist polymer (Positiv 20 Komtakt Chemie, Germany). After cleaning and drying, they were placed in the impregnation oven at 75 ^{o}C and 600 mm Hg (80 kPa) for 10 min (see Figure 2-2b).

Application of photopolymer: After the plates were cooled and impregnated with HMDS, they were sprayed with the photoresist (Positiv 20 Komtakt Chemie, Germany) and were dried at 70 °C for 15 min (see Figure 2-2c).

Exposure to ultraviolet light (UV): When the photoresist was dried, the plates were lined up with the pattern (Photomask) to be transferred to the plate. The plate was placed under a UV lamp for 15 min (see Figure 2-2d).

Developing: The plates exposed to UV light were immersed in a 0.7 w/v NaOH solution. Then, the image was revealed. The plate was first rinsed with tap water and thereafter with distilled water and was dried at 150 °C for 30 min.

Etching: The plates were then immersed in a 3:2 solution of HF:H_2O (v/v) for 8 min and then rinsed with a strong jet of water (see Figs. 2-5f and 2-5g).

Fusion of the plates: After the plate was etched, it was attached to an un-etched glass plate with the same dimensions. Both plates (one over the other) were placed in a muffle furnace at 680 °C for 20 min (see Figure 2-2h).

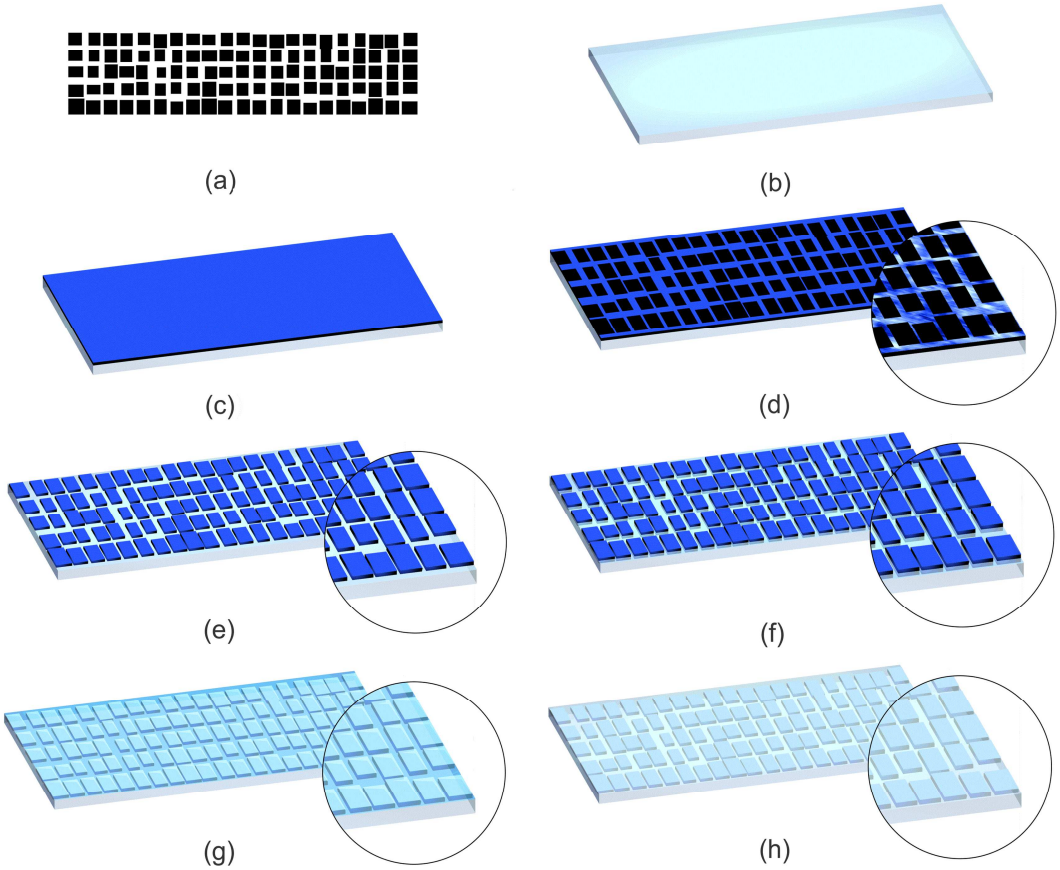

Figure 2-2: Photo-etching process diagram showing: (a) the pattern printed on a transparent film (photomask); (b) the glass plate with hydrophobic surfaces; (c) the glass surface coated with photoresist; (d) the alignment of the photomask for UV exposure; (e) the photoresist developed with NaOH; (f) the glass plate etched with hydrofluoric acid (HF); (g) the glass plate etched and clean; (h) the second glass plate fused with the etched glass plate (adapted from Oyarzún and Segura (2009)).

2.2.3 "Deep-fat frying" experiments: moist micromodels immersion in oil

In order to mimic the frying process, the micromodels were previously saturated with deionized water. All sides were closed except from the bottom one, to allow a direct contact with the oil (sunflower oil, Natura, Córdoba, Argentina). It is important to note that no leakage of water was observed when the micromodel was oriented either vertically or horizontally. The micromodel was immersed vertically, up to a depth of ≈ 5 mm, within an oil bath at 190 ± 2 ºC during 20 min until reaching a final water saturation of about 40%. Afterwards, the model was removed from the oil bath keeping the vertical position.

The system containing the heating medium was mounted on a micrometric platform, whereas the micromodel was fixed to a support. Different cameras were used to capture static images and videos of the movement of fluids within the micromodel, in micro or macro view modes. For microscopic view we used a high-resolution CCD color camera, which was used for digital image acquisition (CoolSnap Pro Color, Photometrics Roper Division, Inc., Tucson, AZ, USA) with a resolution of 1,392 × 1,040 pixels^2. The camera was mounted on a boom stand which provided easy vertical or horizontal movement, as well as a stable support for the camera at 30 cm. A partially telecentric video lens (55 mm F2.8, Edmund Optics, NJ, USA) with a 2x converter was mounted on the video camera. For macroscopic view, we used a HD video camera (Sony, Handycam DCR-SX43, China) to record videos as well as a digital camera (Sony, Cibershot DSC-HX9V, China) mounted at 25 cm.

2.2.4 Fluorescence microscopy

In order to capture the final oil distribution within the system, the micromodel was immersed in an oil bath that was previously stained with Nile Red (0.05 g/l), a heat-resistant fluorochrome (Pedreschi & Aguilera, 2002). After complete cooling, the micromodel was observed using a stereomicroscope SZX2-ILST (Olympus, Tokyo,

Japan), using the fluorescence mode. Images were acquired using a CoolSnap Pro Color digital camera, which was mounted on the microscope.

2.2.5 Drying and oil profiles determination

Images of the total area of micromodels were acquired with a digital camera (Sony Cibershot DSC-HX9, China) every 10 s. The camera was mounted at 25 cm from the micromodel. The iris and lens aperture were operated in automatic mode, without flash. The camera was grey-balanced before each imaging session and a uniform diffuse light was used to illuminate the micromodel. The images were stored in JPEG (Joint Photographic Experts Group) format using high resolution and superfine quality for further processing and analysis. The spatial resolution was approximately 15 pixels/mm. The images were processed using Image Pro-plus 4.1 software (Media Cybernetics, Silver Spring, U.S.A.). To do so, images were transformed to grey level images, which were then binarized using a grey-level threshold of 150. This procedure allowed obtaining a clear image of the water moving front and oil deposition. Saturation was defined as the percentage of total volume that was occupied by water (or oil). All volumes were calculated using image analysis, considering the depth of the capillaries (R_{ah}).

2.2.6 Determination of surface oil

The oil available for absorption into the micromodel during cooling is limited, and corresponds to the fraction that remains attached to the open side of the micromodel after the immersion. An image of the oil profile that adhered to that side was taken after 10 s. This time was chosen, since no oil was observed to drain after that period of time and because oil suction only started afterwards (this is consistent with results obtained by Bouchon and Pyle (2005b) in potato cylinders). Side-view images were taken with the CoolSnap Pro Color digital camera using a partially telecentric video lens (55 mm F2.8, Edmund Optics, NJ, USA). Images were spatially calibrated using a micro-ruler with an accuracy of 100 microns. Image Pro-plus 4.1 software was used for image processing and analysis, to determine the radius of the semicircle formed by the oil

layer over the open side of the micromodel. The volume of surface oil was calculated from: $\pi r^2 * h/2$, where r is the radio of the semicircle and h is the length of the side of the micromodel.

2.2.7 Statistical analysis

Experiments were carried out in triplicate. Data were tested by analysis of variance (ANOVA) and means separation was achieved using LSD method at 95% confidence, using Statgraphics plus 5.1 (Manugistics, Inc., Rockville, M.D., U.S.A).

2.3. Results & discussion

2.3.1. The immersion period

The micromodel saturated with deionized water was immersed about 5 mm within the oil bath as shown in Figure 2-3. The micromodel was heated and bubbling started a few seconds later (boiling point). Bubbling occurred through preferential pathways (large pores, in the range of 200 to 260 microns of radii), from which the steam outlet was vigorous. This behavior is consistent with the one observed in capillary flow (Dullien, 1992), where larger capillaries with a lower capillary pressure, offer a lower resistance for water bubbles release. In relation to bubble formation, we observed that bubbles tended to coalesce into larger ones, at a high frequency, as shown in Figure 2-4.

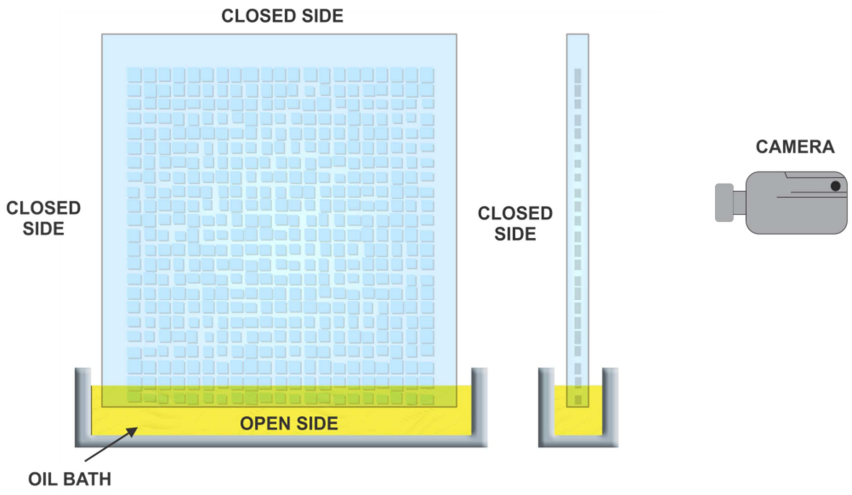

Figure 2-3: Front and side view of the experimental frying system; the camera was mounted in front of the micromodel.

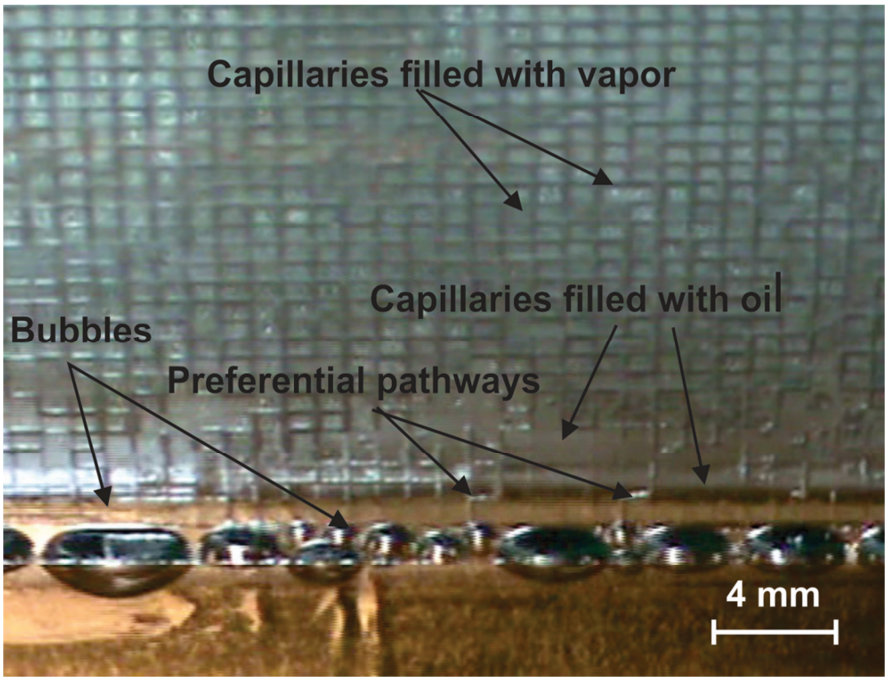

Figure 2-4: Digital image of the glass micromodel during the immersion period, showing bubbles escape, bubbles coalescence, bubbles preferential pathways and structural oil (oil fraction absorbed during the immersion period).

2.3.2. Water evaporation

Even though it was possible to observe in some way an advancing evaporation front, the macroscopic view did not show a stable displacement (see Figure 2-5). An irregular front was determined, reflecting the existence of preferential pathways. This unstable behavior could be linked to the orientation of the plate (gravity effect) and the associated capillary pressure of the different pores.

As reported by Benselama et al. (2011), the force of gravity may affect the shape of the meniscus, changing the equilibrium of capillary forces across the liquid-vapor interface. Pores with different sizes will have different capillary pressures. Since drying is a hierarchical process, larger pores, which have a lower capillary pressure, will tend to dry first. However, pores with the same size may have different capillary pressures due to differences in height (Laurindo & Prat, 1996, 1998).

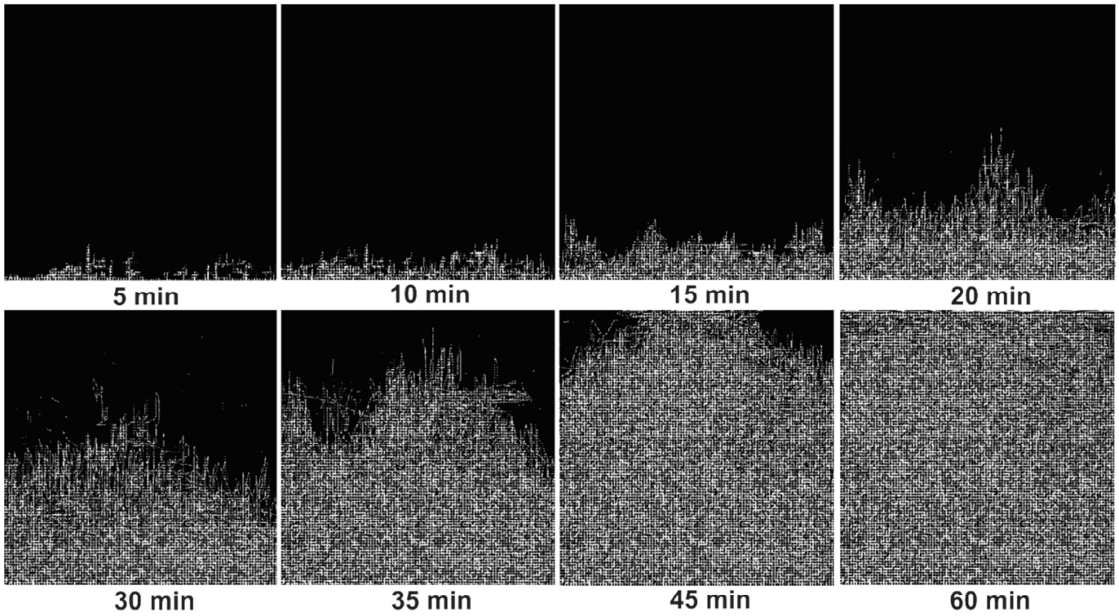

Figure 2-5: Drying front (in white) after 5, 10, 15, 25, 30, 35, 45 and 60 min of frying, on a dark background (capillaries filled with water and solid part of the matrix), after image processing.

These observations are in accordance with those determined by Laurindo and Prat (1996) who studied the effect of gravity on the drying front of a micromodel. In their study they considered 3 basic situations depending on the Bond number B (dimensionless), which is defined as:

$$\boldsymbol{B} = \frac{\Delta\boldsymbol{\rho}\cdot\boldsymbol{g}\cdot\boldsymbol{\delta}^{\mathbf{2}}\cdot\boldsymbol{sin\theta}}{\boldsymbol{\gamma}} \qquad \text{(Eq. 2-1)}$$

where δ (m) is the distance between two nodes, g (m/s^2) is the gravitational acceleration, $\Delta\rho$ = density $_{liquid}$ − density $_{gas}$ (kg/m^3), γ (N/m) is the interfacial tension (between the liquid and the gas) and θ is the angle between the micromodel and a horizontal axis (rad). In the first scenario, the micromodel was placed horizontally and the gravity force was negligible (B = 0). In the second case, the micromodel was placed vertically with the open side upwards and the gravity forces tended to stabilize the invasion process (B > 0). Finally, in the last case, the micromodel was placed with the open side downwards and the gravity force tended to destabilize the invasion process (B < 0), as in this research.

Figure 2-6 shows the drying curve of the micromodel for increasing frying times. Data were obtained after image processing and analysis. Reported results correspond to the percentage of the total volume of the micromodel filled with liquid water at time t. Overall, a traditional drying curve was obtained, with an initial linear decrease of water content through time followed by decreasing moisture lost rates.

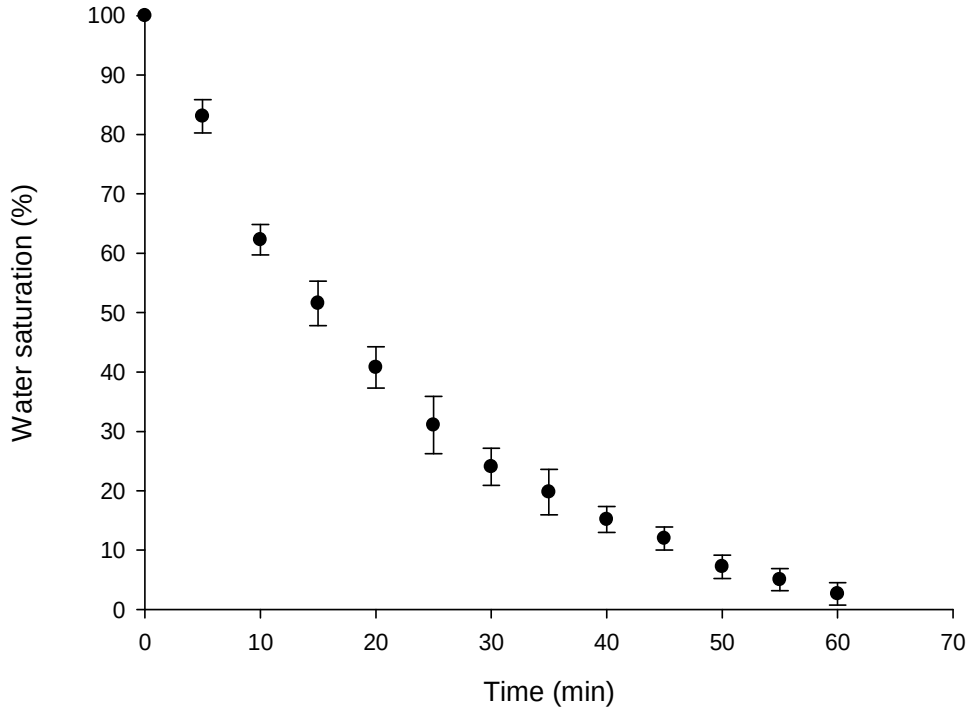

Figure 2-6: Water saturation (percentage of the total volume of the micromodel filled with liquid water) during the immersion period for increasing frying times. Points are means ± standard error (n=3).

2.3.3. Dry out and rewetting of capillaries

During the immersion period, bubbles were released at a very high frequency as in a normal frying operation. A powerful advantage of this experimental set-up was that we were able to follow in real time the fluids motion within the pore network, to assess most relevant displacement patterns during the high-speed vapor release. Overall, the vapor-liquid interface moved continuously inside the capillaries. The high-frequency release of bubbles on the open side of the micromodel produced a sudden change in pressure within the capillary that could induce different motions (see Figure 2-7). Water escape did not follow a traditional local pattern, as the one observed during normal drying, where dry capillaries do not rewet after drying. It rather followed a pattern similar to the one observed in boiling drying (Wang, Peng, & Liu, 2002), where the sudden pressure

drop in the capillary induced by the fast release of vapor, could induce liquid water displacement within it. In this study, rewetting could be produced either by the liquid water (within the micromodel) or by the oil phase (mainly from the surrounding oil at the open side). As the pressure in each node (pressure field) was continuously modified, a reconfiguration of the fluids within the micromodel could be observed in several moments and locations. Wang et al. (2002) observed a similar behavior when studying boiling drying of a bead-packed structure (porous media) using different heat fluxes (low, medium, and high). They found that in high heat fluxes a disorderly behavior in the movement of fluids occurred, where a continuous dry out and rewetting of pores was observed, as in our study.

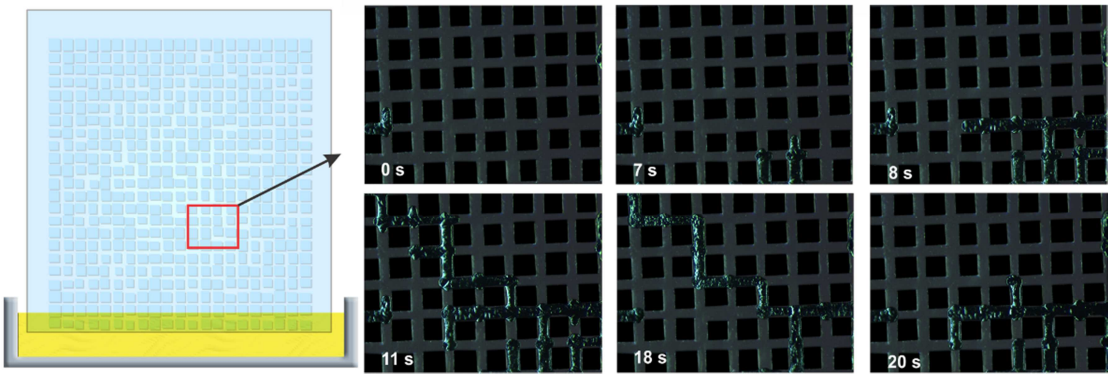

Figure 2-7: Microview of the micromodel during the immersion period. Images were taken at approximately 4 cm from the open side of the micromodel. The advancing evaporation pathways can be clearly seen and distinguished at the microscopic level (lighter capillaries).

In accordance, we observed that moisture changes could occur in a series of abrupt menisci movements within the micromodel. This movement of fluids is often referred as a “Haines jump”. In a Haines jump, either a sudden local evaporation or a pressure gradient–driven liquid flow removes liquid in single bodies or assembly of bodies and interconnecting throats (L. A. Segura & Toledo, 2005b). A Haines jump is a dynamic event, involving a complex interplay of viscous, inertia, and capillary forces in a

complex geometrical-topological environment (L. A. Segura & Toledo, 2005a). We were able to observe such phenomenon in different locations at a time.

2.3.4. Liquid water transport

In addition to the aforementioned displacements and probably due to the same nature, we observed the ejection of liquid water from the micromodel into the oil. The movement of liquid water was fostered in this case by the force of gravity. A microview of the abrupt movement and transport of liquid water into the oil can be observed in Figure 2-7, after 15 s. Although it is commonly accepted that the expansion of bubbles in the inner part of porous media induces liquid flow (Oyarzún & Segura, 2009), free water movement in void structures is still not well understood. Badillo et al. (2011), when studying vacuum impregnation, observed that when large pressure gradients are imposed on a system, the liquid–air menisci advance simultaneously by several throats of the micromodel, preferentially through larger ones. These rapid movements of fluids near an open side may cause liquid water to be expelled off the micromodel, giving rise to violent evaporation within the oil, a phenomenon known as splutter. This phenomenon has been reported by Vitrac et al. (2003) in materials with high water content, and may be observed in domestic life during frying.

2.3.5. Oil penetration during the immersion period

Oil immersion of a glass micromodel has certainly some differences from oil immersion of a food material. For instance, glass micromodels are non-hygroscopic, have a fixed structure and are 100% saturated with water. Food materials, on the other hand, are composted of several components and the porous structure develops during the process. In starchy foods for instance, a major food category, starch gelatinization affects the formation and structure of the porous media that is developed during frying, where pores may also expand or collapse during the process. But, the use of glass micromodels allows the direct observation of transport phenomena, which has not been possible to be achieved in a food system. Particularly, we were able to recognize visually all the

periods that have been identified by Farkas et al. (1996), the initial heating period, which lasted just a few seconds before bubbling started, as well as the surface boiling, falling rate and bubble-end point periods.

In relation to oil absorption, it was possible to witness that only a small fraction of oil was able to penetrate into the capillaries during the immersion period in the external layers of the micromodel, since the vigorous escape of water generated a barrier that prevented oil migration into the porous structure. This is shown in Figure 2-4 where it is possible to distinguish vapor-filled capillaries in a light whiter color from oil-filled capillaries, which had a grey intensity. Bouchon et al. (2003) coined this fraction as "structural oil" and found that it was restricted to a minimum (less than 10% of the total oil) in products with a high final water content upon frying.

2.3.6. The post-frying cooling period

After the micromodel was removed from the oil bath, the vigorous escape of steam continued for nearly 50 s. During that period of time the micromodel started to cool down and a thin layer of oil, which was attached to the bottom open-side of the micromodel, was quickly set-up.

Porous oil suction has been suggested to start once the pressure within the crust region is low enough to allow the imbibition (Bouchon and Pyle, 2005a). In our experiments, once the escape of steam stopped (after 50 s), oil-uptake began abruptly and oil movement into the pores could be clearly identified (see figure 2-8 for a microscopic view).

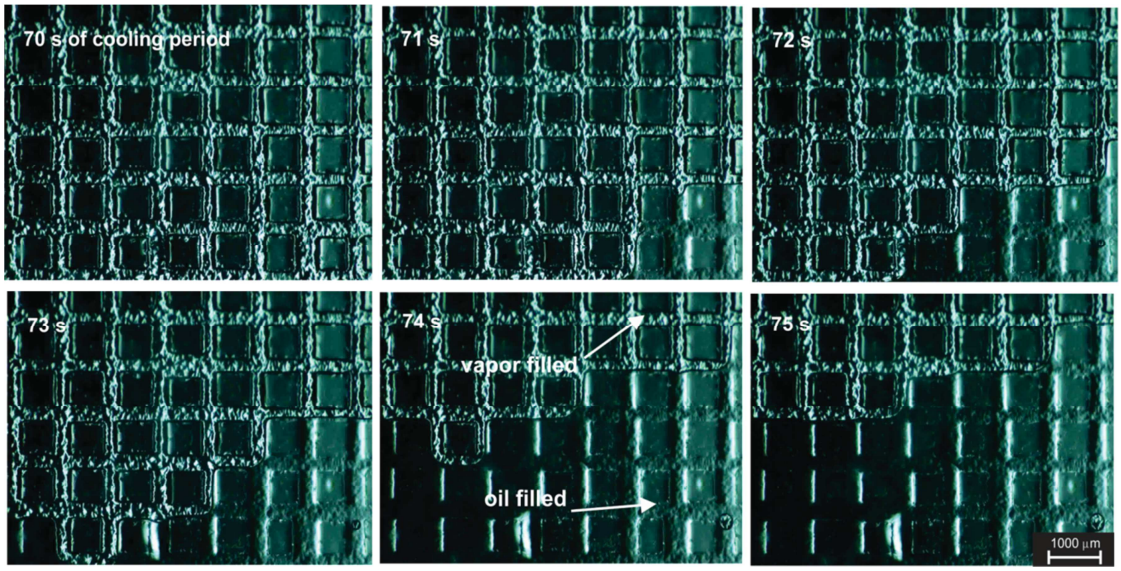

Figure 2-8: Microscopic view of the oil moving front (dark capillaries) within the empty network (lighter capillaries filled with vapor). Images were taken every 1 s at approximately 4 cm from the open side of the micromodel, starting 70 s after cooling.

As reported by Bouchon and Pyle (2005b), the time elapsed before suction starts can be on the order of several seconds, since after frying, there is still a thermal gradient that is able to provide a heat flux towards the interior for a period of time, postponing oil suction. Certainly, the size of the capillaries also plays a fundamental role, since thinner ones would induce oil suction much faster. This effect may be understood through Equation 2-2 (Bouchon and Pyle, 2005a), which is a modified form of the Washburn equation that models the oil flow through a uniform pore (perfect cylinder of radius r). In addition to capillary pressure, the total driving pressure includes a new term that represents the unbalanced atmospheric pressure due to the change of the water vapor pressure as well as the influence of gravity.

$$\Delta P^{*} = P_{atm} - P_{pore} = P_{atm} - \left(P_{V} - \frac{2\sigma\cos\phi}{r} \pm \rho\, g\, h \cos\alpha \right) \qquad \text{(Eq. 2-2)}$$

Where ΔP^* is the piezometric pressure difference (Pa), P_V is the water-vapor pressure (Pa), σ is the oil surface tension ($N.m^{-1}$), ϕ is the contact angle (rad), r is the pore radius (m), ρ is the oil density ($kg.m^{-3}$), g is the acceleration due to gravity ($m.s^{-2}$), h is the oil penetration distance (m) and α is the angle between the capillary and a vertical axis (rad). To allow oil infiltration the pressure driving force has to be positive, that is (since h=0 at the beginning):

$$P_{atm} - P_V + \frac{2\sigma\cos\theta}{r} > 0 \qquad \Leftrightarrow \qquad P_V < P_{atm} + \frac{2\sigma\cos\theta}{r} \qquad \text{(Eq. 2-3)}$$

In this system, since capillaries had a pore-throat radius of 150 µm ± 60 µm, the cooling effect should prevail over the capillary effect, since $2\sigma\cos\theta/r$ is much lower than P_{atm} and P_V. This fact allows explaining the delay in oil absorption, as well as the fast oil uptake, which only occurs once the vapour pressure is low enough to allow oil imbibition, after some cooling.

2.3.7. Oil absorption kinetics

Figure 2-9 shows the oil advancing front during post-frying cooling, after an immersion period of 20 min. The initial image (just upon removing the micromodel from the oil bath) shows an initial amount of oil, which largely corresponds to the amount of oil that was able to penetrate within the micromodel during the immersion period. Oil uptake started after approximately 50 s; images show the advancing front after 70, 80 and 90 s of cooling. As in the period of immersion, the force of gravity affects the movement of the moving front. In this case the force of gravity seems to stabilize the advancing front of the oil, which develops in a stable manner. At pore-level the configuration used herein (upward configuration) tends to restrict the capillary penetration, as explained by Bouchon and Pyle (2005a).

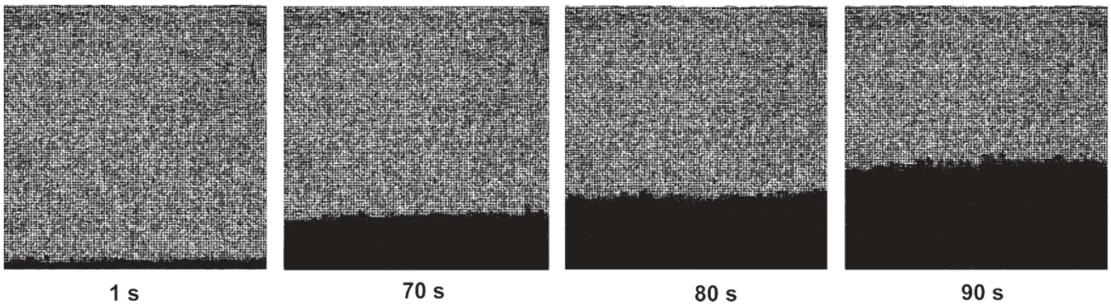

Figure 2-9: Oil moving front during cooling (after 1 s and up to 90 s upon cooling), after an immersion period of 20 min.

The oil uptake kinetics showed a rather linear increase (Figure 2-10), which started after 50 s of cooling and lasted for around 30 s. In addition, the graph shows the amount of oil that was able to get into the structure during the immersion period (structural oil).

The amount of oil that is available to be absorbed by the micromodel is limited to the oil fraction that remains attached to the micromodel after removal from the oil bath, which was determined to be 8.687 x 10^{-7} m^3. The end of oil uptake was defined by the moment when air penetrated, and the pressure field was balanced. This occurred as soon as the oil film lost its continuity, allowing the air to quickly fill the empty spaces within the network. Since the oil layer that was attached to the open side was much larger (thickness of the glasses, 5 mm) than the capillaries that led to that open side (microns), the amount of oil that remained on the surface was much larger (97%; 8.412 x 10^{-7} m^3) than the fraction that was able to penetrate within the structure during cooling (3%; 2.756 x 10^{-8} m^3). Thus, oil absorption stopped due to air penetration, despite the fact that there still was a big amount of oil on the surface.

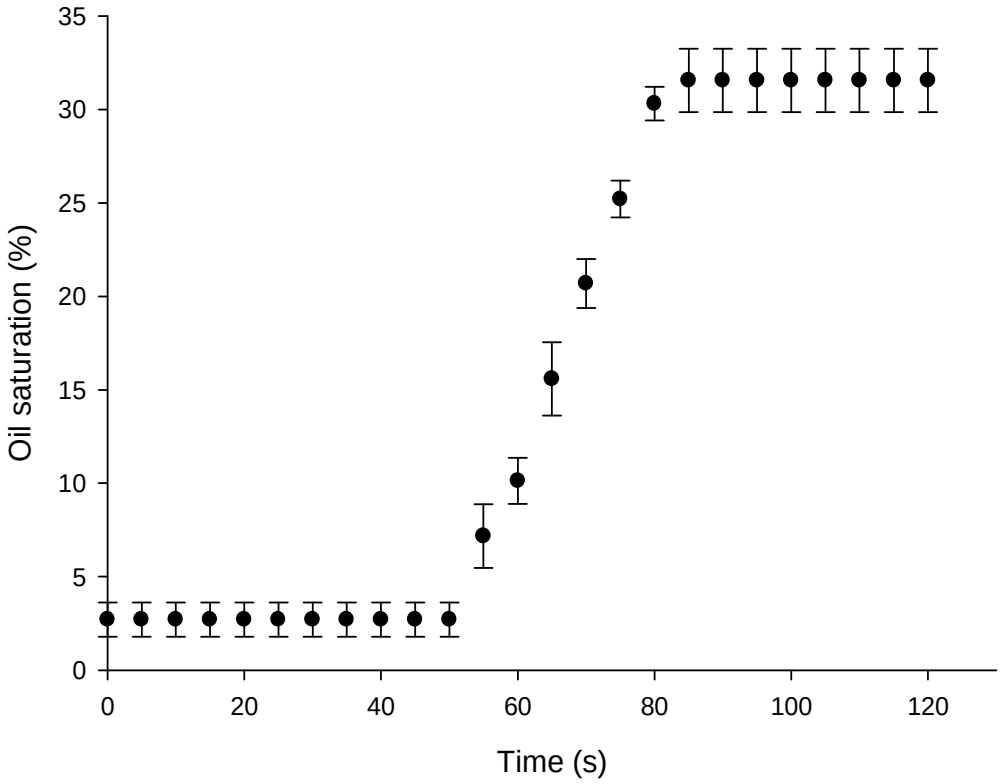

Figure 10: Oil uptake (percentage of the total volume of the micromodel filled with oil) during cooling after an immersion period of 20 min. Points are means ± standard error (n=3).

Figure 2-8 shows how the oil advancing front quickly stops when the air gets into the structure, despite the fact that there is still a fair amount of empty space available within the micromodel. As a matter of fact, when the micromodel was submerged in oil under similar conditions, but was allowed to cool down within the oil bath (unlimited amount of oil without air interference), about 95% of the available space was impregnated with oil, in micromodels that were dehydrated up to a final content of 15% (final water saturation).

2.3.8. Oil location

The images obtained by fluorescence microscopy allowed a clear distinction of the oil (in red) within the micromodel (see Figure 2-11). The figure was built-up using the images captured on microview mode, which were then pasted together (with a 1-mm gap) to get a continuous section up to the central part of the micromodel. This allowed assessing the oil distribution from the open side of the micromodel (bottom of the image) up to the center of the micromodel (top of the image).

After oil immersion and cooling, the pores that were closer to the open side incorporated a vast amount of air (black capillaries surrounded by a thin oil film), whereas the inner ones were mostly filled with oil (red capillaries). At a deeper distance, it was possible to distinguish additional capillaries filled with air as well as pores filled with oil (D), possibly due to the penetration of air through preferential paths. At a furthest distance (E), a thin oil film surrounding the inner wall of the capillaries could be seen, suggesting a film flow transport into the structure (E). Similar observations have been made in studies with micromodels in petroleum science (Ryazanov, van Dijke, & Sorbie, 2009), where an oil film was observed to move on top of a film layer of water that wetted the capillary walls, due to gas injection. In our case, it could be hypothesized an analogous phenomenon, where oil would move on top of a condensed liquid water layer, driven by the air flow during cooling. Laurindo and Prat (1998) demonstrated the existence of film flow during drying, through direct observation using a micromodel. Future work is needed to understand the importance of such mechanism during frying.

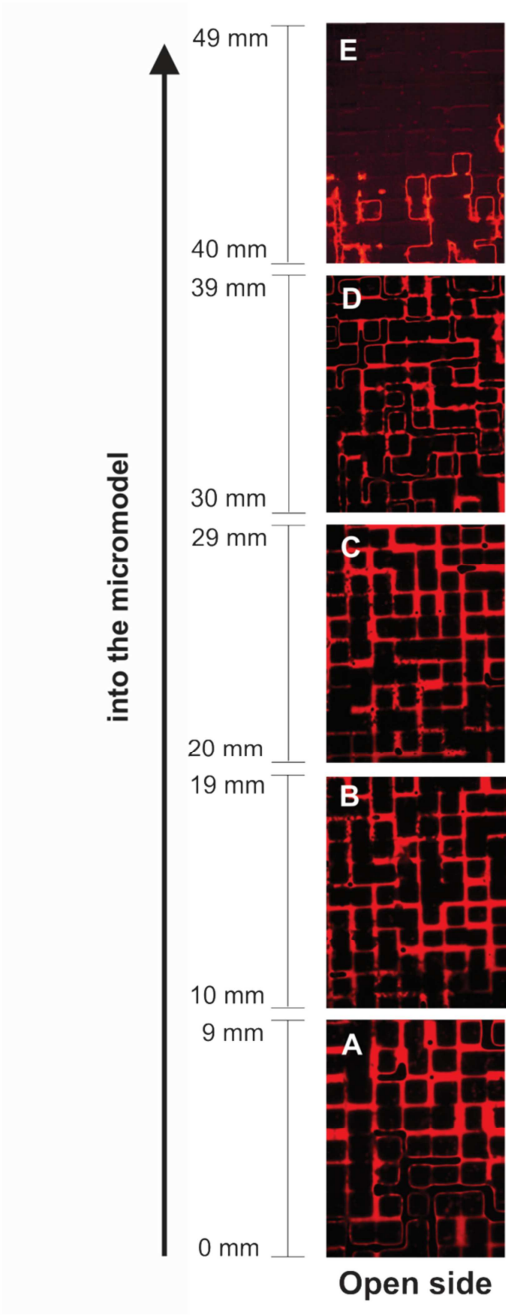

Figure 2-10: Fluorescent microscopy showing the oil distribution (in red) from the bottom of the micromodel (open side, A) up to the central region (E). Images were collected and pasted together with a 1-mm gap to get an overall idea of the oil distribution.

2.4. Conclusions

We were able to successfully develop an experimental set-up that allowed us observing most important transport phenomena occurring during oil immersion within a micromodel. A powerful advantage of this experimental procedure was that it allowed following in real time the fluids motion within the pore network, to get some visual evidence of most relevant displacement patterns during the high-speed vapor release. In addition, we were able to visualize the meniscus motion mechanisms of oil inhibition within the micromodel, together with the use of fluorescence microscopy.

During the immersion period, bubbles were released at a very high frequency as in a normal frying operation, thus, we confirmed that only a small fraction of oil was able to penetrate within the capillaries during that interval. Once the escape of steam stopped, after some initial cooling, oil-uptake began abruptly and oil movement into the pores could be clearly identified. The end of oil uptake was defined by the moment when air penetrated, as soon as the oil film lost its continuity.

Overall, this experimental approach can give us important clues about most relevant transport phenomena occurring during the frying process of a thick product with high water content. It also allows getting some experimental evidence that may be used to test some hypotheses in relation to water loss and oil uptake during post-frying cooling.

Overall, the former technique illustrates how glass micromodels may be used to visualize and provide valuable information to understand key transport phenomena during processing, an approach that may well be used to characterize and understand additional unit operations in other domains.

2.5. References

Badillo, G.M., Segura, L.A., Laurindo, J.B., (2011). Theoretical and experimental aspects of vacuum impregnation of porous media using transparent etched networks. International Journal of Multiphase Flow 37(9), 1219-1226.

Benselama, A.M., Harmand, S., Sefiane, K., (2011). Equilibrium profile of extended isothermal meniscus with gravity inclination effect. Colloids and Surfaces a: Physicochemical and Engineering Aspects 391(1-3), 158-169.

Bouchon, P., Aguilera, J.A., (2001). Microstructural analysis of frying potatoes. International Journal of Food Science and Technology 36(6), 669-676.

Bouchon, P., Aguilera, J.M., Pyle, D.L., (2003). Structure oil-absorption relationships during deep-fat frying. Journal of Food Science 68(9), 2711-2716.

Bouchon, P., Pyle, D.L., (2004). Studying oil absorption in restructured potato chips. Journal of Food Science 69(3), E115-E122.

Bouchon, P., Pyle, D.L., (2005a). Modelling Oil Absorption During Post-Frying Cooling: I: Model Development. Food and Bioproducts Processing 83(4), 253-260.

Bouchon, P., Pyle, D.L., (2005b). Modelling Oil Absorption During Post-Frying Cooling: II: Solution of the Mathematical Model, Model Testing and Simulations. Food and Bioproducts Processing 83(4), 261-272.

Buckley, J.S., (1991). Multiphase displacements in micromodels, in: Morrow, N.R. (Ed.), *Interfacial phenomena in petroleum recovery*. Marcel Dekker Inc., New York, pp. 157-189.

Dullien, F.A.L., (1992). Capillarity in porous media, *Porous media: fluid transport and pore structure*. Academic press San Diego, San Diego, USA.

Farkas, B.E., Singh, R.P., Rumsey, T.R., (1996). Modeling heat and mass transfer in immersion frying .1. Model development. Journal of Food Engineering 29(2), 211-226.

Karathanos, V.T., Kanellopoulos, N.K., Belessiotis, V.G., (1996). Development of porous structure during air drying of agricultural plant products. Journal of Food Engineering 29(2), 167-183.

Laurindo, J.B., Prat, M., (1996). Numerical and experimental network study of evaporation in capillary porous media. Phase distributions. Chemical Engineering Science 51(23), 5171-5185.

Laurindo, J.B., Prat, M., (1998). Numerical and experimental network study of evaporation in capillary porous media. Drying rates. Chemical Engineering Science 53(12), 2257-2269.

Mellema, M., (2003). Mechanism and reduction of fat uptake in deep-fat fried foods. Trends in Food Science & Technology 14(9), 364-373.

Moreira, R.G., Barrufet, M.A., (1998). A new approach to describe oil absorption in fried foods: a simulation study. Journal of Food Engineering 35(1), 1-22.

Moreira, R.G., Sun, X.Z., Chen, Y.H., (1997). Factors affecting oil uptake in tortilla chips in deep-fat frying. Journal of Food Engineering 31(4), 485-498.

Moreno, M.C., Brown, C.A., Bouchon, P., (2010). Effect of food surface roughness on oil uptake by deep-fat fried products. Journal of Food Engineering 101(2), 179-186.

Oyarzun, C.A., Segura, L.A., (2009). Design and Construction of Glass Micromodels for the Study of Moisture Transport in Softwoods. Drying Technology 27(1), 14-29.

Pedreschi, F., Aguilera, J.M., (2002). Some changes in potato chips during frying observed by confocal laser scanning microscopy (CLSM). Food Science and Technology International 8(4), 197-201.

Prat, M., (1993). Percolation model of drying under isothermal conditions in porous media. International Journal of Multiphase Flow 19(4), 691-704.

Ryazanov, A., van Dijke, M.I.J., Sorbie, K.S., (2009). Two-Phase Pore-Network Modelling: Existence of Oil Layers During Water Invasion. Transport in Porous Media 80(1), 79-99.

SanMartin, F.A., Laurindo, J.B., Segura, L.A., (2011). Pore-Scale Simulation of Drying of a Porous Media Saturated with a Sucrose Solution. Drying Technology 29(8), 873-887.

Segura, L.A., Oyarzún, C.A., (2012). Experimental evidence of mass transfer mechanisms during freeze-drying in a capillary porous medium. International Journal of Refrigeration 35(8), 2102-2109.

Segura, L.A., Toledo, P.G., (2005a). Pore-level modeling of isothermal drying of pore networks - Effects of gravity and pore shape and size distributions on saturation and transport parameters. Chemical Engineering Journal 111(2-3), 237-252.

Segura, L.A., Toledo, P.G., (2005b). Pore-level modeling of isothermal drying of pore networks. Evaporation and viscous flow. Latin American Applied Research 35(1), 43-50.

Ufheil, G., Escher, F., (1996). Dynamics of oil uptake during deep-fat frying of potato slices. Food Science and Technology-Lebensmittel-Wissenschaft & Technologie 29(7), 640-644.

Vitrac, O., Dufour, D., Trystram, G., Raoult-Wack, A.-L., (2002). Characterization of heat and mass transfer during deep-fat frying and its effect on cassava chip quality. Journal of Food Engineering 53(2), 161-176.

Vitrac, O., Trystram, G., Raoult-Wack, A.L., (2000). Deep-fat frying of food: heat and mass transfer, transformations and reactions inside the frying material. European Journal of Lipid Science and Technology 102(8-9), 529-538.

Wang, Z., Peng, X.F., Liu, T., (2002). Visualization of boiling phenomena in a bead-packed structure. Experimental Heat Transfer 15(3), 177-189.

Ziaiifar, A.M., Achir, N., Courtois, F., Trezzani, I., Trystram, G., (2008). Review of mechanisms, conditions, and factors involved in the oil uptake phenomenon during the deep-fat frying process. International Journal of Food Science and Technology 43(8), 1410-1423.

3. THE EFFECT OF GRAVITY ON MOISTURE LOSS AND OIL ABSORPTION PROFILES DURING A SIMULATED FRYING PROCESS USING GLASS MICROMODELS

Abstract:

New trends in nutrition have driven the development of research on fried products with lower oil content, thus, great efforts have been made to elucidate the mechanisms responsible for oil absorption. This understanding can be certainly improved through direct visual observation. Accordingly, the goal of this study was to analyze transport phenomena that develop during oil immersion by using glass micromodels submerged in oil (190 ºC), to visualize the mechanisms responsible for water evaporation and oil absorption within a matrix, as well as the effect of gravity using three different configurations (g=0, g<0, g>0). Moisture and oil profiles were imaged during the frying process in order to obtain water and oil saturation maps. Drying curves were constructed using image analysis, and fractal analysis was performed to describe the morphology of the evaporation and oil fronts. If g<0 (open side of the micromodel at the bottom) drying times were shorter and gravity tended to destabilize the drying front, which had a mean fractal dimension of 1.818±0.032 that was significantly higher than those obtained in other set-ups. Largely, evaporation fronts tended to take the form of temperature profiles as reflected by infrared thermal imaging. The morphology of the advancing oil fronts was similar in all configurations. However, g severely affected oil content. When g=0, less oil was absorbed with a final oil saturation of 32%. Overall, these results and approach may help scientists to describe the physical mechanisms that develop during oil immersion and may aid food manufacture to develop fried foods with lower oil content.

.

Keyword: *micromodel; frying; oil uptake; pore network; square capillaries.*

3.1. Introduction

Over the past 20 years, several of the heat and mass transfer phenomena occurring during or immediately after deep frying have been described. Different contributions have suggested that oil does not penetrate the food product while there is an overpressure inside (Dana & Saguy, 2006; Farinu & Baik, 2005; Mellema, 2003). Thus, oil would be mostly absorbed during cooling, since the vigorous escape of water vapor would preclude oil absorption during most of the immersion period, as was indirectly determined by Bouchon et al. (2003). Accordingly, the pressure drop generated during cooling has been suggested as one of the main driving forces to control oil absorption (Bouchon & Pyle, 2005a; Mellema, 2003; Ziaiifar et al., 2008), although some authors have mainly related it to capillary pressure (R. G. Moreira & Barrufet, 1998). Bouchon and Pyle (2005a) considered both effects, developing a modified form of the Washburn equation, which in addition to capillary pressure, included a new term that represented the unbalanced atmospheric pressure due to the change of the water vapor pressure during cooling, as well as the influence of gravity.

So far, all of the models described have been developed from a macroscopic viewpoint and many authors have used diagrams with an ideal pore to explain the oil absorption phenomenon (Mellema, 2003). Reality is more complex because the pores are interconnected in a food matrix and present different states. Pores can be filled or partly filled with water, air, vapor or oil, and their evolution will depend on the condition of their neighboring pores. The evolution of pressure and temperature fields also influence whether the pores dry or fill with air, water, or oil.

The pore network approaches have several advantages over the continuum approach (*e.g.* diffusion model) in which the microscopic complexities are lumped (*e.g.* effective diffusivities), which mostly are empirical constants (Gueven & Hicsasmaz, 2013). Experimentally, they include the use of micromodels, which are transparent networks of pores and constrictions that simulate the complexity of a porous media nature (Oyarzún

& Segura, 2009). The applications of micromodels are varied (Badillo et al., 2011; Laurindo & Prat, 1998; SanMartin et al., 2011; L. A. Segura & Oyarzún, 2012; L. A. Segura & Toledo, 2005b) and are increasing, since they allow us to see the movement of the fluid interface and to distinguish between mechanisms that have similar behavior with respect to other phenomena.

Lenormand et al. (1988) conducted extensive work through pore network simulations and experiments with transparent micromodels in order to show the different displacement drain type mechanisms (a wetting fluid displaces a non-wetting) of two immiscible fluids according to the capillary number (C) and the viscosity ratio (M). C is a dimensionless number that is a ratio between the viscous forces and capillary forces. In porous media for low capillary numbers, flow is dominated by capillary forces whereas for high capillary number the capillary forces are negligible compared to viscous ones, as shown in Equation 3-1:

$$\boldsymbol{C = \frac{q \cdot \mu_w}{A \cdot \gamma \cdot \cos \varphi}} \qquad \text{(Eq. 3-1)}$$

where the numerator is the displacing fluid flow q (m^3/s) times the viscosity of the wetting fluid μ (kg/(m.s)) and the denominator is the flow cross-sectional area A (m^2) times the interfacial tension of the wetting fluid γ (N/m) and the cos of contact angle φ (for water/glass ~ °0). M is the ratio between the viscosity of the non-wetting fluid (in the case of the immersion period, it is the vapor) and the viscosity of the wetting fluid (water), as defined in Equation 3-2:

$$\boldsymbol{M = \frac{\mu_{nw}}{\mu_w}} \qquad \text{(Eq. 3-2)}$$

Lenormand and Zarcone (1989) and Lenormand et al. (1988) developed a model that can reproduce flow transitions from capillary forces-dominated to viscous forces-dominated. These authors established the existence of a "phase diagram" for the displacement of two immiscible phases that is reproduced in Figure 3-1, based on the capillary number (C) and the viscosity ratio (M), which define the existing flow patterns and regions.

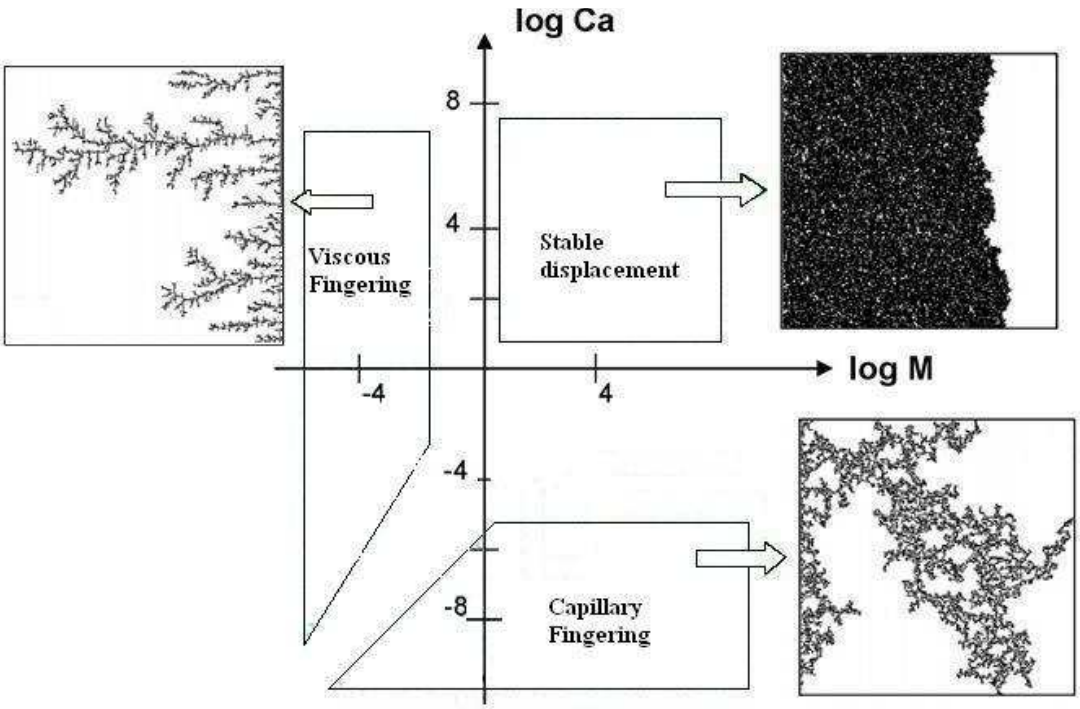

Figure 3-1: Phase diagram proposed by Lenormand (1988), for drainage showing the different areas and types of profile found, adapted from Badillo et al. (2011).

In addition, the flow in a porous medium may be affected by additional factors including the direction in which this flow occurs in relation to the force of gravity. Laurindo and Prat (1996) studied the effect of gravity on the drying front of a micromodel. They considered three basic situations depending on the Bond number B, which is defined as:

$$\boldsymbol{B = \Delta\rho \cdot g a^2 \cdot \sin\theta / \gamma} \quad \text{(Eq. 3-3)}$$

where **α** (m) is the distance between two nodes of the network, **g** (m/s^2) is the gravity vector intensity, $\boldsymbol{\Delta\rho = \rho_{liquid} - \rho_{gas}}$ (kg/m^3), θ is the angle between the open side of the micromodel and the horizontal plane (rad), and **γ** (N/m) is the interfacial tension between wetting fluid and non-wetting. The first case is the one where the micromodel was placed horizontally and the gravity forces are negligible, *i.e.* B = 0. The second case

is where the micromodel was placed vertically with the open side up. Here the force of gravity tended to stabilize the invasion process, *i.e.* B > 0. In the third case, the micromodel was placed with the open side down and the force of gravity tended to destabilize the invasion process, *i.e.* B < 0.

As previously stated, understanding transport phenomena during/after frying is of importance because it forms the basis of the development of predictive models, which save time and cost, and allow revealing most important mechanisms. This understanding can certainly be reinforced through direct visual observation. In accordance, the aim of this study was to obtain evidence of the transport phenomena that occur during oil immersion and to study the effect of gravity on the dynamics of water evaporation and oil uptake using glass micromodels.

3.2. Materials and methods

Micromodels (2D transparent porous media) were manufactured using a photolithographic technique using the protocol described by Oyarzún and Segura (2009). The size of micromodels was (15 x 15 cm^2) and contained 100x100 pores (nodes), which were built using statistical data on the microstructure of potatoes (Karathanos et al., 1996), as explained in Cortés et al. (2014). The pore-throat (bonds) radius was a random variable which followed a log-normal distribution with a mean size of 150 μm, a standard deviation of 60 μm and a center-to-center pore distance of 1,000 μm. Each channel had an approximately constant depth of 35 μm.

3.2.1 Photolithographic manufacturing process

A diagram of the manufacturing protocol is shown in Figure 3-2. A detailed description of the protocol, based on that described by Oyarzún and Segura (2009), is provided below. *Conditioning of glass plates:* The plates (2.5 mm thickness) were buffed with sandpaper to remove sharp edges. Next, the plates were immersed in a 2% detergent

solution. They were then submerged in a 4:1:1 solution of H_2SO_4:H_2O_2:H_2O (v/v) for 120 min. Next, they were rinsed with distilled water and dried in an oven for 30 min at 150 ºC.

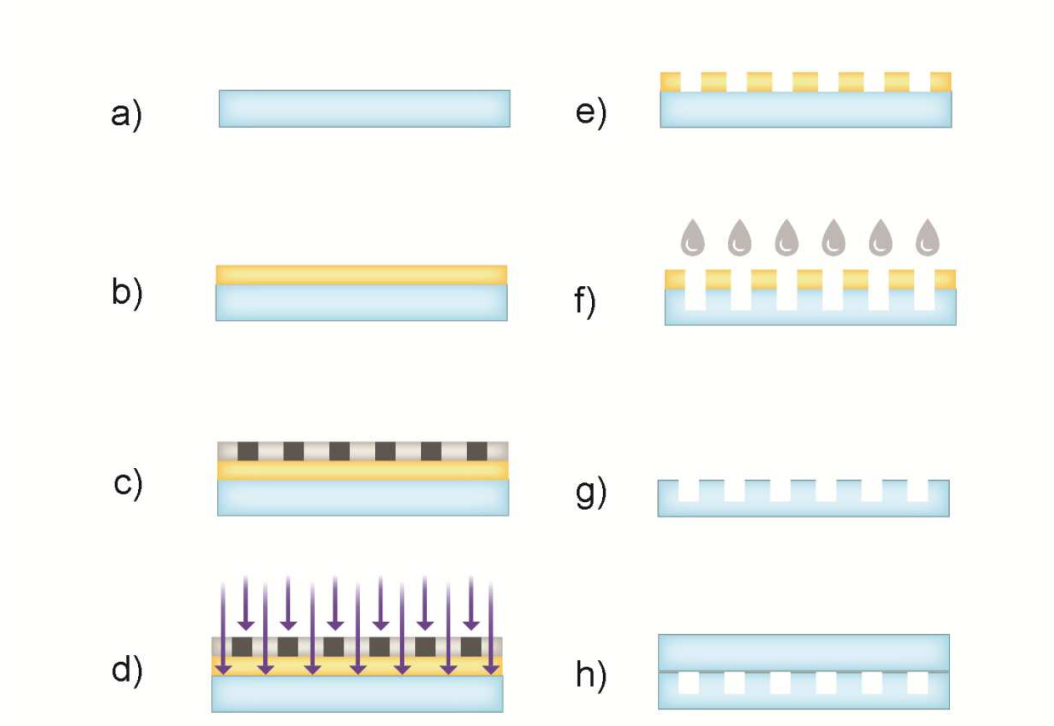

Figure 3-2: Photo-etching process diagram showing: (a) the glass plate with hydrophobic surfaces; (b) the glass surface coated with photoresist; (c and d) the alignment of the photomask for UV exposure; (e) the photoresist developed with NaOH; (f) the glass plate etched with hydrofluoric acid (HF); (g) the glass plate etched and clean; (h) the second glass plate fused with the etched glass plate (adapted from Oyarzún and Segura (2009)).

Hydrophobization: The plates were impregnated with hexamethyldisilazane (HMDS) in order to improve the adhesion of the photoresist polymer (Positiv 20 Komtakt Chemie, Germany). Using a controlled temperature of 75°C, the cleaned and dried plates were placed in the impregnation oven and vacuum was applied up to a pressure of 600 mm Hg (80 kPa). After 10 min of soaking, the vent valve was opened. The plates were placed in a container with silica gel for cooling (see Figure 3-2a).

Application of photopolymer: After the plates were cooled and impregnated with HMDS, they were sprayed with the photoresist (Positiv 20 Komtakt Chemie, Germany). Plates with a uniform photoresist film and which were free of defects and particles were dried at 70°C for 15 min (see Figure 3-2b).

Exposure to ultraviolet light (UV): When the photoresist had dried, the plates were lined up with the pattern (Photomask) to be transferred onto the plate. Each plate was placed under a UV lamp, which was inside a black box impervious to light. The aligned plate-pattern was placed under the lamp at 20 cm, the box was closed and the UV light was turned on for 15 min (see Figure 3-2c and 3-2d).

Developing: The plates exposed immersed in a 0.7 w/v NaOH solution and the image was revealed. The plate was first rinsed with tap water and then distilled water. The developed and rinsed plate with the pattern was then dried at 150 °C for 30 min.

Etching: After drying, the plates were immersed in a 3:2 solution of $HF:H_2O$ (v/v) for 8 min. The etched plates were rinsed with a strong jet of water and vigorously brushed to remove the remaining photoresist and deposits that were formed during the reaction (see Figs. 3-2f and 3-2g).

Fusion of the plates: After the plate was etched, it was attached to a plain glass plate of the same size that had been cleaned according to the protocol. Both plates (one over the other) were placed in a muffle furnace at 680°C for 20 min (see Figure 3-2h).

3.2.2 Experimental setup of the frying system

In order to mimic the frying process and place the micromodel in different positions with respect to gravity, an acrylic glass device was built (see Figure 3-3). This device has two main areas. The first is a receptacle containing oil (sunflower oil, Natura, Córdoba, Argentina). The second area is isolated by rubber sealing (temperature proof).

The micromodel is held by the upper and lower edges in the chamber using rubber insulators.

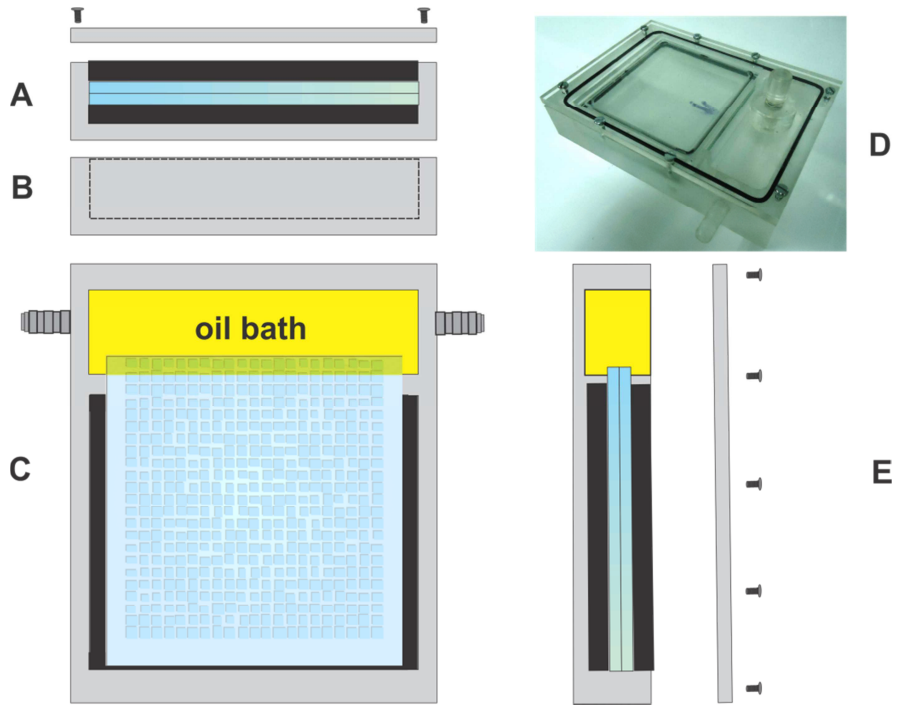

Figure 3-3: The front and side view of experimental frying system, the camera was mounted in front of the micromodel. (A) internal view of oil receptacle, (B) external view of oil receptacle, (C) top view of device, (D) full view of device, (E) side view of device.

The micromodel does not have contact with the acrylic. The whole system has a 4 mm acrylic lid which is attached to the rest of the device, sealing it completely. Figures 3-3A and 3-3B show a front view of the device from the outside and the oil inside the receptacle. The micromodel appears to be located between two layers of rubber sealant. Figure 3-3C presents a top view of the device that allows the viewer to identify the two different areas and see how the micromodel is placed inside this. Figure 3-3D presents a picture of the entire device. Figure 3-3E presents a side view of the device.

3.2.3 Frying experiments

First, the micromodels were saturated with deionized water by immersing the micromodel in water and submitting it to vacuum. After the vacuum was broken, it reached a water saturation of 100%. The micromodels have three closed sides and one open. The open side allows for direct contact with the oil while immersing the micromodels in a ≈5 mm-depth oil bath that was maintained at 190ºC (first receptacle). The receptacle has an inlet and outlet connected to a thermo-regulated electric fryer at 190°C (Somela, Model DF535T, Santiago, Chile) through a peristaltic pump (Masterflex model LS 7521, Illinois, USA), ensuring complete filling of the oil receptacle inside of the acrylic device.

The acrylic fryer device with the micromodel mounted inside of it was placed in three different positions as seen in Figure 3-4. Different types of cameras were used to capture static images and videos of the movement of fluids within the micromodel during immersion and cooling in micro and macro view modes. At the end of the immersion period, the receptacle of the acrylic device that contained the oil was quickly emptied, and the oil available for absorption was only attached to the open side of the micromodel. Also, a valve on the acrylic device opened in order to leave the oil receptacle open to the environment. The same position was used during the immersion and the cooling periods.

Depending on the purpose of the image and required resolution, the acrylic device was backlit using D65 lamps with built-in light diffusers. Lamps were placed at an angle of 45° with the aim of standardizing the light incident on the micromodel, and this is a key to image quality and proper processing.

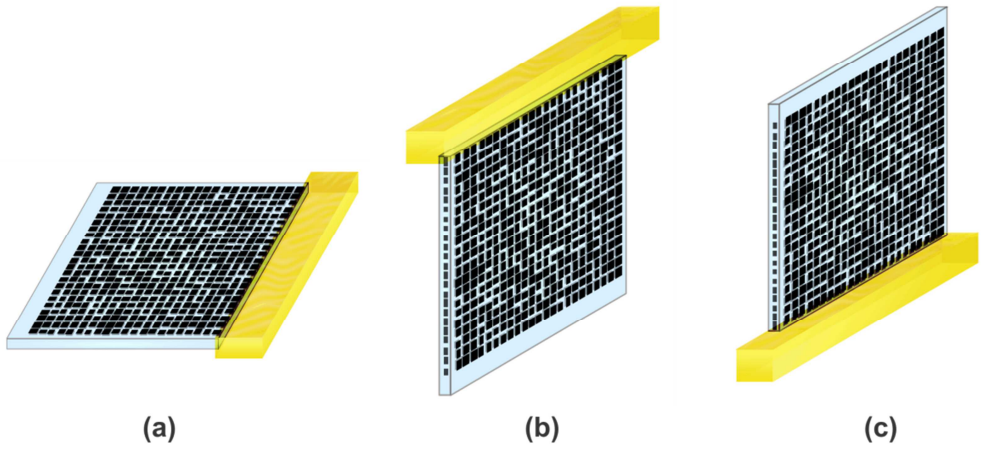

Figure 3-4: Scheme of the three basic configurations of the micromodels used in oil immersion experiments showing the 3 configurations under study (g=0, g<0, g>0).

We used a high-resolution CCD color camera (CoolSnap Pro Color, Photometrics Roper Division, Inc., Tucson, AZ, USA) with a resolution of 1,392 × 1,040 pixels to capture the image of the microscopic view. The camera was mounted on a boom stand which provided easy vertical or horizontal movement and stable support for the camera. A partially telocentric video lens (55 mm F2.8, Edmund Optics, NJ, USA) with a 2x converter was mounted on the video camera. For macroscopic view, an HD video camera (Sony, Handycam DCR-SX43, China) was used to obtain video and a digital camera with 16.2 megapixels (Sony, Cybershot DSC-HX9V, China) was used for stills.

3.2.4 Evaporation and oil profiles determination

Images of total area of micromodels were acquired using a digital camera (Sony Cybershot DSC-HX9, China) every 60 seconds. The camera was mounted at 5 cm of micromodels. The iris and lens aperture were operated in automatic mode, no flash. The camera was gray-balanced before each imaging session and uniform diffuse lighting was used to illuminate the micromodels. The images were stored in JPEG (Joint Photographic Experts Group) format at high resolution and superfine quality for further processing and analysis. The spatial resolution was approximately 15 pixel/mm of the

micromodels surface. The images were processed using Image Pro-plus 4.1 software (Media Cybernetics, Silver Spring, USA). These were converted into grey level images and then binarized with a threshold of 150 units of grey level. Images of a moving front were obtained to calculate profiles of moisture and oil inside of the micromodels during the frying process and ascertain the shape of the drying and oil fronts as well as the moisture loss and oil uptake kinetics.

The saturation of micromodels with water and oil was calculated as the percentage of empty volume of the micromodel occupied by water or oil separately. The empty volume was calculated using the area of the empty capillaries measured by image analysis and depth of the capillary (35 µm) by scanning electron microscopy SEM (Jeol JSM 25SII, Tokio, Japan). The volume occupied by water and oil was calculated by multiplying the occupied micromodel area and the depth of the capillary.

3.2.5 Fractal analysis of evaporation and oil profiles

Fractal geometry has the ability to describe irregular objects that traditional Euclidean geometry fails to analyze (Xu, Mujumdar, & Yu, 2008). Thus, we used the fractal dimension (D_F) to differentiate, quantify and classify the drying or oil advance patterns. Mathematically, D_F is defined as:

$$D_F = 1 - \frac{\log(F)}{\log(L)} \quad \text{(Eq. 3-4)}$$

where F is the total extent of the pattern under consideration and L is the metric (or length scale) on which it is measured. For a given pattern of invasive phase (vapor or oil) within the micromodel, the fractal dimension is expected to lie in the range of $1 < D_F < 2$. In order to determine D_F numerically, a plug-in of fractal analysis (FRACLAC, version 2.5) for Image J version 1.47 (image analysis software) was used (Wayne Rasband, National Institute of Health, USA). D_F was calculated in triplicate for three different water saturations (Sw: 0.87, 0.50, 0.10) in all configurations studied with

respect to gravity, and two different oil saturations (So: 0.15, 0.25) in all configurations during the cooling period. The FRACLAC plug-in requires an initial configuration in which the most relevant parameter is the number of grids used to determine D_F. It was four in all images, so the software calculates 4 slopes per image and an average value of the four calculations.

3.2.6 Temperature profiles

Temperature profiles were obtained using an infrared camera model 760 (Inframetrics, Waltham, USA). Images were also taken with a digital camera (Sony Cybershot DSC-HX9, China) to compare the temperature profiles to the evaporation profiles.

3.2.7 Phase diagrams

The capillary number (C) was calculated for the immersion and cooling periods using Equation 3-1. Equation 3-2 was used to calculate the viscosity ratio (M). The fluid properties listed on Table 3-1 were used and the displaced fluid flows were calculated using image analysis from saturation maps for both processes.

Table 3-1: Fluids properties at atmospheric pressure (Perry, Green, & Maloney, 2008)

Description	Temperature K	Symbol	Value	Units
Water viscosity	373.15	μ	0.282×10^{-3}	kg/m s
Vapor viscosity	373.15	μ	1.227×10^{-5}	kg/m s
Vapor viscosity	463.15	μ	1.537×10^{-5}	kg/m s
Oil viscosity	463.15	μ	0.0257	kg/m s
Water surface tension	373.15	γ	0.0859	N/m
Water density	373.15	φ	958.4	kg/m^3
Oil surface tension	463.15	γ	0,0354	N/m

3.2.8 Statistical analysis

Experimental data were tested by analysis of variance (ANOVA) and means separation was achieved using LSD method at 95% confidence using Statgraphics plus 5.1 (Manugistics, Inc., Rockville, M.D., U.S.A).

3.3. Results and discussion

This section explores the effect of gravity on evaporation profiles and drying curves during the immersion period, i.e., B = 0 (g = 0, θ= 0), B = 0.025 (g>0, θ= π/2) and B = -0.129 (g<0, θ= - π/2). We conducted the same analysis for oil profiles and oil penetration curves during the cooling period for the three gravity conditions. The Bond number was calculated using Equation 3 and the fluid properties listed on Table 3-1 at 373.15 K, which is approximately the interface vapor-water temperature.

3.3.1 The immersion period

As stated above, the main phenomenon that occurs during the immersion period is water evaporation, reason why frying is considered a dehydration process. Drying has been extensively studied using the microscopic approach through experiments and modeling at pore level (Laurindo & Prat, 1996; Metzger, Irawan, & Tsotsas, 2007; Prat, 2002a; L. A. Segura, 2007). Most of the research found in the literature is focused on the study of drying under isothermal conditions. Some articles discuss drying simulation at the pore level (Huinink, Pel, Michels, & Prat, 2002; Plourde & Prat, 2003), while others describe micromodels experiments that consider temperature gradients (Louriou & Prat, 2012). However, temperatures, gradients and heat transfer rates are very low compared to those found in frying.

3.3.2 The effect of gravity on water evaporation

Figure 3-5 shows the effect of gravity on the evaporation curves (water saturation v/s time) for the three configurations (g>0, g=0 and g<0). It can be seen that when the gravity vector moves in the same direction as the velocity vector of the drying front (i.e.,

g>0 and B>0, open side on top), the gravity force tends to stabilize the interface and the drying rate is lower by comparison when there are no gravitational effects or g<0, the latter being sped-up by gravity. Similar results were reported by Laurindo and Prat (1996) in experiments with micromodels during isothermal drying.

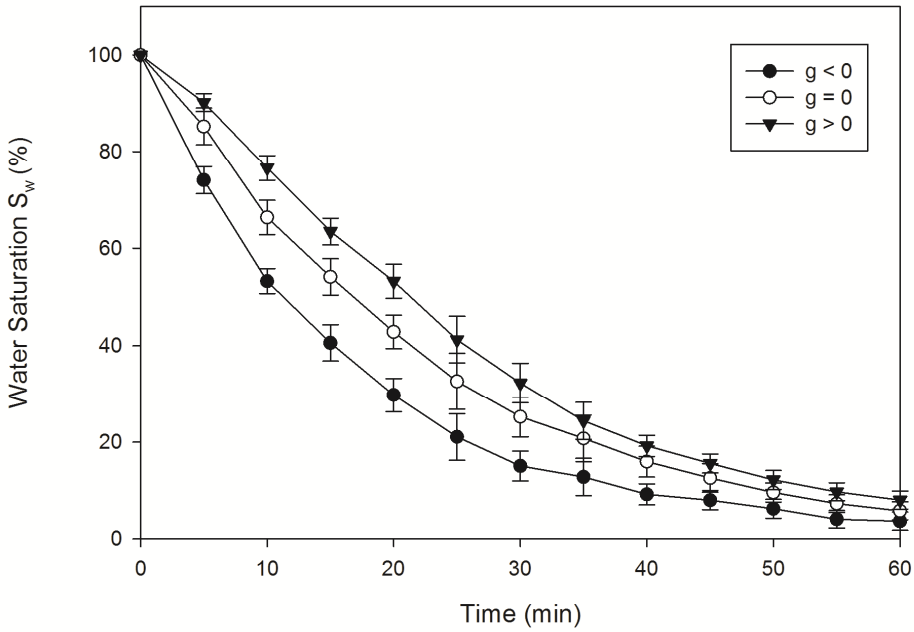

Figure 3-5: Water saturation (Sw) *versus* time (evaporation curves) for the 3 configurations under study (g=0, g<0, g>0) during the immersion period (mean values ± standard error, n=3).

Figure 3-6 shows a microview of the evaporation front within the micromodel for g<0 condition (open side on the bottom) that shows capillaries filled with water vapor and capillaries filled with liquid water, which illustrates the process. The drying of the pores follows a hierarchical progression where pores with lower capillary pressure dry first (in the absence of gravitational effects). However, same-sized pores may have different capillary pressures due to height differences when gravitational effects are present (Laurindo & Prat, 1996, 1998). Basically, the force of gravity affects the shape of the meniscus and changes the equilibrium of capillary forces across the liquid-vapor interface (Benselama et al., 2011).

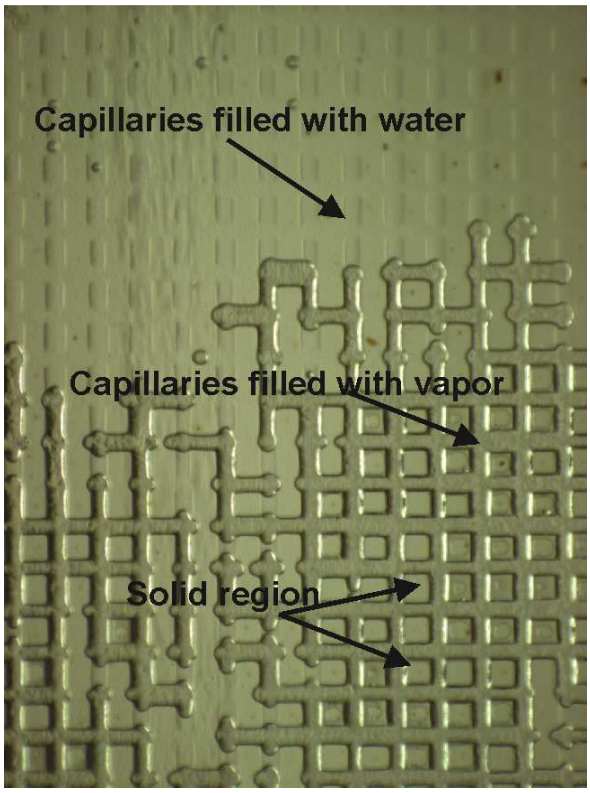

Figure 3-6: Microview of the micromodel during the immersion period; images were taken approximately at 4 cm from the open side of the micromodel, showing the movement of fluids and the drying progress through the capillaries.

When there are gravitational effects, in order to be invaded, the throat must meet the criterion of the lower value of the potential U (r_t, Z), which depends on the throat radius (r_t) and the relative position (Z) as defined by equation 5 (L. A. Segura & Toledo, 2005a). Where, γ is the interfacial tension (N/m), r_t is the throat radius (m), $\Delta\rho$ is $\rho_{water} - \rho_{vapor}$ (kg/m^3), g is gravitational force (m/s^2), Z is the position relative at bottom of micromodel (m) , θ is the angle between the open side of the micromodel and horizontal plane (rad).

$$U(r_t, Z) = \frac{2\gamma}{r_t} + \Delta\rho g Z \cdot \sin\theta \qquad \text{(Eq. 3-5)}$$

Figure 3-7 compares binarized images of evaporation fronts at an approximately equal percentage of saturation (S_w), which is obtained after different immersion times for the different orientations, due to the different drying rates. Drying fronts (white region) in the images are displayed from top to bottom for all configurations (g>0, g=0 and g<0). They are only shown this way in order to allow for a better comparison.

Overall, this figure shows similar behaviors of gravitational effects (producing changes in saturation maps) to those observed during isothermal drying, but with a less intensity (Laurindo & Prat, 1996; L. A. Segura & Toledo, 2005a)**.** A fractal analysis of the evaporation fronts was conducted in order to describe their morphology. Yiotis et al. (2010) conducted pore network simulations of isothermal drying in order to provide better information on the structure of drying patterns (two-dimensional) both in the presence and absence of gravity. Their results for the fractal dimension of the invading gaseous phase (Dp = 1.88±0.03) and the drying front perimeter (De = 1.34±0.06) in the absence of gravity were in agreement with reported experimental and theoretical values for drying in the literature. As such, the fractal analysis appears to be a good tool for describing the irregular shapes of the fronts of evaporation during frying.

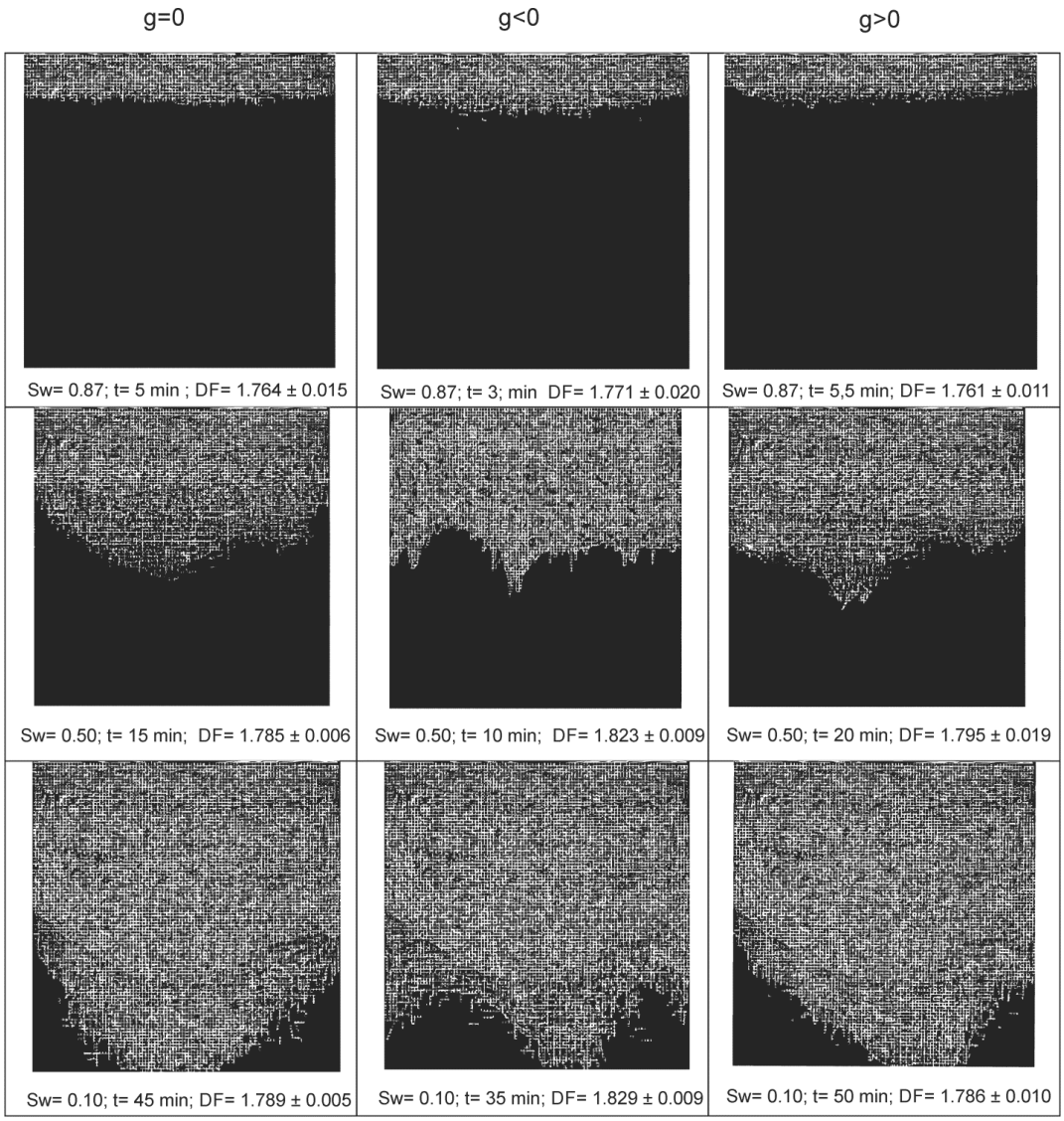

Figure 3-7: Saturation maps of water for the 3 configurations under study (g=0, g<0, g>0) during the immersion period for the same level of water saturation. The time at which this occurs as well as the fractal dimension are also shown.

Figure 3-7 also summarizes the effects of gravity on the evaporation fronts and delivers the value of the fractal dimensions (D_F) for each configuration, which are within the expected theoretical range. The higher the degree of disorder in the evaporation front, the higher the value of D_F found. At low saturation, saturation maps show a profile

development that is similar to the three configurations studied, both in form and in the degree of disorder. No significant differences of D_F were found among the different configurations at a saturation level of 0.87 with $\alpha = 0.05$ (p-value = 0.643). For a Sw of 0.50, there are visible differences between the profiles shapes, and the D_F value for $g<0$ is higher than the other configurations with $\alpha = 0.05$ (p-value = 0.005). Finally, for Sw of 0.10 D_F shows a significantly higher value for $g<0$ compared to the other configurations with $\alpha = 0.05$. D_F proved to be a good tool for studying the evaporation patterns and supports the statement that the evaporation front is more disordered and D_F is greater as the capillary forces dominate the process.

3.3.3 The effect of temperature on the evaporation front

Thermal imaging of the temperature profiles was monitored with an infrared camera using the set-up shown in Figure 3-8, after removing the micromodel from the device. In our experiments, evaporation fronts tended to take the form of temperature profiles, showing that areas that contained liquid water in the micromodels had temperatures lower than the boiling point of water, while areas containing water vapor presented a temperature above 100°C. Similar results were reported by Figus *et al.* (1999) using pore-network simulation where the shape of the evaporation front was influenced both by the thermal gradient and the pore size distribution. These studies were conducted in a partially heated network with the aim of designing capillary pumped loops (CPL), which are systems for the thermal management of spacecraft with high power loads. Using simulation of drying at the pore level with temperature gradients and gravity effects, Surasani et al. (2009) obtained similar results where the shape of the drying fronts tended to take the form of temperature gradients.

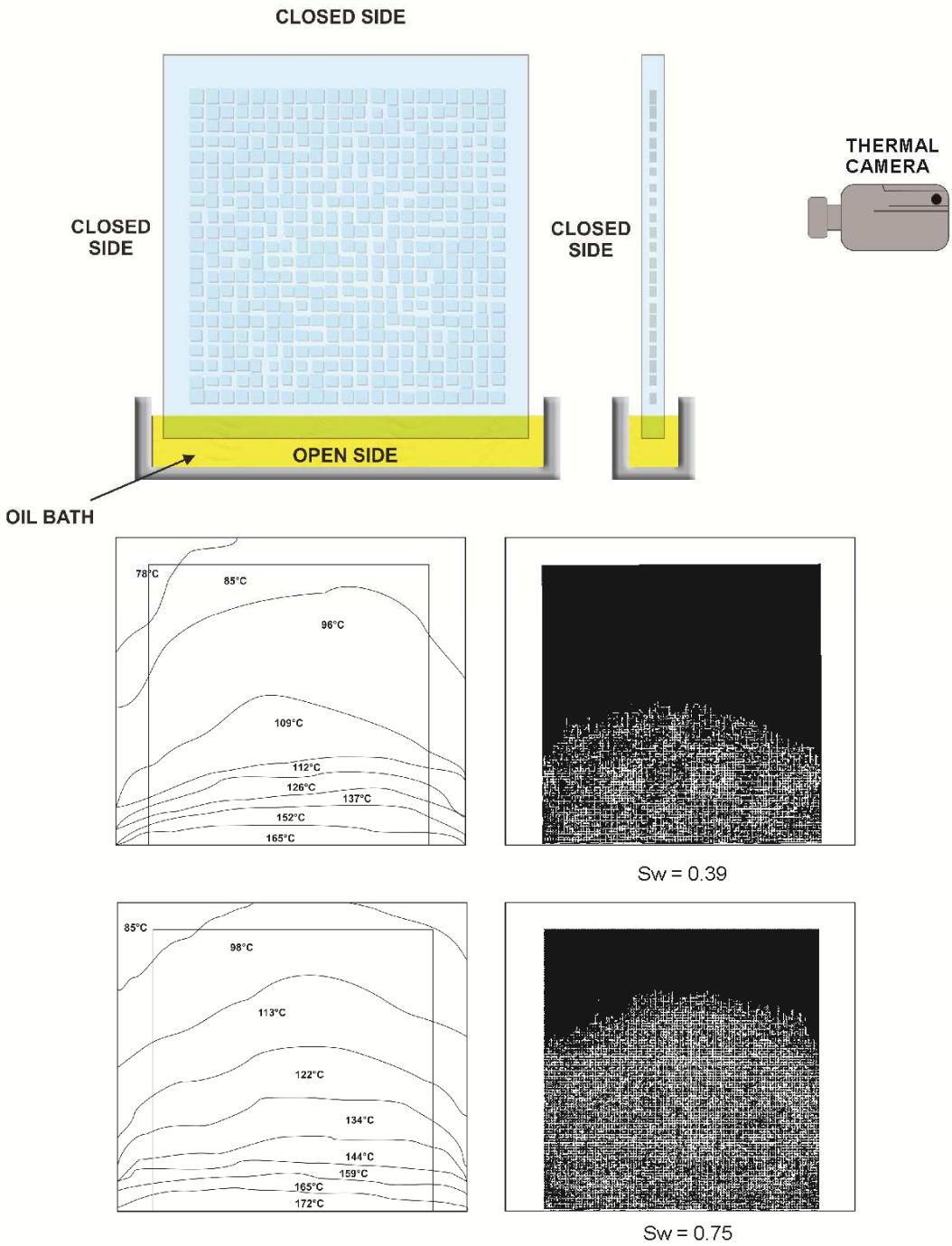

Figure 3-8: Temperature profiles acquired by infrared thermal imaging and saturation maps obtained during the immersion period for g<0 configuration.

It is important to note that during isothermal dehydration, when g = 0, g <0 and g> 0, the shape of the drying front has been reported to vary widely, that is they are importantly affected by gravity (Laurindo & Prat, 1996). These results have been extensively studied and very good correlation of the fronts obtained from experiments with micromodels and those obtained by simulation at pore level have been reported (Prat, 2002b). In view of that, based on the evaporation fronts and temperature profiles that we obtained, we can infer that in our set of experiments the thermal effect seems to be more important than the gravitational effect due to the high temperature gradients applied, which are much higher than those found during drying. In the absence of thermal gradients, the shape of our evaporation front should be similar to those found during isothermal drying. In relation to frying, the temperature profiles are consistent with those found during food deep-fat frying (Bouchon & Pyle, 2005b), confirming the importance of the moving front during the process.

3.3.4 Phase diagram for the immersion period

While frying is not a drainage process in which there is an invasive phase and a defender phase, as is the case with drying, there are similarities that allow us to apply the approach used for the immersion period during frying in which water is displaced by vapor. In order to compare the results of this study with the classical phase diagram developed for drainage processes by Lenormand et al. (1988), capillary number (C) and viscosity ratio (M) were computed for the immersion period. The results are shown as triangles in Figure 3-9. According to the phase diagram, the results range from a mixture of viscous fingering and capillary fingering mechanisms (in the early stages of the process) to domination only by the capillary fingering mechanism in the final stages. As can be seen in Figure 3-7, as the evaporation front progresses, it begins to be more disordered (increases the value of D_F), which would indicate that given a lower thermal gradient, capillary forces begin to dominate the flow in the final stages. Initially, the process progresses quickly and pores are drying simultaneously, but as time passes it gradually becomes slower and capillary forces begin to dominate over viscous forces,

causing slow movement of the menisci through smaller radii throats of the micromodel (about 50-80 µm). This movement is typical of capillary fingering.

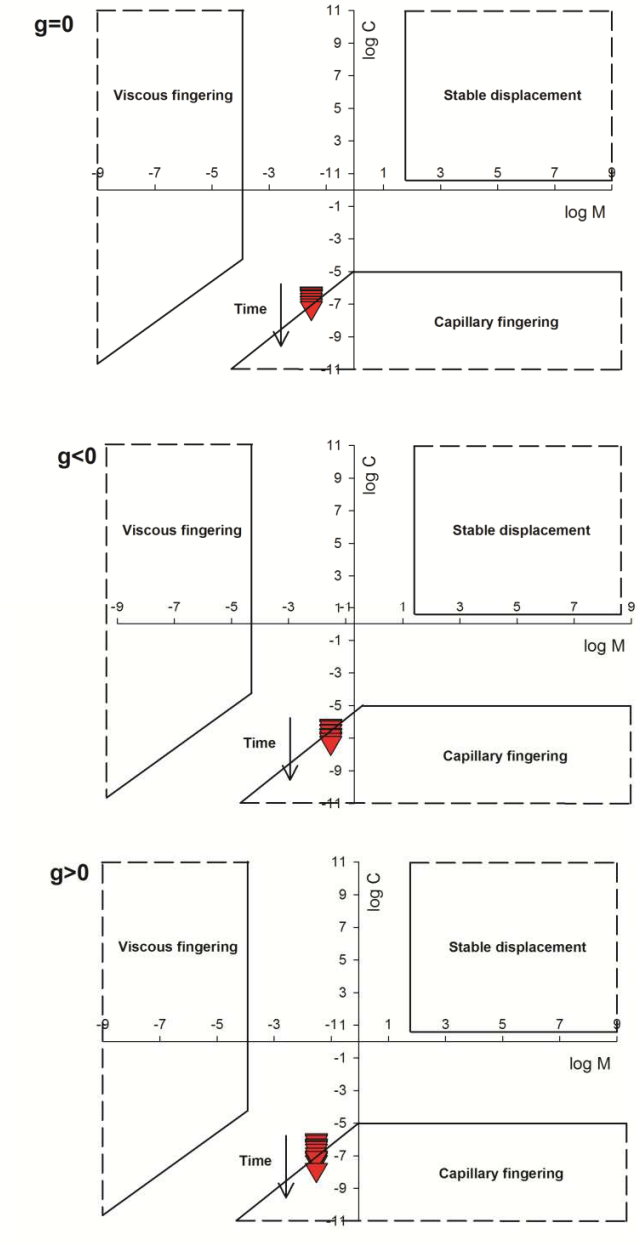

Figure 3-9: Phase diagram adapted from Lenormand et al. (1988), showing the trajectory during the immersion period for the 3 configurations under study (g=0, g<0, g>0).

No important differences were observed in the phase diagrams for the different configurations. This is due to the fact that this diagram shows a relationship of the mechanisms that dominate the flow during the process under study, and observed differences are given for the time at which this change of mechanisms occurs.

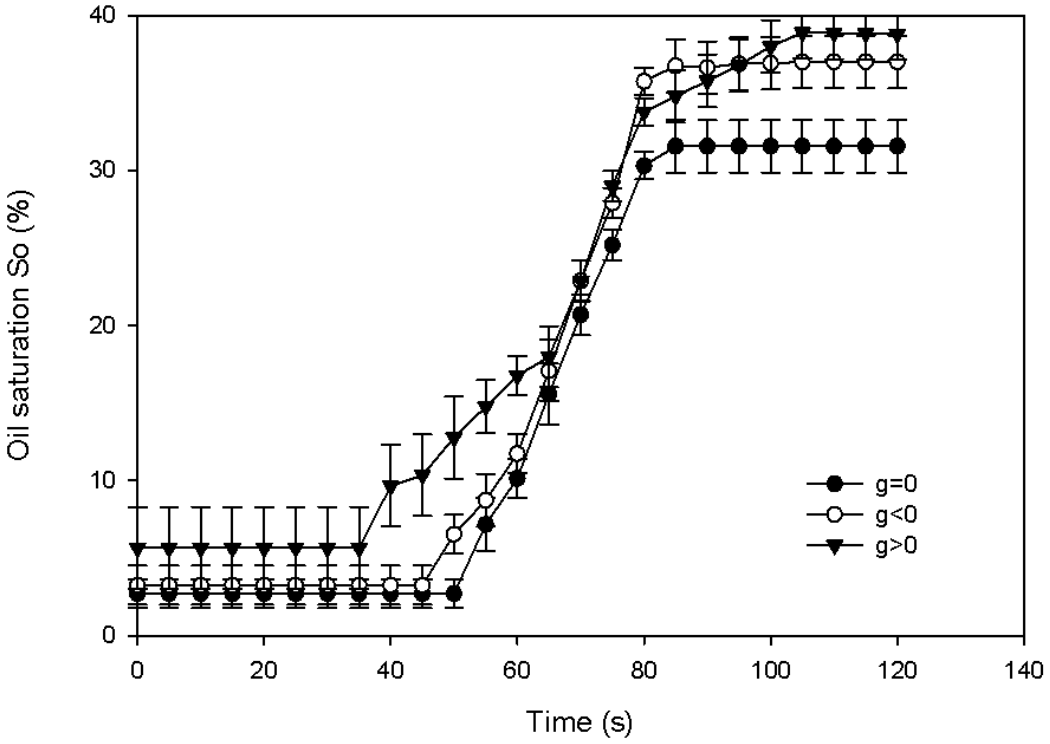

Figure 3-10: Oil uptake *versus* cooling time for the 3 configurations under study (g=0, g<0, g>0) (mean values ± standard error, n=3). The upper amount is limited by the oil available for absorption.

3.3.5 The cooling period

The literature reviewed strongly suggests that the largest proportion of oil that ends up in a fried food is sucked into the porous crust after the food is removed from the oil bath (Bouchon et al., 2003). In an earlier study, we obtained experimental evidence using micromodels that the oil mostly penetrates the matrix during the cooling period (Cortés et al., 2014). Overall, we observed a similar behavior in all configurations (g>0, g=0 and

g<0), where the vigorous escape of water vapor precluded oil absorption during the immersion period, which mostly begun upon cooling. When the open side of the micromodel was removed from the oil bath (emptying the oil receptacle of the acrylic device), the internal overpressure was released, which drew the remnant oil on the surface (the only available oil fraction to be absorbed) within the structure. During the first few seconds of cooling, bubbling (release of vapor from inside the micromodel) was vigorous. As time progressed, the vapor escape decreased in intensity until it stopped a few seconds after surface oil absorption begun. The oil front advanced quickly until the air penetrated the micromodel, which offset the internal and external pressure, halting the suction.

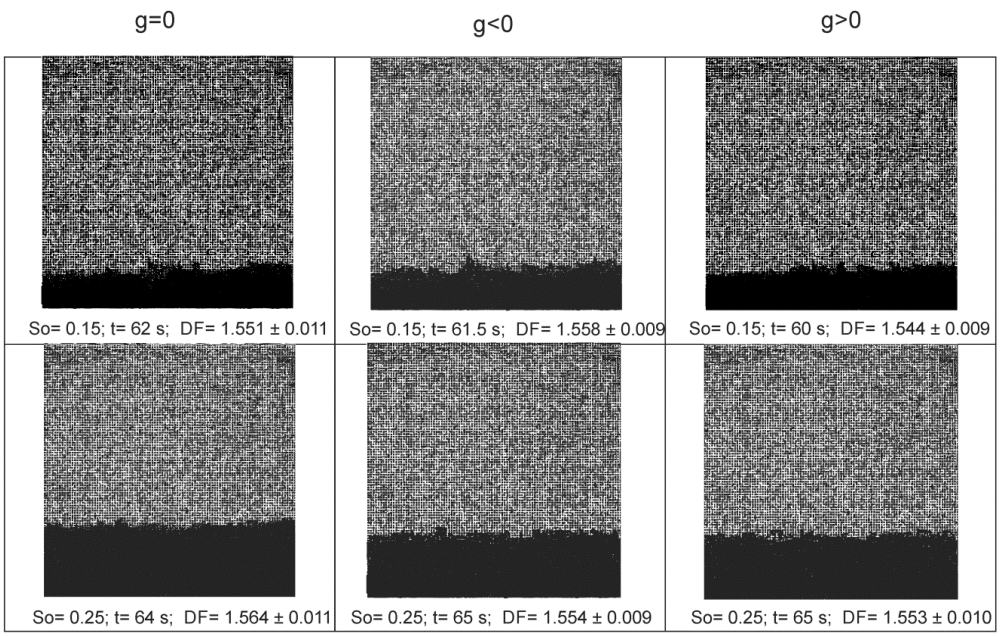

Figure 3-11: Saturation maps of oil for the 3 configurations during the cooling period for the same level of oil saturation. The time at which this occurs as well as the fractal dimension are also shown.

3.3.6 The effect of gravity on oil absorption

Figure 3-10 shows the oil saturation increase during post-frying cooling (So v/s time) for the three orientations. It can be noted that the lowest amount of final oil is achieved in the configuration g=0, a set-up that may favor oil surface drainage. By contrast, the orientations that achieved higher final oil content were g>0 and g<0, which were not significantly different (α= 0.05).

The morphology of the advancing oil fronts was very similar in all configurations as shown in Figure 3-11, which compares binarized images of oil fronts with approximately equal percentages of oil saturation obtained after different cooling times. The fractal analysis shows stabilized oil fronts with fractal dimensions (D_F) that are not significantly different (α = 0.05). These results suggest that the effect of suction due to the great pressure drop during cooling may stabilize the oil front, which also makes the oil to move forward quickly within the micromodel. Thus, the capillary forces would be negligible. The abrupt intake of air, which competes with oil to fill the empty pores once the surface oil layer breaks, would balance the internal pressure with the external suction. This would drop the oil flux to a very low value driven only by capillary forces. At the speed at which this occurs, the effect of gravity would be negligible.

3.3.7 Phase diagram for the cooling period

Phase diagrams for a draining process were also developed (where a wetting fluid is displaced by a non-wetting fluid). Lenormand (1988) developed a similar diagram for a process of embedding, which displaced a non-wetting fluid (vapor) by a wetting fluid (oil).

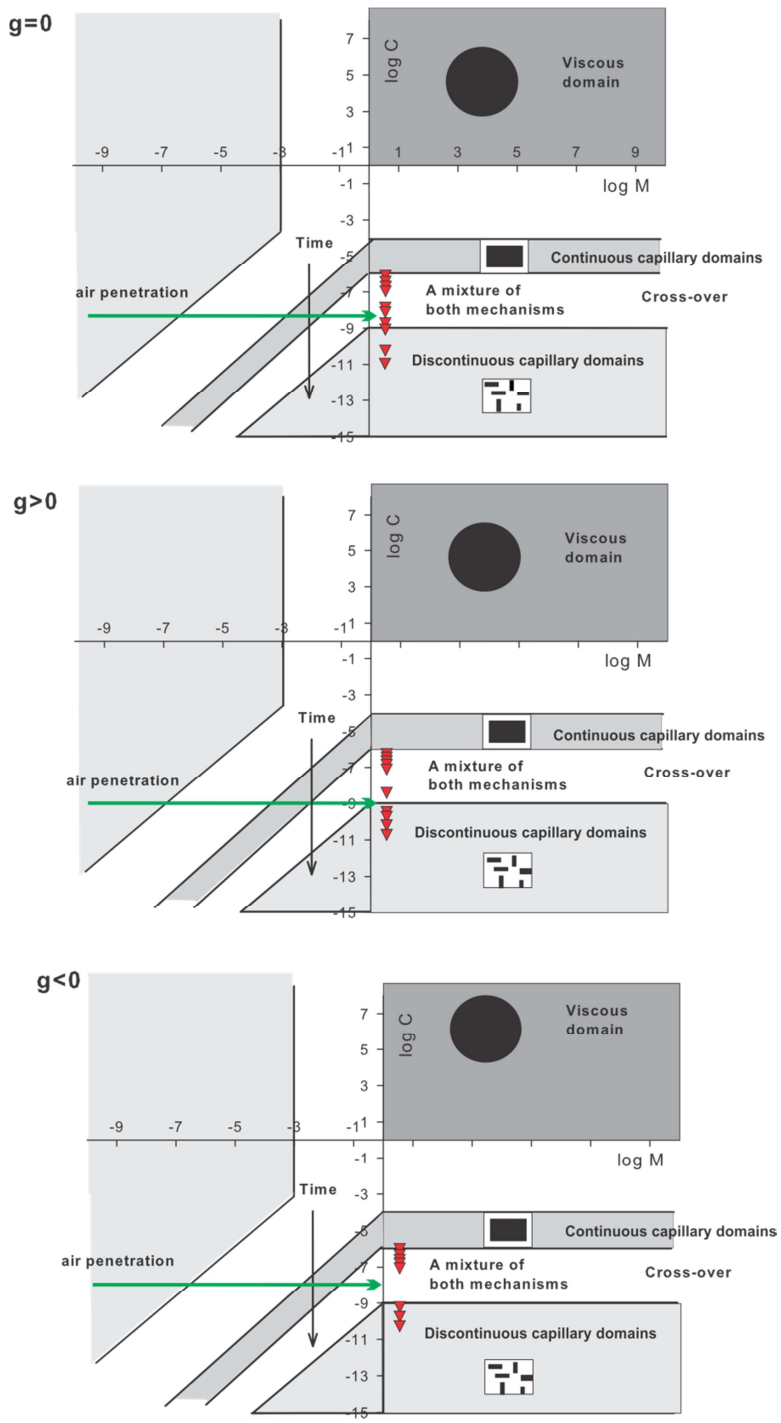

Figure 3-12: Phase diagram adapted from Lenormand et al. (1988), showing the trajectory during the cooling period for the 3 configurations under study (g=0, g<0, g>0).

As in the immersion period, the results were compared to the imbibition phase diagram developed by Lenormand et al. (1988) and Lenormand and Zarcone (1989) (see Buckley, 1991 for a review). The results are shown as triangles in Figure 12, which shows the progress through time (arrow) as well as the moment when the air enters within the micromodel. According to the imbibition phase diagram, the liquid transport mechanism during imbibition ranges from a mixture of mechanisms of the continuous and discontinuous capillary domains to only discontinuous capillary domains. When the air has penetrated, oil developments within the model are much slower, moving from an area where there is a mixture of mechanisms to an area where discontinuous capillary domains dominate.

3.4. Conclusion

An experimental approach to the study of the effect of gravity ($g=0$, $g<0$, $g>0$) on the dynamics of water evaporation and oil uptake, using glass micromodels submerged in oil, was successfully developed. While it was not possible to arrive to a total decoupling of the phenomena, it was possible to conclude that gravity affected water evaporation, favoring it when the evaporation front moved against this force ($g<0$). The evaporation fronts morphology showed none of the characteristics observed in analogous drying experiments, which suggested that thermal effects had a dominant role. In relation to oil absorption, the morphology of the advancing oil fronts was similar in all configurations. However, the force of gravity affected oil content. In fact, the lowest amount of final oil was achieved in the configuration $g=0$, a set-up that may favor oil surface drainage. Overall, the microscopic approach to frying has proven to be very useful for arriving at a better understanding of the transport phenomena that occur during this unit operation and opens up a range of possibilities for developing new studies in this area.

3.5. References

Badillo, G. M., Segura, L. A., & Laurindo, J. B. (2011). Theoretical and experimental aspects of vacuum impregnation of porous media using transparent etched networks. *International Journal of Multiphase Flow, 37*(9), 1219-1226.

Benselama, A. M., Harmand, S., & Sefiane, K. (2011). Equilibrium profile of extended isothermal meniscus with gravity inclination effect. *Colloids and Surfaces a: Physicochemical and Engineering Aspects, 391*(1-3), 158-169. doi: 10.1016/j.colsurfa.2011.03.068

Bouchon, P., Aguilera, J. M., & Pyle, D. L. (2003). Structure oil-absorption relationships during deep-fat frying. [Article]. *Journal of Food Science, 68*(9), 2711-2716.

Bouchon, P., & Pyle, D. L. (2004). Studying oil absorption in restructured potato chips. *Journal of Food Science, 69*(3), E115-E122.

Bouchon, P., & Pyle, D. L. (2005a). Modelling Oil Absorption During Post-Frying Cooling: I: Model Development. *Food and Bioproducts Processing, 83*(4), 253-260.

Bouchon, P., & Pyle, D. L. (2005b). Modelling Oil Absorption During Post-Frying Cooling: II: Solution of the Mathematical Model, Model Testing and Simulations. *Food and Bioproducts Processing, 83*(4), 261-272.

Buckley, J. S. (1991). Multiphase displacements in micromodels. In N. R. Morrow (Ed.), *Interfacial phenomena in petroleum recovery* (Vol. 36, pp. 157-189). New York: Marcel Dekker Inc.

Cortes, P., Badillo, G., Segura, L. A., & Bouchon, P. (2014). Experimental evidence of water loss and oil-uptake during simulated deep-frying process using glass micromodels. *Journal of Food Engineering, 140*, 19-27.

Dana, D., & Saguy, I. S. (2006). Review: Mechanism of oil uptake during deep-fat frying and the surfactant effect-theory and myth. *Advances in Colloid and Interface Science, 128-130*, 267-272.

Farinu, A., & Baik, O. D. (2005). Deep fat frying of foods-transport phenomena. *Food Reviews International, 21*(4), 389-410. doi: 10.1080/87559120500222896

Figus, C., Bray, Y. L., Bories, S., & Prat, M. (1999). Heat and mass transfer with phase change in a porous structure partially heated: continuum model and pore network simulations. *International Journal of Heat and Mass Transfer, 42*(14), 2557-2569. doi: http://dx.doi.org/10.1016/S0017-9310(98)00342-1

Gueven, A., & Hicsasmaz, Z. (2013). *Pore structure in food - simulation, measurement and applications* New York: Springer.

Huinink, H. P., Pel, L., Michels, M. A. J., & Prat, M. (2002). Drying processes in the presence of temperature gradients --Pore-scale modelling. *The European Physical Journal E, 9*(1), 487-498. doi: 10.1140/epje/i2002-10106-1

Karathanos, V. T., Kanellopoulos, N. K., & Belessiotis, V. G. (1996). Development of porous structure during air drying of agricultural plant products. *Journal of Food Engineering, 29*(2), 167-183.

Laurindo, J. B., & Prat, M. (1996). Numerical and experimental network study of evaporation in capillary porous media. Phase distributions. [Article]. *Chemical Engineering Science, 51*(23), 5171-5185.

Laurindo, J. B., & Prat, M. (1998). Numerical and experimental network study of evaporation in capillary porous media. Drying rates. [Article]. *Chemical Engineering Science, 53*(12), 2257-2269.

Lenormand, R., Touboul, E., & Zarcone, C. (1988). Numerical models and experiments on immiscible displacements in porous media. *Journal of Fluid Mechanics, 189*(9), 165-187.

Lenormand, R., & Zarcone, C. (1984). *Role of roughness and edges during imbibition in square capillaries.*

Lenormand, R., & Zarcone, C. (1989). Capillary fingering: Percolation and fractal dimension. *Transport in Porous Media, 4*(6), 599-612. doi: 10.1007/bf00223630

Louriou, C., & Prat, M. (2012). Pore network study of bubble growth by vaporisation in a porous medium heated laterally. *International Journal of Thermal Sciences, 52*(0), 8-21. doi: http://dx.doi.org/10.1016/j.ijthermalsci.2011.09.008

Mellema, M. (2003). Mechanism and reduction of fat uptake in deep-fat fried foods. *Trends in Food Science & Technology, 14*(9), 364-373.

Metzger, T., Irawan, A., & Tsotsas, E. (2007). Influence of pore structure on drying kinetics: A pore network study. *Aiche Journal, 53*(12), 3029-3041. doi: 10.1002/aic.11307

Moreira, R. G., & Barrufet, M. A. (1998). A new approach to describe oil absorption in fried foods: a simulation study. *Journal of Food Engineering, 35*(1), 1-22.

Oyarzun, C. A., & Segura, L. A. (2009). Design and Construction of Glass Micromodels for the Study of Moisture Transport in Softwoods. [Article]. *Drying Technology, 27*(1), 14-29. doi: 10.1080/07373930802565731

Perry, R. H., Green, D. W., & Maloney, J. O. (2008). *Perry's chemical engineers' handbook* (Vol. 7): McGraw-Hill New York.

Plourde, F., & Prat, M. (2003). Pore network simulations of drying of capillary porous media. Influence of thermal gradients. *International Journal of Heat and Mass Transfer, 46*(7), 1293-1307. doi: http://dx.doi.org/10.1016/S0017-9310(02)00391-5

Prat, M. (2002a). Recent advances in pore-scale models for drying of porous media. *Chemical Engineering Journal, 86*(1-2), 153-164.

Prat, M. (2002b). Recent advances in pore-scale models for drying of porous media. *Chemical Engineering Journal, 86*(1–2), 153-164. doi: http://dx.doi.org/10.1016/S1385-8947(01)00283-2

San martín, F. A., Laurindo, J. B., & Segura, L. A. (2011). Pore-Scale Simulation of Drying of a Porous Media Saturated with a Sucrose Solution. *Drying Technology, 29*(8), 873-887. doi: 10.1080/07373937.2010.547968

Segura, L. A. (2007). Modeling at pore-scale isothermal drying of porous materials: Liquid and vapor diffusivity. *Drying Technology, 25*(10), 1677-1686. doi: 10.1080/07373930701590889

Segura, L. A., & Oyarzún, C. A. (2012). Experimental evidence of mass transfer mechanisms during freeze-drying in a capillary porous medium. *International Journal of Refrigeration, 35*(8), 2102-2109. doi: http://dx.doi.org/10.1016/j.ijrefrig.2012.08.014

Segura, L. A., & Toledo, P. G. (2005a). Pore-level modeling of isothermal drying of pore networks - Effects of gravity and pore shape and size distributions on saturation and transport parameters. *Chemical Engineering Journal, 111*(2-3), 237-252. doi: 10.1016/j.cej.2005.02.004

Segura, L. A., & Toledo, P. G. (2005b). Pore-level modeling of isothermal drying of pore networks. Evaporation and viscous flow. *Latin American Applied Research, 35*(1), 43-50.

Surasani, V. K., Metzger, T., & Tsotsas, E. (2009). A Non-isothermal Pore Network Drying Model with Gravity Effect. *Transport in Porous Media, 80*(3), 431-439. doi: 10.1007/s11242-009-9372-7

Xu, P., Mujumdar, A. S., & Yu, B. (2008). Fractal Theory on Drying: A Review. *Drying Technology, 26*(6), 640-650. doi: 10.1080/07373930802045932

Yiotis, A. G., Tsimpanogiannis, I. N., & Stubos, A. K. (2010). Fractal Characteristics and Scaling of the Drying Front in Porous Media: A Pore Network Study. *Drying Technology, 28*(8), 981-990. doi: 10.1080/07373937.2010.497087

Ziaiifar, A. M., Achir, N., Courtois, F., Trezzani, I., & Trystram, G. (2008). Review of mechanisms, conditions, and factors involved in the oil uptake phenomenon during the deep-fat frying process. *International Journal of Food Science and Technology, 43*(8), 1410-1423. doi: 10.1111/j.1365-2621.2007.01664.x

4. THE EFFECT OF DIFFERENT POROUS MEDIA ON MOISTURE LOSS AND OIL ABSORPTION PROFILES DURING FRYING USING GLASS MICROMODELS

Abstract

The importance of food microstructure in food processing has been extensively reported and deep-fat frying is not an exception. Microstructure plays a pivotal role to understand oil absorption mechanisms. The aim of this work was to improve our understanding of the relationship between microstructure and oil absorption, through the use of glass micromodels to obtain direct evidence of transport phenomena in different porous networks. Porous patterns were developed based on key descriptors of three food matrices (potato, apple and carrot). They were saturated with water and immersed in oil at 190°C. Moisture and oil profiles were imaged to get water and oil saturation maps. Image and fractal analyses were performed to describe the morphology of the evaporation and oil fronts. Results showed that higher porosity facilitated the removal of moisture from the matrix and promoted greater oil absorption during cooling. The fractal dimension showed that microstructures with a relatively high number of fine capillaries were less stable and propitiated fingering during the advance of the evaporation front, whereas the shape of the oil front was not affected in any system. In all matrices, the disruption of the surface oil film due to air penetration was a critical factor to stop oil imbibition. Thus, the amount of surface oil was not a limiting factor.

Keywords: *micromodel, frying, oil uptake, pore network, capillaries, dehydration.*

4.1. Introduction

Oil uptake is a phenomenon that has gained great importance in the food industry, because the amount of fat absorbed during the frying process is one of the most important quality parameters of fried foods. This runs counter to recent consumer trends towards healthier food and low fat products (Bouchon & Pyle, 2004).

Oil absorption is heavily linked to moisture loss since it determines the extent of crust formation, the microstructure of which has been considered to be a key product-related determinant of the final oil uptake of deep-fat fried food (Bouchon, Hollins, Pearson, Pyle, & Tobin, 2001). It has been found that most of the oil is confined to the surface region of the fried product (Bouchon & Aguilera, 2001; Farkas et al., 1996; I. S. Saguy, Ufheil, & Livings, 1998). Also, there is evidence to suggest that it would be mainly penetrate during the cooling period, since the vigorous escape of water vapor would prevent oil migration during most of the immersion period (Bouchon et al., 2003; Cortés et al., 2014; R. G. Moreira et al., 1997; Ufheil & Escher, 1996), as it was recently confirmed by Cortes, Badillo, Segura, & Bouchon (2014) through visual observation using glass micromodels. This suggests that oil uptake is essentially a surface-related phenomenon resulting from the competition between drainage and suction into the porous crust once the food is removed from the oil (Bouchon & Aguilera, 2001). Accordingly, Moreno, Brown and Bouchon (2010), found a direct relationship between oil absorption and surface roughness, using laser scanning microscopy. Nevertheless, they could not extend this relationship when comparing products of different categories (gluten- or potato-based laminated dough), suggesting that other food-related properties, such as product porosity, should be examined. This also seems to play a critical role in vacuum frying, as determined by (Dueik, Robert, & Bouchon, 2010) when analyzing the behavior of three different food matrices: potatoes, carrots and apples. However, information about the effect of different porous media in oil absorption is still scarce.

The use of micromodels may be a good means to get additional information to improve our knowledge in this respect. Micromodels are transparent pores and constriction networks that simulate the complexity of natural porous media. They have been used to

visualize flow phenomena at microscopic levels (Buckley, 1991) to better understand transport phenomena in different fields of science, including food processes such as drying (L. A. Segura & Toledo, 2005a), vacuum impregnation (Badillo et al., 2011), freeze-drying (L. A. Segura & Oyarzun, 2012) and recently, frying (Cortés et al., 2014). The pioneers in the use of micromodels to study transport phenomena at the pore level were Lenormand, Touboul and Zarcone (1988). These researchers conducted extensive work on pore networks through simulations and experiments. They analyzed the different drain type mechanisms (where a wetting fluid displaces a non-wetting fluid) during the displacement of two immiscible fluids, according to the capillary number (C) and the viscosity ratio (M). C is a dimensionless number that represents the ratio between viscous and capillary forces, according to Equation 4-1:

$$C = \frac{q \cdot \mu_w}{A \cdot \gamma \cdot cos\, \varphi} \quad \text{(Eq.4-1)}$$

The numerator is the displacing fluid flow q (m^3/s) times the viscosity of the wetting fluid μ_w (kg/(m.s)) and the denominator is the flow cross-sectional area A (m^2) times the interfacial tension of the wetting fluid (γ in N/m) and the cosine of the contact angle φ (for water/glass ~ °0). On the other hand, M represents the ratio between the viscosity of the non-wetting fluid (the water vapor, in the case of the immersion period during deep-fat frying) and the viscosity of the wetting fluid (liquid water), as defined in Equation 4-2:

$$M = \frac{\mu_{nw}}{\mu_w} \quad \text{(Eq. 4-2)}$$

In accordance, they developed a model that can reproduce flow transitions from capillary forces-dominated to viscous forces-dominated and defined a "phase diagram" that allowed them to map the displacement of two immiscible phases based on the capillary number and the viscosity ratio, which may be of great interest to understand flow patterns during deep-fat frying.

Within this framework, the aim of this research was to develop an experimental set-up based on the use of glass micromodels to obtain direct evidence of moisture loss and oil uptake in three different porous networks in order to improve our understanding of the relationship between microstructure and oil absorption during oil immersion.

4.2. Materials and Methods

Micromodels (2D transparent porous media) were manufactured using a photolithographic technique in accordance with the protocol described by Oyarzún and Segura (2009). The size of the micromodels was 15x15 cm^2 and they contained 100x100 pores (nodes), which were built using statistical data on food microstructure, as Cortés et al. (2014) explain in greater detail. The statistical information for three different food matrixes: carrots (Diaz, Acuña, & Segura, 2011), potatoes (Karathanos et al., 1996), and apples (Rahman et al., 2005) was used as a basis for the design of three distinct models with low, medium and high porosity, respectively. The aim was to define three different structures, with different porosity and pore size distribution, to understand the effect of these variables in transport phenomena. The pore-throat (bonds) radius was a random variable which followed a log-normal distribution for all cases, with the mean size and standard deviation of pore-throat shown in Table 4-1. Each channel had an approximately constant depth of 35 μm. The values were amplified 50 times in the case of carrots and 100 times in the case of potatoes in order to obtain adequate resolution for the photolithographic technique at the micron range.

4.2.1. Computer-Designed Photomask

The photolithographic process involves transferring a transparent printed pattern (called a photomask) with the network design onto a glass plate. The pattern is etched into the glass plate in order to obtain a network of capillaries with a specific pattern. This photomask must be carefully designed to capture all of the topological and geometric features of the porous structure. In this study, we used computer-designed patterns to describe the microstructure of the three matrices. The first step was to generate random

numbers of throats-radii. Then, a macro was written in Visual Basic Application (VBA). These values were loaded and the network was drawn using the vector graphics drawing program AutoCAD (version 2010, Autodesk Inc.). The patterns were printed on transparent films using a laser printer (HP Designjet Z5200) with a resolution of 2,400 x 1,200 dpi. A section of 10x10 nodes of photomask for each food matrix studied is shown in Figure 1 in order to visualize the differences in pore size distribution between them. Additional characteristics of the micromodels are shown in Table 4-1.

Table 4-1: Pore media parameters used to design the micromodels.

Pore media parameter	Symbol	Low Porosity	Medium Porosity	High Porosity
Average pore size (μm)	A_{ps}	22	75	109
Pore size standard deviation (μm)	SD_{ps}	15	30	82
Pore body to pore body length (m)	L	1×10^{-3}	1×10^{-3}	1×10^{-3}
Throat and body depth (m)	R_{ah}	3.5×10^{-5}	3.5×10^{-5}	3.5×10^{-5}
Porosity (dimensionless)	P	0.17	0.26	0.30
Total pore space volume (m^3)	V_r	6.07×10^{-12}	9.09×10^{-12}	1.06×10^{-11}
Cross-sectional area (m^2)	Σ	1.78×10^{-7}	2.95×10^{-3}	3.47×10^{-3}

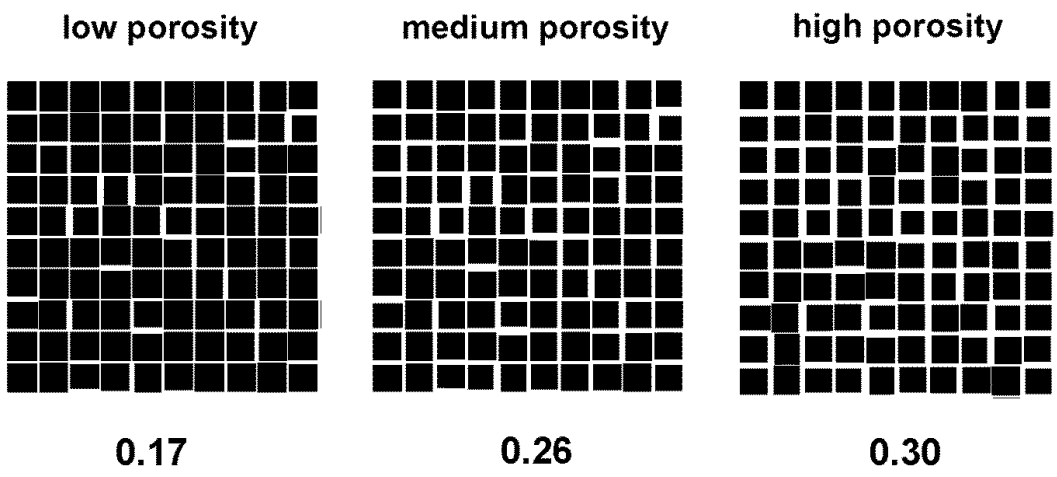

Figure 4-1: A section of 10x10 nodes of photomask for the three matrices showing the differences between each micromodel.

4.2.2. Photolithographic Process

The photolithographic technique allows the pattern printed (photomask) to be etched onto the glass plates. A diagram of the manufacturing protocol is shown in Figure 4-2, and a detailed description of the protocol can be found in Cortés et al. (2014), which is based on Oyarzún and Segura (2009).

The main steps in the manufacture of micro-models are described below:

1) *Conditioning of glass plates:* This step is meant to produce clean plates (see Figure 4-2a);
2) *Hydrophobization:* This operation helps with the fixation of the photopolymer (see Figure 4-2b).
3) *Application of photopolymer:* The photopolymer allows the printed pattern to be transferred (see Figure 4-2c).

4) *Exposure to ultraviolet light (UV):* UV light activates the photopolymer areas that are not protected by the printed pattern, i.e. are exposed (see Figure 4-2d).
5) *Developing:* Using NaOH, the photopolymer which has been activated by UV light is removed, leaving exposed areas of the glass that will be etched.
6) *Etching:* The glass is etched with acid in the areas that are not protected by the photopolymer (see Figures 4-2f and 4-2g).
7) *Fusion of the plates:* The etched glass plate is fused to a clean plate to generate the micromodel (see Figure 4-2h).

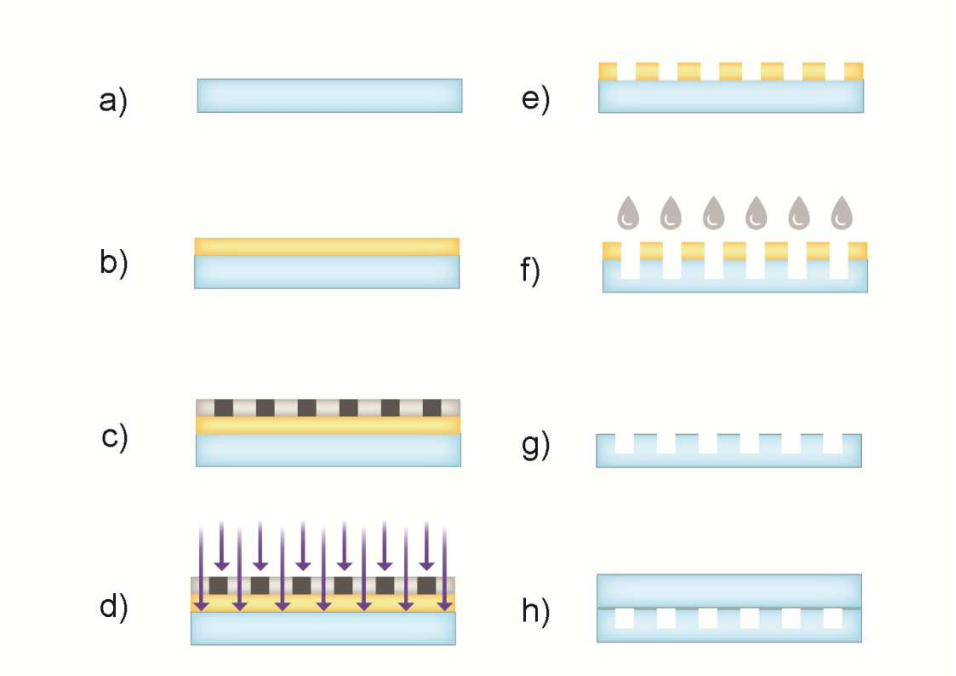

Figure 4-2: Photo-etching process diagram showing: (a) the glass plate with hydrophobic surfaces; (b) the glass surface coated with photoresist; (c and d) the alignment of the photomask for UV exposure; (e) the photoresist developed with NaOH; (f) the glass plate etched with hydrofluoric acid (HF); (g) the glass plate etched and clean; (h) the second glass plate fused with the etched glass plate (adapted from Oyarzún and Segura (2009)).

4.2.3. Oil immersion experiments

In order to mimic the frying process, the micromodels were saturated with deionized water. All sides were closed except from the bottom to allow for direct contact with the oil (sunflower oil, Natura, Córdoba, Argentina) and provide a pathway for steam release and oil to be absorbed. The micromodel was immersed vertically to a depth of ≈ 5 mm in an oil bath at 190 ± 2 ºC for 60 min. The model was removed from the oil bath keeping a vertical position. The system containing the heating medium (oil) was mounted on a micrometric platform and the micromodel was attached to a support as shown in Figure 4-3. The camera was mounted on a boom stand which provided easy vertical or horizontal movement as well as stable support for the camera at 25 cm from the micromodels. Proper position of micromodels was checked in all experiments with a level to avoid inclinations in both the micromodel and the camera.

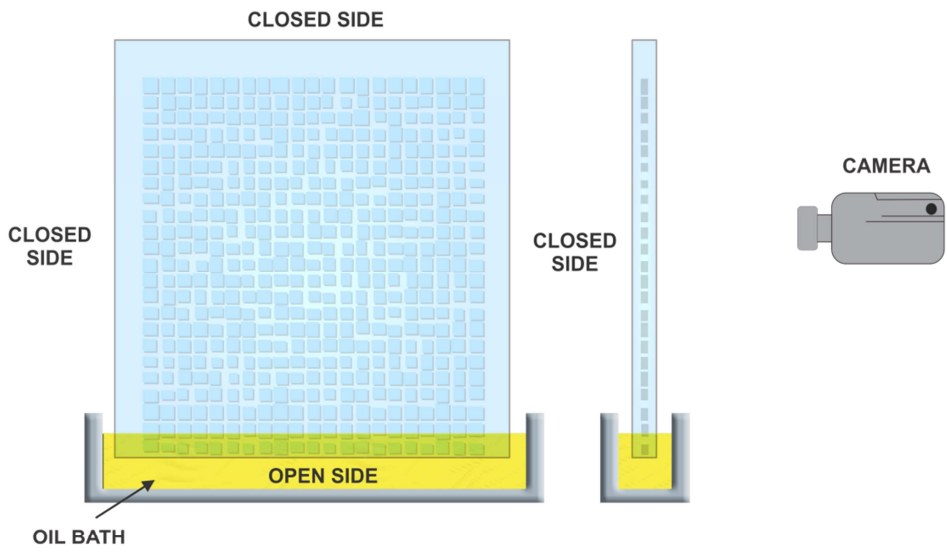

Figure 4-3: Front and side view of the experimental oil immersion system; the camera was mounted in front of the micromodel.

4.2.4. Determination of evaporation and oil profiles

In order to construct evaporation and oil profiles, digital images of the total area of the micromodels were acquired using a digital camera (Sony Cybershot DSC-HX9, China) every 10 s. The useful regions were extracted. The camera was mounted 25 cm in front of the micromodel. The iris and lens aperture were operated in automatic mode without flash. The camera was grey-balanced before each imaging session and a uniform diffuse light (D65 lamps) was used to back-light the micromodel. The images were stored in JPEG (Joint Photographic Experts Group) format using high resolution and superfine quality for further processing and analysis. The spatial resolution of the images was approximately 15 pixels/mm. The images were processed using Image Pro-plus 4.1 software (Media Cybernetics, Silver Spring, U.S.A.). Then, they were transformed to grey level images, which were binarized using a grey-level threshold of 150. This procedure allowed obtaining a clear image of the advance of water and oil fronts. These images were then used to construct the saturation maps of oil and water. Evaporation and oil uptake curves were plotted using the saturation of water and oil, respectively. Saturation was defined as the percentage of total volume that was occupied by water (or oil). All volumes were calculated using areas determined by image analysis and based on the depth of the capillaries.

4.2.5. Determination of surface oil

After the immersion period, the oil available for absorption into the micromodel during cooling is limited, and corresponds to the fraction that remains attached to the open side of the micromodel after the immersion. Images of the oil profile that adhered to that side were taken after 10 s in the three matrices. This time was chosen because no oil drained after that period of time and because oil suction started after said interval. Side-view images were taken with a CoolSnap Pro Color digital camera using a partially telecentric video lens (55 mm F2.8, Edmund Optics, NJ, USA). Images were spatially calibrated using a micro-ruler with an accuracy of 100 microns. Image Pro-plus 4.1 software was used for image processing and analysis to determine the radius of the semicircle formed

by the oil layer over the open side of the micromodel. The volume of surface oil was calculated from: $\pi r^2 * h/2$, where r is the radio of the semicircle and h is the length of the side of the micromodel. No significant differences in surface oil content were found between the threes matrices.

4.2.6. Fractal analysis of evaporation and oil profiles

In order to describe and quantify the form of the evaporation and the oil profiles, the fractal dimension was computed. Fractal geometry is useful for describing irregular objects that traditional Euclidean geometry fails to analyze (Xu et al., 2008). Thus, we used the fractal dimension (D_F) to differentiate, quantify and classify the evaporation and oil advance patterns. Mathematically, D_F is defined as:

$$D_F = 1 - \frac{\log(F)}{\log(L)} \qquad \text{(Eq. 4-3)}$$

where F is the total extent of the pattern under consideration and L is the metric (or length scale) on which it is measured. In order to determine D_F numerically, a plug-in of fractal analysis (FRACLAC, version 2.5) for Image J version 1.47 (image analysis software) was used (Wayne Rasband, National Institute of Health, USA). D_F was calculated in triplicate for three different water saturations (Sw: 0.75, 0.50, 0.10) in all matrices studied during the immersion period and for two different oil saturations (So: 0.15, 0.25) in all matrices during the cooling period. The FRACLAC plug-in requires an initial configuration in which the most relevant parameter is the number of grids used to determine D_F. It was four in all images, so the software calculates four slopes per image and an average value of the four calculations.

4.2.7. Statistical analysis

Experiments were carried out in triplicate for each food matrix studied. Data were tested by analysis of variance (ANOVA) and means separation was achieved using LSD

method at 95% confidence, using Statgraphics plus 5.1 (Manugistics, Inc., Rockville, M.D., U.S.A.).

4.3. Results & discussion

4.3.1. Effect of the matrix on water evaporation during oil immersion

During the immersion period, water vigorously escaped from the micromodel as vapor. The evaporation front first moved quickly and then slowed down as the process advanced. Figure 4-4 shows the effect of the matrix on the evaporation curves (water saturation v/s time) for the different models under study. As can be seen, the micromodels of low porosity had a significantly lower moisture loss rate than micromodels of medium and high porosity ($\alpha = 0.05$). This may be also related to the lower size of capillaries in this matrix compared to the other two, which may impair water loss.

Figure 4-5 compares the binarized images of the evaporation fronts at an equal percentage of water saturation (S_w), which is obtained after different immersion times for the three matrices due to the different drying rates. Evaporation fronts (white region) in the images advance from bottom (open side) to top for all matrices. The fractal dimension is also displayed in the Figure to better describe the drying patterns. Overall, D_F values are in the range of those reported by Yiotis et al. (2010) during isothermal drying (two-dimensional).

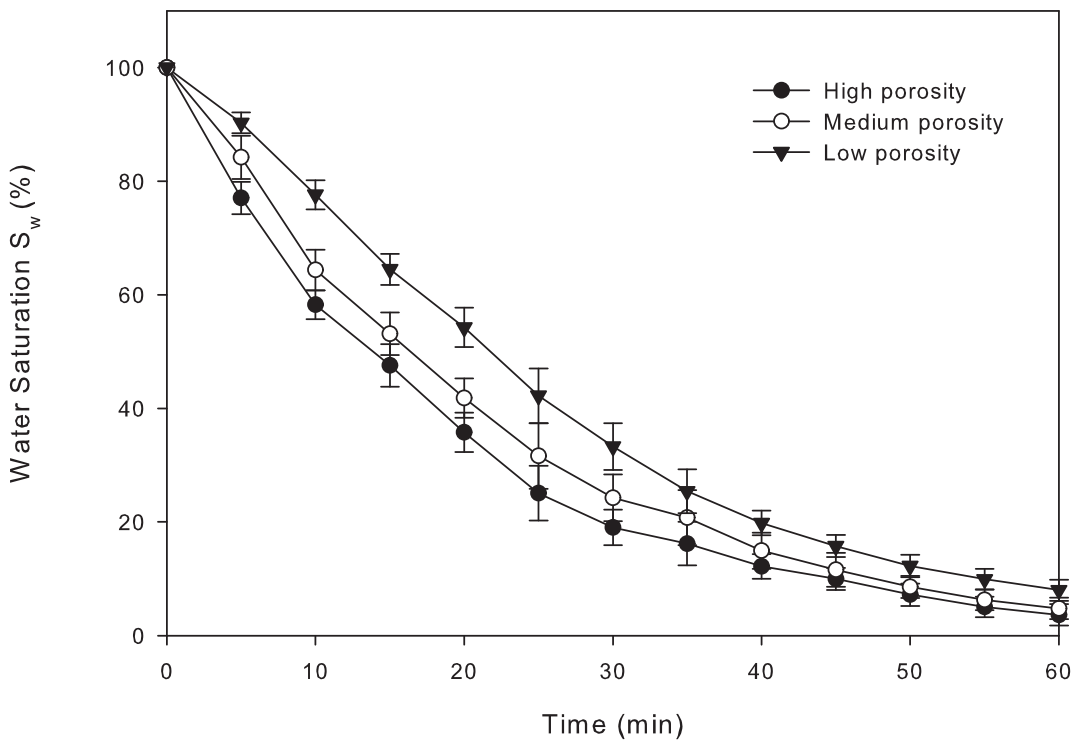

Figure 4-4: Water saturation (percentage of the total volume of the micromodel filled with liquid water) during the immersion period for increasing frying times for each food matrix under study. Points are means ± standard error (n=3).

In the initial stages of the process, the thermal gradient caused the evaporation front to advance in a more stable form in all matrices (Sw=0.75). As the process proceeded, the front speed decreased and fingering was more pronounced, increasing the degree of disorder, as reflected by the higher D_F value. When comparing the different matrices, the low porosity matrix showed a D_F value that was significantly higher compared to the other two matrices at 0.5 and 0.1 water saturation levels. This could be because of the relatively high number of fine capillaries found in this model, which may propitiate fingering during the advance of the evaporation front.

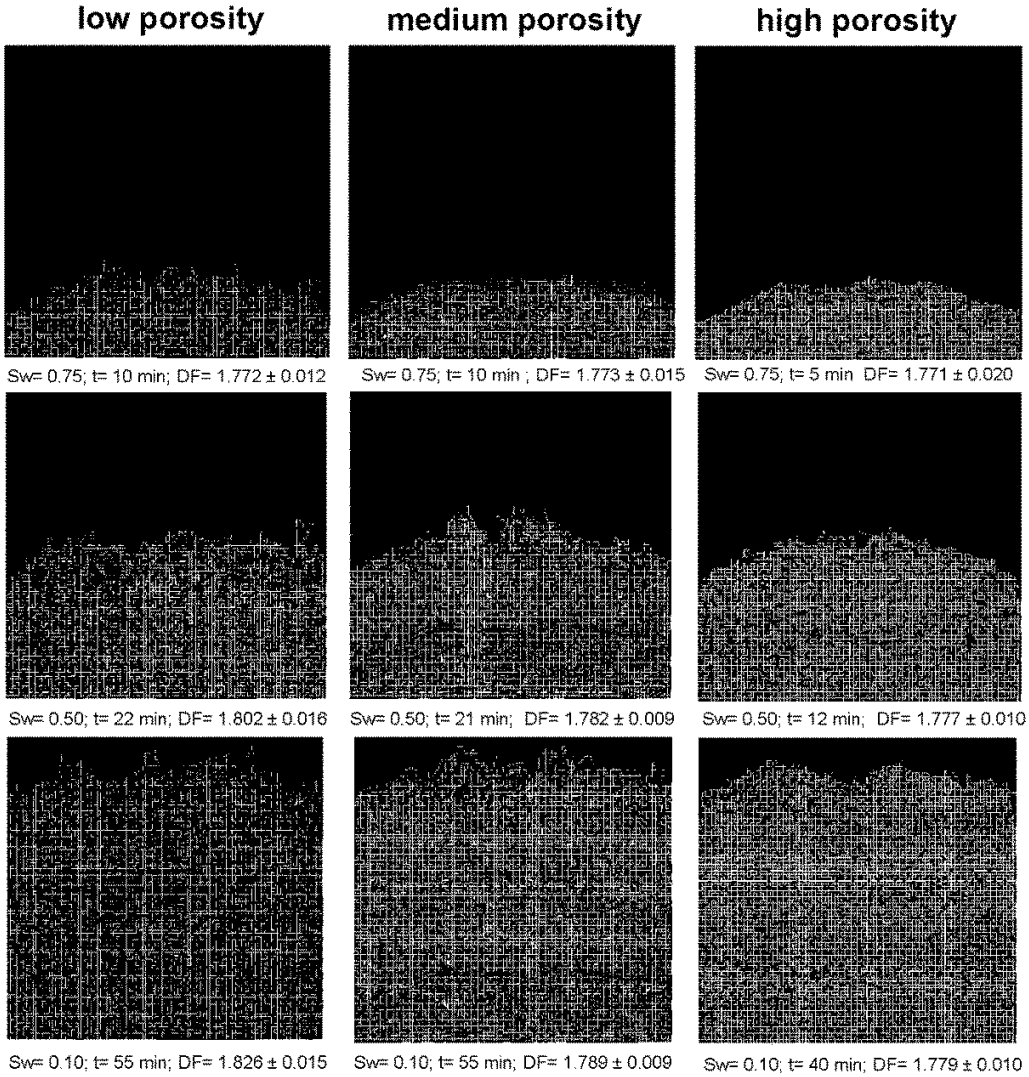

Figure 4-5: Water saturation maps of water for the three food matrices under study during the immersion period for the same level of water saturation. The time at which this occurs as well as the fractal dimension are also shown.

4.3.2. Phase diagram for water evaporation during the immersion period

As explained in the introduction , Lenormand et al. (1988) pioneered the development of a phase diagram to identify the dominant mechanism for fluid displacement during drainage (where a wetting fluid is displaced with a non-wetting fluid). We used this diagram to display our results, since it is possible to consider the immersion period of frying as a drainage process in which a wetting fluid (water) is displaced by its vapor, a non-wetting fluid. To do so, we computed and plotted the capillary number (C) and the viscosity ratio (M) at different times during the immersion period, according to Equations 4-1 and 4-2, respectively.

Figure 4-6 shows the phase diagrams for the immersion period for the three matrices under study. The red triangles show the progress of the water loss and time elapses from top to bottom. According to the phase diagram, in the early stages of the process, a mixture of viscous fingering mechanisms is dominant in all matrices. As the process proceeds, capillary fingering begins to dominate and in the final stages capillary forces seem to dominate the flow. This is consistent with fractal dimension measurements, which showed an increase in D_F as dehydration progressed (Figure 4-5). The process initially progresses quickly, and pores dry simultaneously probably driven by the high thermal gradient, but as time passes, it gradually becomes slower and capillary forces seem to dominate over viscous forces, causing slow movement of the menisci through smaller radii throats of the micromodel.

No important differences were observed in the phase diagrams for the different matrices. That is, the mechanisms that dominated the flow during the process in all matrices under study were similar. Differences were only found with respect to the time at which the change in mechanism occurred in the different matrices, in accordance to Figures 4-4 and 4-5.

.

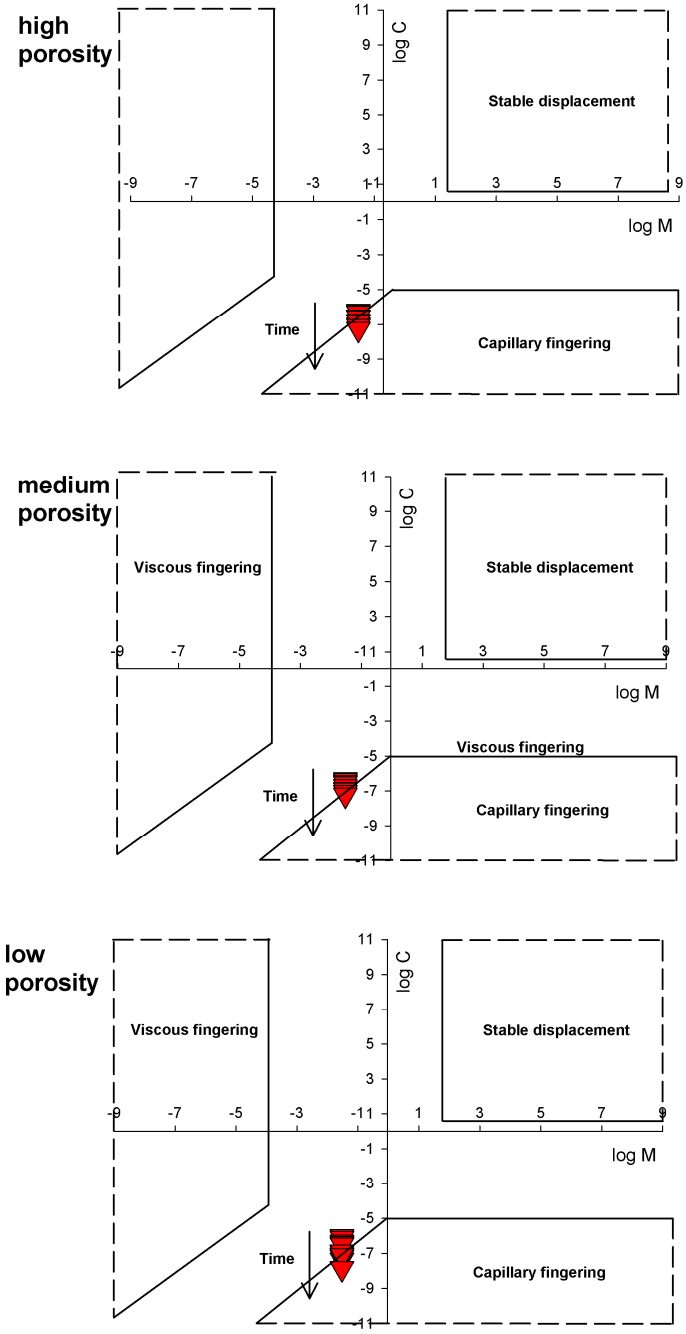

Figure 4-6: Phase diagram showing the trajectory (red triangles) due to water evaporation during the immersion period for the three matrices under study.

4.3.3. The effect of the matrix on oil absorption

During the cooling period, a series of coupled phenomena occurred including vapor condensation, drainage of surface oil and oil suction within the structure in competition with air. Our experimental results confirmed that most of the oil was absorbed during this period in all matrices. Figure 4-7 shows that the oil saturation at the end of the immersion period was below 8% in all models and increased significantly during the post-frying cooling (So v/s time) for the three matrices. The lowest amount of final oil was achieved for low and medium porosity micromodels (34.8 and 37% final oil saturation, respectively). By contrast, the matrix that achieved the highest final oil content was the high porosity micromodel (41.5% of oil saturation), which was significantly different from the other two (α= 0.05) and in absolute terms represents an even higher difference. Dueik et al. (2012) determined that apple chips absorbed twice as much oil as potato and carrot chips when frying under atmospheric or vacuum conditions, probably due to the higher porosity of the matrix.

It is important to note that the oil available to be absorbed was approximately the same for all experiments and was about 8.5×10^{-7} m^3, which remained attached to the end of the micromodel submerged after being removed from the oil bath. This amount was far larger than the one that finally penetrated the structure, and therefore was not a limiting factor. In fact, oil absorption stopped due to air penetration even though there still was a large amount of oil on the surface.

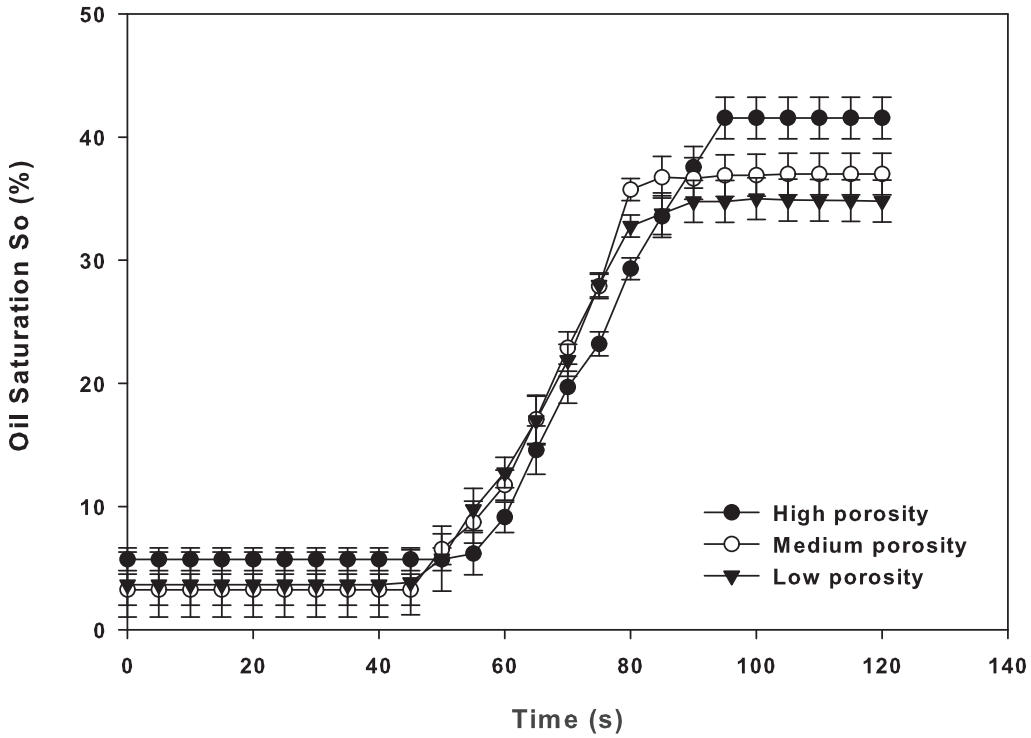

Figure 4-7: Oil uptake (percentage of the total volume of the micromodel filled with oil) during cooling, after an immersion period of 20 min, for the three food matrices under study. Points are means ± standard error (n=3).

Figure 4-8 shows the oil saturation maps during the cooling period at two different saturation levels. No significant differences in the fractal dimension (D_F) of oil profiles between the three different matrices ($\alpha = 0.05$) were found. Thus, the big pressure drop during cooling seemed to cause a stable advance of the oil front in all matrices. No fingering was observed in any set-up. The oil suction began abruptly after a few seconds in all matrices and stopped when the air penetrated into the micromodels and the internal pressure was equal to external pressure, despite the fact that the surface could still contain a fair amount of oil on top of it. These results may have some interesting practical implications. For instance it could be possible to design a post-processing step

aiming to destabilize the surface layer of oil, to facilitate the entrance of air into the matrix to decrease oil absorption.

.

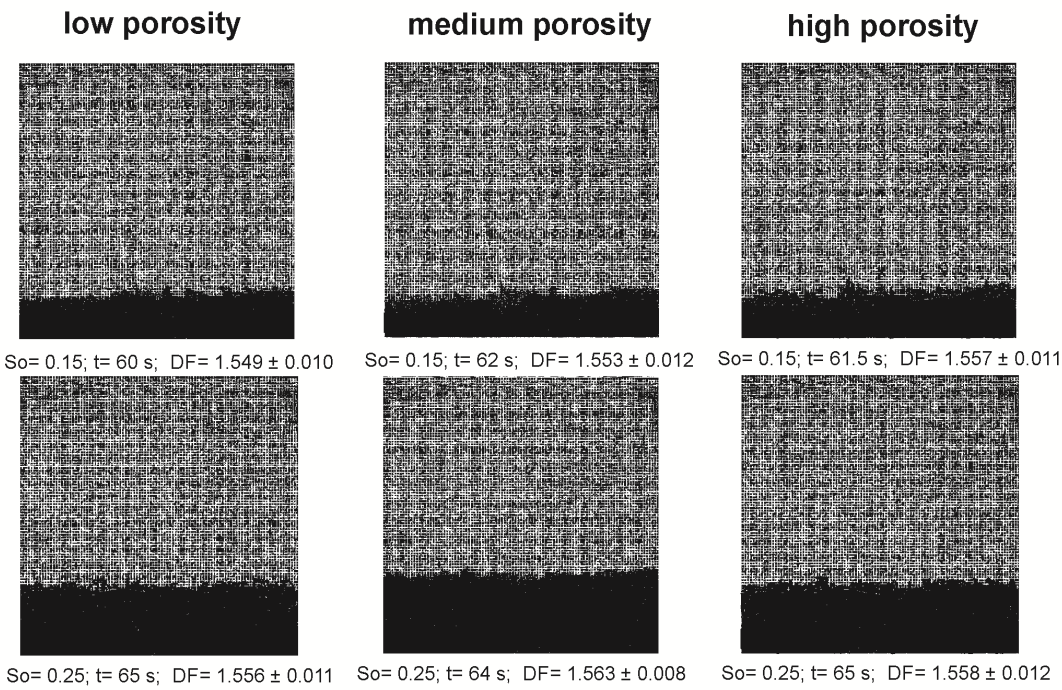

Figure 4-8: Oil saturation maps for the three food matrices under study during the post-frying cooling period for the same level of oil saturation. The time at which this occurs as well as the fractal dimension are also shown.

4.3.4. Phase diagram for oil absorption during the cooling period

In order to better characterize the flow pattern of oil penetration during cooling, we used the phase diagram for an embedding process developed by Lenormand et al. (1988), which represents the displacement of a non-wetting fluid (vapor) by a wetting one (oil).

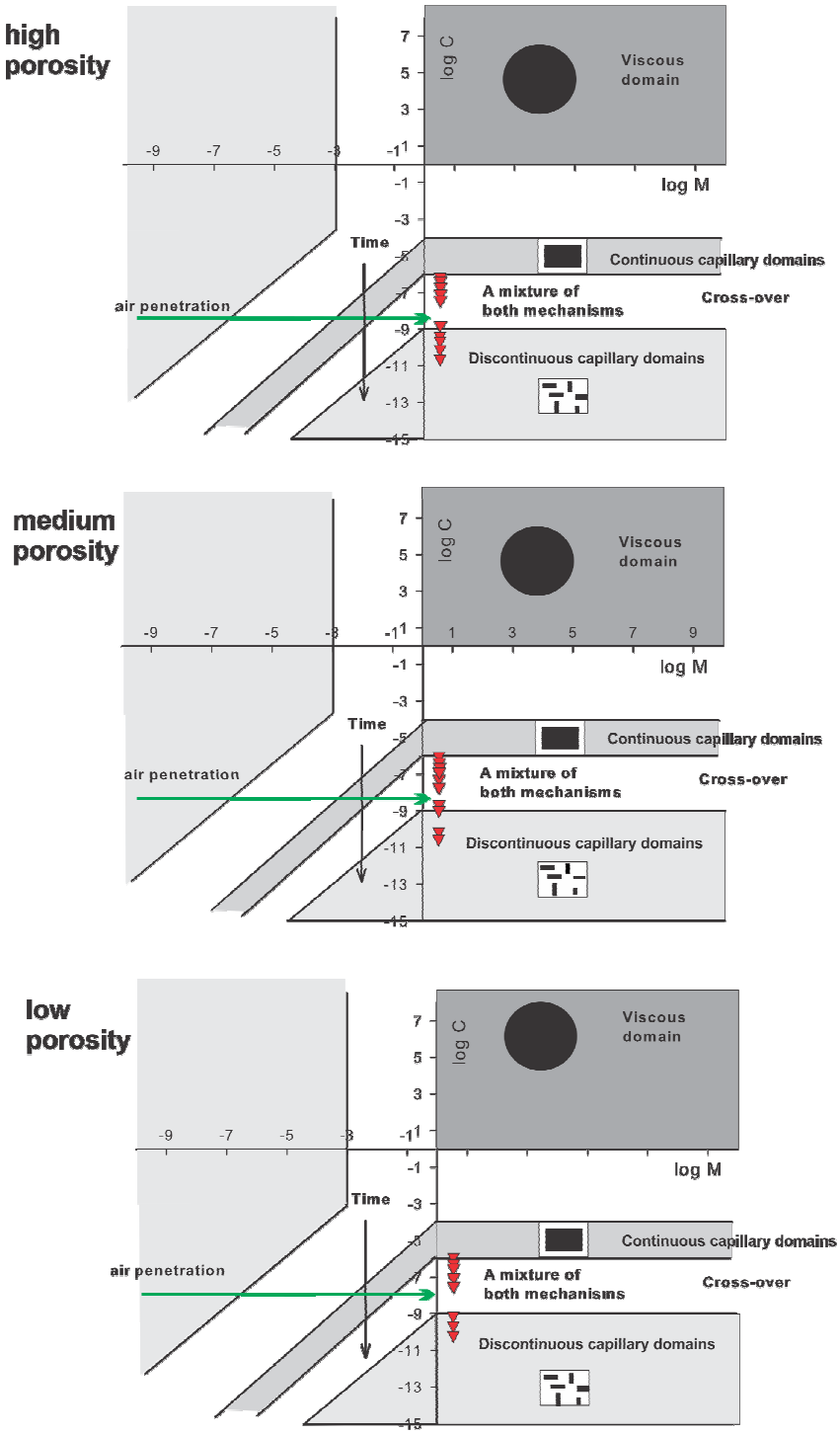

Figure 4-9: Phase diagram showing the trajectory (red triangles) due to oil uptake during the cooling period for the three matrices under study.

The capillary number and the viscosity ratios were calculated according to Equations 4-1 and 4-2, and plotted in this diagram, as shown in Figure 4-9. Results are represented as red triangles, which characterize the trajectory over time (arrow). Also, the moment when the air gets into the micromodel and stops the suction is also shown. Overall, all matrices showed that once air penetrated, discontinuous capillary domains prevailed, highlighting the importance of capillary fingering only at this stage. However, this oil fraction was restricted to a minimum.

4.4. Conclusions

This study showed that the experimental procedure based on the use of glass micromodels is a useful technique to analyze the effect of different porous media on transport phenomena during frying. Specifically, it can be concluded that the microstructural characteristics of the porous matrix do have a significant effect on the kinetics of moisture loss and oil uptake. Higher porosity and larger pore sizes, in the micron range, facilitate the removal of moisture from the matrix during the immersion period and promote greater oil absorption during the cooling period. Fractal analysis was instrumental to describe the shape of the saturation maps for water and oil, during the immersion and cooling periods, respectively. The fractal dimension indicated that the stability of the evaporation front was affected by the different porous media, showing that microstructures with a relatively high number of fine capillaries were less stable and propitiated fingering during the advance of the evaporation front. On the other hand, the shape of the oil front was not affected by the matrix during the cooling period. This behaviour could be explained by the high pressure drop due to water vapour condensation within the micromodel during the cooling period.

In all matrices, the disruption of the surface oil film was a critical factor to stop oil imbibition. Once this occurred, air was able to quickly penetrate within the micromodel, halting the suction. Thus, the amount of surface oil was not a limiting factor.

Overall, the use of micromodels, notwithstanding its limitations in reproducing actual food processing conditions, expands the range of model systems to be used in food

engineering. They allow a direct observation of phenomena, which can help researchers to better understand the mechanisms involved in the different stages of a process to innovate in the challenging field of food product design.

4.5. References

Badillo, G. M., Segura, L. A., & Laurindo, J. B. (2011). Theoretical and experimental aspects of vacuum impregnation of porous media using transparent etched networks. *International Journal of Multiphase Flow, 37*(9), 1219-1226.

Benselama, A. M., Harmand, S., & Sefiane, K. (2011). Equilibrium profile of extended isothermal meniscus with gravity inclination effect. *Colloids and Surfaces a: Physicochemical and Engineering Aspects, 391*(1-3), 158-169. doi: 10.1016/j.colsurfa.2011.03.068

Bouchon, P., & Aguilera, J. A. (2001). Microstructural analysis of frying potatoes. *International Journal of Food Science and Technology, 36*(6), 669-676.

Bouchon, P., Aguilera, J. M., & Pyle, D. L. (2003). Structure oil-absorption relationships during deep-fat frying. *Journal of Food Science, 68*(9), 2711-2716.

Bouchon, P., Hollins, P., Pearson, M., Pyle, D. L., & Tobin, M. J. (2001). Oil Distribution in Fried Potatoes Monitored by Infrared Microspectroscopy. *Journal of Food Science, 66*(7), 918-923.

Bouchon, P., & Pyle, D. L. (2004). Studying oil absorption in restructured potato chips. *Journal of Food Science, 69*(3), E115-E122.

Bouchon, P., & Pyle, D. L. (2005a). Modelling Oil Absorption During Post-Frying Cooling: I: Model Development. *Food and Bioproducts Processing, 83*(4), 253-260.

Bouchon, P., & Pyle, D. L. (2005b). Modelling Oil Absorption During Post-Frying Cooling: II: Solution of the Mathematical Model, Model Testing and Simulations. *Food and Bioproducts Processing, 83*(4), 261-272.

Buckley, J. S. (1991). Multiphase displacements in micromodels. In N. R. Morrow (Ed.), *Interfacial phenomena in petroleum recovery* (Vol. 36, pp. 157-189). New York: Marcel Dekker Inc.

Cortés, P., Badillo, G., Segura, L. A., & Bouchon, P. (2014). Experimental evidence of water loss and oil-uptake during simulated deep-frying process using glass micromodels. *Journal of Food Engineering, 140*, 19-27.

Dana, D., & Saguy, I. S. (2006). Review: Mechanism of oil uptake during deep-fat frying and the surfactant effect-theory and myth. *Advances in Colloid and Interface Science, 128-130*, 267-272.

Danowska-Oziewicz, M., & Karpinska-Tymoszczyk, M. (2005). Quality changes in selected frying fats during heating in a model system. [Article]. *Journal of Food Lipids, 12*(2), 159-168.

Diaz, R. E., Acuña, S. M., & Segura, L. A. (2011). Construction of 2D transparent micromodels in polyester resin with porosity similar to carrots. *Ciencia E Tecnologia De Alimentos, 31*(4), 960-966.

Dueik, V., Moreno, M. C., & Bouchon, P. (2012). Microstructural approach to understand oil absorption during vacuum and atmospheric frying. *Journal of Food Engineering, 111*(3), 528-536. doi: 10.1016/j.jfoodeng.2012.02.027

Dueik, V., Robert, P., & Bouchon, P. (2010). Vacuum frying reduces oil uptake and improves the quality parameters of carrot crisps. *Food Chemistry, 119*(3), 1143-1149. doi: 10.1016/j.foodchem.2009.08.027

Dullien, F. A. L. (1992). Capillarity in porous media *Porous media: fluid transport and pore structure* (Vol. 2). San Diego, USA: Academic press San Diego.

Farinu, A., & Baik, O. D. (2005). Deep fat frying of foods-transport phenomena. [Review]. *Food Reviews International, 21*(4), 389-410. doi: 10.1080/87559120500222896

Farkas, B. E., Singh, R. P., & Rumsey, T. R. (1996). Modeling heat and mass transfer in immersion frying .1. Model development. *Journal of Food Engineering, 29*(2), 211-226.

Figus, C., Bray, Y. L., Bories, S., & Prat, M. (1999). Heat and mass transfer with phase change in aporous structure partially heated: continuum model andpore network simulations. *International Journal of Heat and Mass Transfer, 42*(14), 2557-2569. doi: http://dx.doi.org/10.1016/S0017-9310(98)00342-1

Gamble, M. H., Rice, P., & Selman, J. D. (1987). Distribution and morphology of oil deposits in some deep fried products. [Note]. *Journal of Food Science, 52*(6), 1742.

Gueven, A., & Hicsasmaz, Z. (2013). *Pore structure in food - simulation, measurement and applications* New York: Springer.

Halder, A., Dhall, A., & Datta, A. K. (2007a). An improved, easily implementable, porous media based model for deep-fat frying - Part I: Model development and

input parameters. [Article]. *Food and Bioproducts Processing, 85*(C3), 209-219. doi: 10.1205/fbp07033

Halder, A., Dhall, A., & Datta, A. K. (2007b). An improved, easily implementable, porous media based model for deep-fat frying - Part II: Results, validation and sensitivity analysis. [Article]. *Food and Bioproducts Processing, 85*(C3), 220-230. doi: 10.1205/fbp07034

Huinink, H. P., Pel, L., Michels, M. A. J., & Prat, M. (2002). Drying processes in the presence of temperature gradients --Pore-scale modelling. *The European Physical Journal E, 9*(1), 487-498. doi: 10.1140/epje/i2002-10106-1

Karathanos, V. T., Kanellopoulos, N. K., & Belessiotis, V. G. (1996). Development of porous structure during air drying of agricultural plant products. *Journal of Food Engineering, 29*(2), 167-183.

Laurindo, J. B., & Prat, M. (1996). Numerical and experimental network study of evaporation in capillary porous media. Phase distributions. [Article]. *Chemical Engineering Science, 51*(23), 5171-5185.

Laurindo, J. B., & Prat, M. (1998). Numerical and experimental network study of evaporation in capillary porous media. Drying rates. [Article]. *Chemical Engineering Science, 53*(12), 2257-2269.

Lenormand, R., Touboul, E., & Zarcone, C. (1988). Numerical models and experiments on immiscible displacements in porous media. *Journal of Fluid Mechanics, 189*(9), 165-187.

Lenormand, R., & Zarcone, C. (1984). *Role of roughness and edges during imbibition in square capillaries.*

Lenormand, R., & Zarcone, C. (1989). Capillary fingering: Percolation and fractal dimension. *Transport in Porous Media, 4*(6), 599-612. doi: 10.1007/bf00223630

Louriou, C., & Prat, M. (2012). Pore network study of bubble growth by vaporisation in a porous medium heated laterally. *International Journal of Thermal Sciences, 52*(0), 8-21. doi: http://dx.doi.org/10.1016/j.ijthermalsci.2011.09.008

Mellema, M. (2003). Mechanism and reduction of fat uptake in deep-fat fried foods. *Trends in Food Science & Technology, 14*(9), 364-373.

Metzger, T., Irawan, A., & Tsotsas, E. (2007). Influence of pore structure on drying kinetics: A pore network study. *Aiche Journal, 53*(12), 3029-3041. doi: 10.1002/aic.11307

Moreira, R., Palau, J., & Sun, X. Z. (1995). Simultaneous heat and mass-transfer during the deep fat frying of tortilla chips. *Journal of Food Process Engineering, 18*(3), 307-320.

Moreira, R. G., & Barrufet, M. A. (1996). Spatial distribution of oil after deep-fat frying of tortilla chips from a stochastic model. *Journal of Food Engineering, 27*(3), 279-290.

Moreira, R. G., & Barrufet, M. A. (1998). A new approach to describe oil absorption in fried foods: a simulation study. *Journal of Food Engineering, 35*(1), 1-22.

Moreira, R. G., Sun, X. Z., & Chen, Y. H. (1997). Factors affecting oil uptake in tortilla chips in deep-fat frying. *Journal of Food Engineering, 31*(4), 485-498.

Moreno, M. C., Brown, C. A., & Bouchon, P. (2010). Effect of food surface roughness on oil uptake by deep-fat fried products. *Journal of Food Engineering, 101*(2), 179-186. doi: 10.1016/j.jfoodeng.2010.06.024

Ni, H., & Datta, A. K. (1999). Moisture, oil and energy transport during deep-fat frying of food materials. *Food and Bioproducts Processing, 77*(C3), 194-204.

Oyarzún, C. A., & Segura, L. A. (2009). Design and Construction of Glass Micromodels for the Study of Moisture Transport in Softwoods. *Drying Technology, 27*(1), 14-29. doi: 10.1080/07373930802565731

Pedreschi, F., & Aguilera, J. M. (2002). Some changes in potato chips during frying observed by confocal laser scanning microscopy (CLSM). *Food Science and Technology International, 8*(4), 197-201. doi: 10.1106/108201302027931

Perry, R. H., Green, D. W., & Maloney, J. O. (2008). *Perry's chemical engineers' handbook* (Vol. 7): McGraw-Hill New York.

Plourde, F., & Prat, M. (2003). Pore network simulations of drying of capillary porous media. Influence of thermal gradients. *International Journal of Heat and Mass Transfer, 46*(7), 1293-1307. doi: http://dx.doi.org/10.1016/S0017-9310(02)00391-5

Prat, M. (1993). Percolation model of drying under isothermal conditions in porous media. *International Journal of Multiphase Flow, 19*(4), 691-704. doi: 10.1016/0301-9322(93)90096-d

Prat, M. (2002a). Recent advances in pore-scale models for drying of porous media. *Chemical Engineering Journal, 86*(1-2), 153-164.

Prat, M. (2002b). Recent advances in pore-scale models for drying of porous media. *Chemical Engineering Journal*, *86*(1–2), 153-164. doi: http://dx.doi.org/10.1016/S1385-8947(01)00283-2

Rahman, M. S., Al-Zakwani, I., & Guizani, N. (2005). Pore formation in apple during air-drying as a function of temperature: porosity and pore-size distribution. *Journal of the Science of Food and Agriculture*, *85*(6), 979-989. doi: 10.1002/jsfa.2056

Ryazanov, A., van Dijke, M. I. J., & Sorbie, K. S. (2009). Two-Phase Pore-Network Modelling: Existence of Oil Layers During Water Invasion. *Transport in Porous Media*, *80*(1), 79-99. doi: 10.1007/s11242-009-9345-x

Saguy, I. S., & Dana, D. (2003). Integrated approach to deep fat frying: engineering, nutrition, health and consumer aspects. *Journal of Food Engineering*, *56*(2-3), 143-152.

Saguy, I. S., Ufheil, G., & Livings, S. (1998). Oil uptake in deep-fat frying: review. *Ocl-Oleagineux Corps Gras Lipides*, *5*(1), 30-35.

SanMartin, F. A., Laurindo, J. B., & Segura, L. A. (2011). Pore-Scale Simulation of Drying of a Porous Media Saturated with a Sucrose Solution. *Drying Technology*, *29*(8), 873-887. doi: 10.1080/07373937.2010.547968

Segura, L. A. (2007). Modeling at pore-scale isothermal drying of porous materials: Liquid and vapor diffusivity. *Drying Technology*, *25*(10), 1677-1686. doi: 10.1080/07373930701590889

Segura, L. A., Mayorga, P., & González, J. (2012). A simple pore-scale network model to transport of water vapor and oxygen in polymeric films. *Latin American Applied Research*, *42*, 185-192.

Segura, L. A., & Oyarzun, C. A. (2012). Experimental evidence of mass transfer mechanisms during vacuum freeze-drying in a capillary porous medium. *International Journal of Refrigeration*, *35*(12), 2102-2109.

Segura, L. A., & Oyarzún, C. A. (2012). Experimental evidence of mass transfer mechanisms during freeze-drying in a capillary porous medium. *International Journal of Refrigeration*, *35*(8), 2102-2109. doi: http://dx.doi.org/10.1016/j.ijrefrig.2012.08.014

Segura, L. A., & Toledo, P. G. (2005a). Pore-level modeling of isothermal drying of pore networks - Effects of gravity and pore shape and size distributions on saturation and transport parameters. *Chemical Engineering Journal*, *111*(2-3), 237-252. doi: 10.1016/j.cej.2005.02.004

Segura, L. A., & Toledo, P. G. (2005b). Pore-level modeling of isothermal drying of pore networks. Evaporation and viscous flow. *Latin American Applied Research, 35*(1), 43-50.

Surasani, V. K., Metzger, T., & Tsotsas, E. (2009). A Non-isothermal Pore Network Drying Model with Gravity Effect. *Transport in Porous Media, 80*(3), 431-439. doi: 10.1007/s11242-009-9372-7

Ufheil, G., & Escher, F. (1996). Dynamics of oil uptake during deep-fat frying of potato slices. *Food Science and Technology-Lebensmittel-Wissenschaft & Technologie, 29*(7), 640-644.

Vitrac, O., Dufour, D., Trystram, G., & Raoult-Wack, A.-L. (2002). Characterization of heat and mass transfer during deep-fat frying and its effect on cassava chip quality. *Journal of Food Engineering, 53*(2), 161-176.

Vitrac, O., Trystram, G., & Raoult-Wack, A. L. (2000). Deep-fat frying of food: heat and mass transfer, transformations and reactions inside the frying material. *European Journal of Lipid Science and Technology, 102*(8-9), 529-538. doi: 10.1002/1438-9312(200009)102:8/9<529::aid-ejlt529>3.3.co;2-6

Wang, Z., Peng, X. F., & Liu, T. (2002). Visualization of boiling phenomena in a bead-packed structure. *Experimental Heat Transfer, 15*(3), 177-189. doi: 10.1080/08916150290082612

Xu, P., Mujumdar, A. S., & Yu, B. (2008). Fractal Theory on Drying: A Review. *Drying Technology, 26*(6), 640-650. doi: 10.1080/07373930802045932

Yamsaengsung, R., & Moreira, R. G. (2002). Modeling the transport phenomena and structural changes during deep fat frying - Part 1: model development. [Article]. *Journal of Food Engineering, 53*(1), 1-10.

Yiotis, A. G., Tsimpanogiannis, I. N., & Stubos, A. K. (2010). Fractal Characteristics and Scaling of the Drying Front in Porous Media: A Pore Network Study. *Drying Technology, 28*(8), 981-990. doi: 10.1080/07373937.2010.497087

Ziaiifar, A. M., Achir, N., Courtois, F., Trezzani, I., & Trystram, G. (2008). Review of mechanisms, conditions, and factors involved in the oil uptake phenomenon during the deep-fat frying process. *International Journal of Food Science and Technology, 43*(8), 1410-1423. doi: 10.1111/j.1365-2621.2007.01664.x

5. GENERAL CONCLUSIONS AND FUTURE PROSPECTS

5.1 General conclusions

The work developed throughout this thesis showed how micromodels may be used to study and gain a better understanding of key transport phenomena during oil immersion from a microscopic point of view. In fact, this approach allowed getting direct visual evidence of the mechanisms involved in the evaporation of water and oil absorption during oil immersion, for the first time, in order to establish the most important flow mechanisms and sequence during the process, identifying when and how the movements of the fluids within the matrix occur. Specifically, it allowed following in real time the fluids motion within the pore network, during the high-speed vapor release. In addition, it was possible to visualize the meniscus motion mechanisms of oil inhibition within the micromodel.

During the immersion period, bubbles were released at a very high frequency as in a normal frying operation. It was confirmed that only a small fraction of oil was able to penetrate within the capillaries during this time interval. Once the escape of steam stopped, after some initial cooling, oil-uptake began abruptly and oil movement into the pores could be clearly identified. The end of oil uptake was defined by the moment when air penetrated, as soon as the oil film lost its continuity. Thus, air played a critical role, as it competed with oil to fill the empty capillaries, which quickly occurred when the continuity of the surface layer of oil was lost. Likewise, the microstructure of the matrix had a significant effect on the kinetics of moisture loss, where larger pores and a higher porosity facilitated moisture loss. In the same way, these microstructural features allowed increasing the final oil content. Using fractal analysis, it was possible to describe the shape of the saturation maps for water and oil, for the immersion and cooling periods, respectively. During the immersion period, the stability of the evaporation front changed as the process was moving forward because the temperature gradient in the early stages produced stable front; however, as the process proceeds, its

shape was more irregular promoting fingering. Also, the evaporation profile was significantly affected by gravity and the type of matrix. During the cooling period, the shape of the oil front was not affected by time and the other factors under the scope of this study (gravity and matrix). This behaviour can be explained by the high pressure gradient produced by water vapour condensation within the micromodel during the cooling period.

Additionally, the analysis of transport phenomena analysis with respect to gravity, using different configurations, showed that gravity affected significantly the water evaporation profiles, favoring them when the evaporation front moved in an opposite direction. However, it was not possible to observe a total decoupling of phenomena. Apparently the temperature gradients, which occurred during the immersion period, had a great effect on the kinetics of evaporation and the shape of fronts, since the temperature profiles overlapped nearly perfectly with the evaporation profiles. The evaporation fronts morphology showed different characteristics to those observed in similar experiments during drying, which suggested that the thermal effects had a dominant role. With respect to oil absorption, the micromodel orientation mostly affected oil drainage from the surface, thus, affecting the final oil content. Specifically, when g=0, a minimum amount of oil absorption was found.

Oil immersion of a glass micromodel has certainly some differences from oil immersion of a food material. For instance, glass micromodels are non-hygroscopic, have a fixed structure and are 100% saturated with water. Food materials, on the other hand, are composted of several components and the porous structure develops during the process. In starchy foods for instance, a major food category, starch gelatinization affects the formation and structure of the porous media that is developed during frying, where pores may also expand or collapse during the process. But, the use of glass micromodels allows the direct observation of transport phenomena, which has not been possible to be achieved in a food system. This evidence may lay the foundations for further knowledge about these phenomena and contribute to the improvement of predictive models,

technology design and processing strategies to develop fried products with lower oil content.

5.2 Future prospects

The work developed throughout this thesis and the developed technique illustrates how glass micromodels may be used to visualize and provide valuable information to understand key transport phenomena during oil-immersion, an approximation that may well be applied in other processes or fields. Thus, the set-up itself already opens new frontiers.

In relation to the oil-immersion process itself, several new questions have arisen. New experiments may be envisaged, in order to get deep of some of the results obtained in this thesis, which may be used to develop new mathematical models of the process, both at the macroscopic and at the pore level. The high temperature gradients observed during frying appear to have a significant role in the kinetics of moisture loss, bubbling, and oil absorption. For instance, it would be ideal to be able to decouple the effect of thermal gradients over gravity effects. A major problem to study the temperature gradients during the immersion period is that glass micromodels are not transparent to infrared radiation, as in thermographic cameras. Thus, a new challenge may be related to the fabrication of micromodels that are transparent to infrared radiation, but at the same time are heat resistant, to avoid temperature shocks.

Another aspect that may be improved in future studies is related to get a better approximation to a real food system. On the one hand, experiments with mixtures of water and others food building blocks, such as starch, proteins, and salts for instance, could be performed in order to study the effect of these components on the kinetics of moisture loss and oil absorption. On the other hand, new materials could be used to diminish the rigidity of the system to get a better approximation to what might occur in a real system. More rigid structures have a higher internal pressure, which can affect the

process. A similar approach to the one recently developed by Segura et al. (2013)[1], to design a micromodel based on a specific type of silicone able to resist the process conditions, could be defined.

Finally, the information obtained from these kinetics studies, performed at pore level, could be used to feed a macroscopic mathematical model to simulate oil absorption and moisture loss under more realistic conditions. Also, it could be possible to simulate the oil immersion process at pore level. The good match with experimental results would indicate the adequacy of the model to capture the essence of key phenomena.

[1] Segura, L.A., Badillo F.V. Villagra, D.L., Garrido, O. (2013) Protocol to build 2D transparent micromodels in PDMS and preliminary applications on drying, *Proceedings of the 6th Nordic Drying Conference*, Copenhagen, Denmark, Editors: Svetlana Goncharova-Alves Odilio Alves-Filho, Trygve M. Eikevik, , ISBN: 978-82-92739-05-1, 11 pages.